DEMOCRATIC REPUBLIC OF ALGERIA

MINISTRY OF HIGHER EDUCATION AND SCIENTIFIC RESEARCH

Blida 01 University

Institute of Aeronautics and Space Studies

Option: Propulsion

Fluid Interaction between Rotor and Stator in a Centrifugal Compressor Stage

In partial fulfillment of the requirements for

The Degree of Master in Aeronautics

A Thesis Submitted by

BEKHTI Adlane

SAYAH Mustapha

under the supervision of

LAAZEB Sebaa

Blida 2023/2024

Acknowledgement

I am infinitely grateful to Allah the great and almighty for blessing my work rewarding my prayers and giving me the strength and knowledge to complete this modest work, this thesis would never be completed without his blessing.

I would like to express my sincere gratitude to all these individuals for mentoring and supporting me in completing this work.

To my parents, their constant encouragement, patience, and understanding have been the pillars of my success.

My teacher LAAZEB Sebaa, for providing me with invaluable insights and direction.

I am grateful to my friends who contributed ideas and perspectives that enriched the project.

Thank you everyone for shaping this project and enhancing my learning experience.

Dedication

It is with great honor and immense joy that I dedicate this modest work to all the people who supported me, particularly to my parents to whom I will never be able to express my gratitude and appreciation, for their love and their support throughout my studies. My brothers and sister, my colleagues and all my teachers. To all my family.

To my teacher LAAZEB Sebaa, whose guidance and encouragement have been instrumental in my academic journey. Your support has inspired me to strive for excellence and pursue my goals with confidence. Thank you for your dedication and belief in my abilities.

To my friends the ones I went through this journey with, the ones who supported me, laughed with me the ones whom I am infinitely grateful.

ملخص

بشكل عام، يتميز التدفق الداخلي في الآلات التوربينية باللزوجة، وقابلية الانضغاط، وثلاثية الأبعاد، ودواماته. كجزء من الأبحاث المختلفة حول ضواغط الطرد المركزي، أجرى العديد من الباحثين دراسات عددية وتجريبية لفهم عملها،

لقد أثبتوا أن العديد من المعلمات الفيزيائية يمكن أن تؤثر بشكل إيجابي أو سلبي على أداء الضاغط. على سبيل المثال، تم إجراء عمليات محاكاة عددية على مراحل الضاغط باستخدام برنامج ANSYS CFX لتحليل المعلمات الهوائية، بما في ذلك تأثير التفاعل بين المكره والناشر على الأداء. تم إجراء هذه المحاكاة باستخدام نموذج الاضطراب kw-sst في الحالة المستقرة.

يعد التفاعل بين العضو الدوار والجزء الثابت في ضواغط الطرد المركزي جانبًا مهمًا في تصميمها وتشغيلها. وهو ينطوي على تحسين المعلمات الهندسية والتشغيلية لتحقيق أقصى قدر من كفاءة الطاقة. يستخدم المهندسون عمليات المحاكاة العددية ونماذج ديناميكيات الموائع الحسابية (CFD) لدراسة هذا التفاعل المعقد، الهدف هو تحسين الأداء العام للضاغط، مما يؤدي إلى استخدام أكثر كفاءة للطاقة وتحقيق مكاسب كبيرة في الكفاءة.

كلمات مفتاحية: سائل قابل للانضغاط، لزج، سائل دوامي، تفاعل دافع-ناشر

Abstract

Generally, the internal flow in turbomachines is characterized by its viscosity, its compressibility, its three-dimensionality and its vortices. As part of various research on centrifugal compressors, many researchers have conducted numerical and experimental studies to understand their operation. They demonstrated that several physical parameters can positively or negatively influence compressor performance. For example, numerical simulations were carried out on compressor stages using ANSYS CFX software to analyze aerothermodynamic parameters, including the effect of interaction between the impeller and diffuser on performance. These simulations were carried out using the kw-sst turbulence model in steady state.

The interaction between the rotor and stator in centrifugal compressors is a crucial aspect of their design and operation. It involves the optimization of geometric and operational parameters to maximize energy efficiency. Engineers use numerical simulations and computational fluid dynamics (CFD) models to study this complex interaction. The goal is to improve overall compressor performance, resulting in more efficient use of energy and significant efficiency gains.

Key word: compressible flow, viscous, vortex flow, impeller-diffuser interaction.

Résumé

De manière générale, le flux interne dans les turbomachines est caractérisé par sa viscosité, sa compressibilité, sa tridimensionalité et ses tourbillons. Dans le cadre de diverses recherches portant sur les compresseurs centrifuges, de nombreux chercheurs ont mené des études numériques et expérimentales pour comprendre leur fonctionnement. Ils ont démontré que plusieurs paramètres physiques peuvent influencer positivement ou négativement les performances du compresseur. Par exemple, des simulations numériques ont été réalisées sur des étages de compresseur en utilisant le logiciel ANSYS CFX afin d'analyser les paramètres aérothermodynamiques, notamment l'effet de l'interaction entre la roue et le diffuseur sur les performances. Ces simulations ont été effectuées en utilisant le modèle de turbulence kw-sst en régime stationnaire.

L'interaction entre le rotor et le stator dans les compresseurs centrifuges est un aspect crucial de leur conception et de leur fonctionnement. Elle implique l'optimisation des paramètres géométriques et opérationnels pour maximiser l'efficacité énergétique. Les ingénieurs utilisent des simulations numériques et des modèles de dynamique des fluides computationnelle (CFD) pour étudier cette interaction complexe. Le but est d'améliorer les performances globales du compresseur, ce qui se traduit par une utilisation plus efficace de l'énergie et des gains d'efficacité significatifs.

Mots clef : fluide compressible, visqueux, tourbillonnaire, interaction roue-diffuseur.

Contents

List of Figures

List of tables

General introduction

Centrifugal compressors are widely used in industry and small gas turbine engines. A high-pressure ratio will be the goal orientation for centrifugal compressors, as this leads to saving energy, reducing emission and raising power density.A stage of a centrifugal compressor consists of a moving part rotor (impeller) and a fixed part stator (diffuser), whose main role is to ensure the correct functioning of the compressor.

Rotor: The rotor is the moving part of the compressor stage. It is made up of blades (or vanes) attached to a central hub and is responsible for accelerating the fluid (gas) by making it swirl.

Stator: The stator is the fixed part of the compressor stage, also made up of blades. Its role is to diffuse the fluid accelerated by the rotor, converting the kinetic energy into an increase in pressure.

Designing the fluid interaction between the rotor and stator often involves numerical simulations and Computational Fluid Dynamics (CFD) models to optimize geometric and operational parameters.

The fluid interaction between the rotor and stator is a complex science, and engineers are continually working on improvements to increase the energy efficiency of centrifugal compressors. This contributes to higher overall performance and more efficient use of energy.

We present this work by four chapters:

Chapter 1: Introduction to the overview and general definition of turbomachinery regarding compressors, especially centrifugal compressors, their classification what follows is a description of the various functions.

Chapter 2: Introducing analytical equations applicable to a certain stage governing equations for centrifugal compressors and CFD models, focusing on Turbulence model exists.

Chapter 3: This chapter is about numerical simulation and representation ANSYS CFX software. Centrifuge geometry modeling Compressor impeller and diffuser and corresponding meshing are described in detail. When representing the turbulence model we use here Research (K-w SST). And the finite volume method of numerical discretization, the equations for this problem are derived from the scenarios in CFD and from the diagrams available in this software.

Chapter 4: the results are presented for the centrifugal compressor stage, and the validation of the results by comparing the numerical results with the experimental results of Ziegler.

BIBLIOGRAPHICAL ANALYSIS

The flow in a centrifugal compressor is generally viscous and turbulent, three-dimensional, unsteady and compressible fluid. For the study and analysis of the flow in this compressor can be done following by two methods, the numerical method and the experimental method.

The numerical method based on the discretization of basic equations in mechanics of fluid to solve the problem, it requires a certain amount of simplification on the system of questions.

The experimental method that several systems require for measurements (pressure, speed, temperature, etc.). Use of visualization techniques for the analysis of different flow structures.

Many researchers have already studied and analyzed the flow in a centrifugal compressor. Among the researchers:

Jeske.H; O.Tepel [1]

They used a numerical method to analyze the transonic flow in the diffuser of a centrifugal compressor with a high pressure ratio, and determination of the flow of the boundary layers over the length of the blades and also calculates the distribution two-dimensional pressure at the hub by the finite difference numerical method and make the comparison with experimental results.

Michal .D; Hathaway; Randall M.chriss; Jerry R.Wood and Anthony J; Stragisar [2] At NASA, they analyzed the flow in a centrifugal compressor at low speed, they used both numerical and experimental methods.

Kai U .Ziegler, Heinz E .Gallus, Reinhard Niehuis [3]

Presents an experimental investigation of the effect of impeller-diffuser interaction on the unsteady and the time averaged flow field configuration in impeller and diffuser and the performance of these components.

Part one deals with the integral flow losses and the diffusion in impeller, diffuser and the entire compressor. The results show that in most cases smaller radial gaps are leading to a more homogeneous flow field at diffuser vane exit and to a higher diffuser pressure recovery resulting in a higher compressor efficiency. On the other hand, impeller efficiency is hardly affected by the radial gap. The second part focuses on the reasons for these effects.

Guillaume Dufour [5]

He studies numerical modeling of flows in compressors centrifugal for design by the laws of similarity and which has the objective improving the quality of centrifugal compressor of conditioning system of air, for this he uses two methods, numerical and experimental.

Numerically, deals with the various parameters which influence the result (the numerical errors, numbers of mesh elements, nodes), the contribution of turbulence model and compares them with the experimental results.

Nicalas Rochuon [6]

He analyzes the three-dimensional and unsteady compressible flow in a centrifugal compressor with a high pressure rate, this analysis of the flow was carried out by two experimental and numerical methods. The experimental method uses the measurements were carried out by LASER velocimetry with Doppler effect. And the numerical method makes stationary in-station simulations with models of different turbulences and making the comparison between the two methods.

Ozturk Tatar [7]

Numerical simulated the incompressible stationary flow through a smooth diffuser centrifugal compressor, using the finite volume method (FVM), coupled with the k-turbulence model standard, using FLUENT code to solve Navier-Stokes equations with design flow condition. Velocity contours, pressure and turbulence kinetic energy were calculated on eight stations across the diffuser, from which turbulent mixing regions are identified. The flow field at the inlet of the diffuser clearly shows the type of jet-wake flow at the wheel. The passing wake is in the vicinity of the envelope side of the diffuser and the mixtures slowly as the flow passes through the diffuser. On the other hand, the blade outlet wake quickly mixes out into the diffuser. Close agreement was observed between the numerical simulation and the experimental results**.**

Maammeur Moustafa [8]

His work deals with a numerical investigation of the three-dimensional flow in a centrifugal compressor, where he shows the affection of the performances by two geometric parameters, the angle of cushioning at the outlet and the section at the inlet of the centrifugal compressor.

The study is based on an aerodynamic approach in turbulent conditions but also in a thermodynamic approach in order to compare them. Due to the presence of the boundary layer, special attention is given to the meshes, and a technique is proposed that allows to specify the density of the mesh near the wall. He also discussed the possible presence of the upstream and downstream domains, respectively the inlet and the volute. Finally it ends with a validation of the results by this of the literature.

CHAPTER 1

Turbomachinery

1. Generality of turbomachinery

1.1 Introduction

A turbomachine is a mechanical system designed to facilitate energy exchange between a flowing fluid and a rotor, typically undergoing uniform rotational motion about its axis.

Turbomachinery encompasses a variety of machines that operate within a continuous thermodynamic cycle, and centrifugal compressors specifically facilitate the exchange of energy between a flowing fluid and a rotating rotor. In essence, a centrifugal compressor is a specific application of turbomachinery designed for compressing gases or air.

Centrifugal compressors have become ubiquitous over the twentieth century across a wide range of applications due to their inherent robustness, good efficiency and broad operating range.

The future of centrifugal compressors seems equally bright with the present focus on environmental goals, including the future decarbonisation of power generation and transportation, with a possible shift to a hydrogen economy. There is ever-increasing pressure to produce higher-efficiency gas turbines at increased cycle pressure ratios for aviation propulsion and ground-based power generation, which also favour the use of centrifugal or axial-centrifugal machines.

1.2Turbomachinery

Turbo machines are rotating machines used to change the state of a working fluid liquids in pumps, gases in compressors and one or the other in turbines. Pumps, fans, ventilators and blowers are used to transport fluids; turbines and wind turbines extract energy from a fluid stream. Turbochargers, propellers and jet engines constitute part of propulsion or transportation devices. This wide remit means that turbomachines span almost all industrial sectors and play a vital role in many of them.

They are often only a small part of a more complex system, which typically imposes the requirements for and constraints on their design. There is a huge range of types, sizes and speeds, with large economic significance in numerous applications. In addition, the technological and scientific interest of fluid dynamics, thermo dynamics and mechanics makes turbomachinery a highly worthwhile subject of engineering study.

Turbomachinery is fundamentally linked to energy conversion in its many forms. Most electrical power is currently generated by steam turbines in nuclear and coal fired plants, but even modern solar or biomass power plants use small steam or gas turbines for energy conversion. Natural gas is the fuel most commonly used for land based gas turbine power plants, and nowadays these are often combined with a steam turbine which, in turn, obtains its heat source from the hot exhaust gases of the gas turbine. Water turbines in hydroelectric schemes and wind turbines use renewable energy sources for power generation.

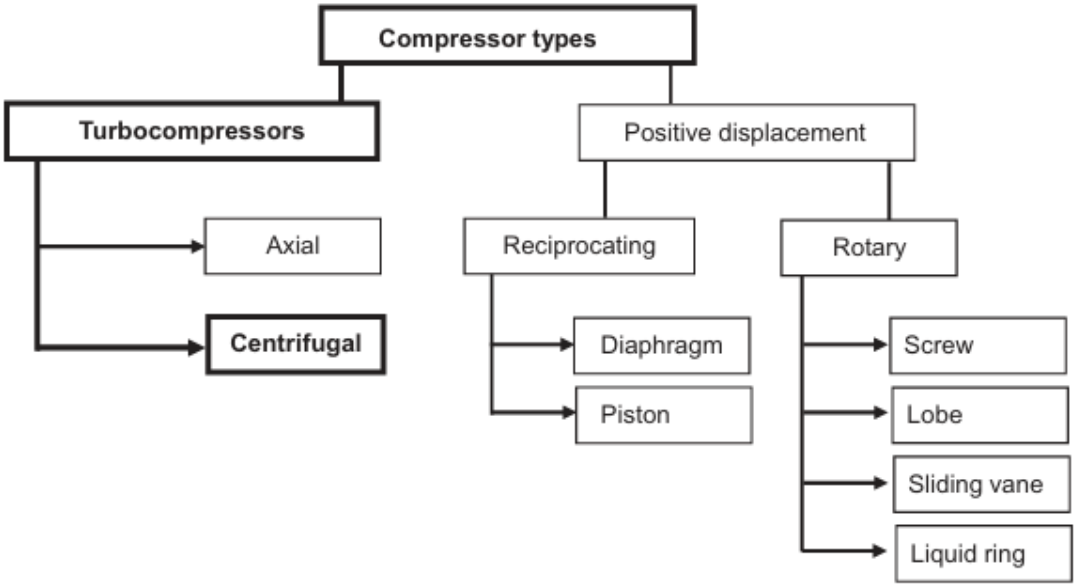

Figure 1-1 Categories of different compressor types [9]

Turbomachinery plays an equally important role in the transportation industry– the gas turbine jet engine is used for propulsion in nearly all aircraft; turbochargers are widely used in ground transportation and as an integral part of diesel propulsion in nearly all ships, lorries and diesel cars and, increasingly, in gasoline-fuelled vehicles. Pumps are the world's most ubiquitous turbomachines, found everywhere where liquid needs to be transported. Compressors and pumps are important to chemical processes, to the use of industrial gases and in the oil and gas industries. Compressors and ventilators are key components in air conditioning, cooling and refrigeration equipment. Turbomachinery can even be found in the medical industry, where pumps are deployed for blood circulation, ventilation-assist fans are used in the treatment of sleep apnoea and in other clinical applications. The drive powering a high-speed dental drill is, in fact, generally a tiny high-speed air-driven turbine.

The distinguishing feature of a turbomachine is that energy is transferred continuously to or from a fluid by the aerodynamic action of the flow around rotating blades in an open system. [9]

1.3 Constitution of turbomachinery

A turbomachine comprises several essential components:

- **A distributor** responsible for guiding the fluid from the inlet section of the machine to the rotor's inlet, imparting the required speed and direction. This distributor can vary from a simple pipe to a fixed ring of blades that can be adjusted to control flow.
- **An impeller** facilitating the transfer of mechanical energy between the fluid and the shaft.
- **A stator**, also known as a diffuser, which gathers the fluid at the rotor outlet and directs it towards the machine's outlet section. The diffuser may include a ring of fixed blades to correct the fluid's direction, typically axial, before its discharge.
- Bearings providing support for the drive shaft.
- Thrust bearings ensuring proper positioning of the rotor within the stator and absorbing axial forces.
- Sealing mechanisms to minimize fluid leakage during operation

1.4 Aerodynamic

The truly key feature of a turbomachine is the aerodynamic forces acting on the blades. It is the motion of the fluid compared to the motion of the machine that is primary. The actual motion of the fluid in a positive displacement machine is, by contrast, generally less well ordered and is secondary to the motion of the components– such as pistons or valves. As the flow passes over the blade surface of a turbomachine, an aerodynamic lift force is generated, similar to the lift force on an aircraft wing. If the blades are moving in the direction of this force, then there is a transfer of work between the fluid and the shaft. This is the essence of turbomachinery, and a good understanding of fluid dynamics is therefore one of the key building blocks in the design of good turbomachines.

As an example of the importance of aerodynamic forces, it is useful to consider the work input into an Archimedean screw. This rotating machine acts as a pump to raise water to a higher level (or as a water turbine when the water is flowing downhill), but it is not a turbomachine because the work input is not related to an aerodynamic force. Instead, it is due to work done against gravitation to lift the weight of the water as it periodically fills and empties from a section of the screw. Similarly, one can distinguish between undershot and overshot water wheels. In an overshot water wheel, the water enters at the top of the wheel and the weight of the water held in each bucket provides the necessary torque. This is not a turbomachine as long as the small impulse from the water entering and leaving the buckets can be neglected. An undershot wheel, by contrast, makes use of the kinetic motion of the fluid to provide a force on the paddle blades. The head of water must first be converted into kinetic energy or the wheel needs to be mounted in a fast running stream. The undershot water wheel is considered to be a turbomachine as its operation is due to an aerodynamic force from the motion of the water acting on the blades. In this case, however, it is a drag force and not an aerodynamic lift force, which is more normal in turbomachines.

The range of types and sizes of turbomachines is vast. Common examples in rough order of increasing size are: high-speed dental drills, computer cooling fans, hair dryers, ventilation fans, turbochargers for cars, water pumps, blowers for air compression, compressors and turbines for helicopter engines, turbochargers for ships' diesel engines, turbines and compressors in aero engines and industrial gas turbines, water turbines, steam turbines and wind turbines in the power generation industry. If world records are considered, wind turbines are the largest (having a rotor tip diameter above 200 m), Francis turbines are the most powerful in terms of the energy from a single blade row (with a power of 800 MW from a single impeller with a diameter of between 5 and 10 m), and the steam turbine is the most powerful turbomachine on a single shaft.

Practical radial turbo compressors can be found in a range of applications with impeller diameters, D2, of between 10 mm and 2000mm, and an impeller tip-speed, u2, of between 100 and 700 m/s. An overview is provided in Figure (2). Low-pressure compressors with low tip-speeds are known as fans and medium-pressure compressors as blowers.

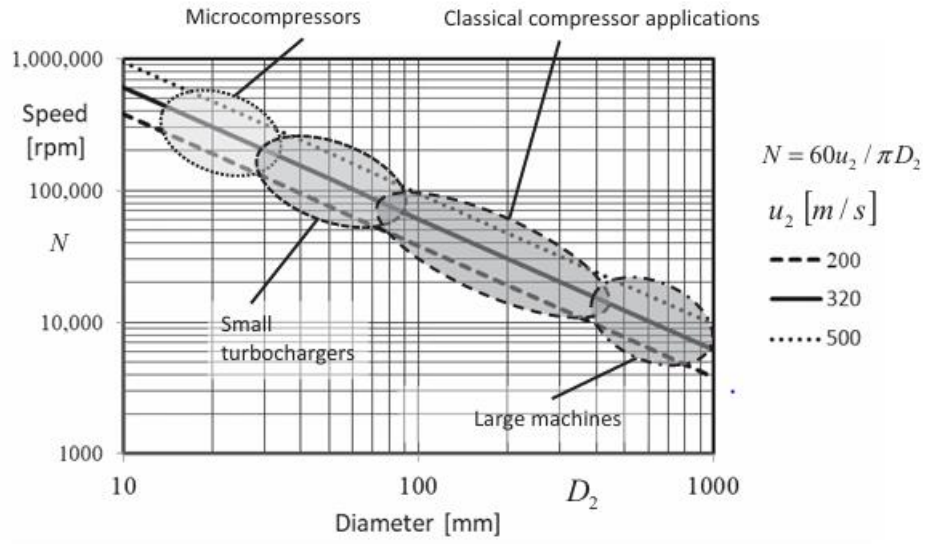

Figure 1-2 an overview of the range of size and rotational speed of radial flow turbocompressors [9]

While most of the fundamental principles of design can be comfortably applied across the range of size and tip-speed, some aspects do not scale. For example, the tip clearance of open impellers is one of the key factors limiting the efficiency of small stages, and the blade thickness tends to become larger relative to the diameter at small size due to manufacturing constraints. In many applications at the larger sizes, it may be more efficient– and may reduce the outer dimensions– to use a smaller axial compressor or an axial-centrifugal compressor. Large centrifugal machines are often preferred, however, as they are more robust and have much wider operating characteristics. [9]

1.5 Classification of Turbomachines

1-Power Consuming and Power Producing Machines

The most fundamental classification is into machines which add energy to a fluid and those which extract energy from a fluid: work-absorbing machines and work-producing machines. The addition or extraction of energy is usually achieved at the expense of the fluid pressure. Turbines have an output of shaft work from the machine which they obtain by converting the internal energy of the fluid into rotational energy of the shaft. In all turbines, except wind turbines, the pressure falls as rotational kinetic energy is generated in upstream components, and this energy is then extracted by the rotor blades. Compressors (and pumps) require work input to the shaft to generate a pressure (or head) rise. The work is first converted into static pressure or enthalpy rise and an increase in kinetic energy in a rotor blade row. The kinetic

energy is then converted into a further pressure rise by a stator blade row. In some low-cost applications, such as ventilator fans, the downstream stator is not present and the exit kinetic energy is simply discarded.

2-Thermal and Hydraulic Machines

The distinguishing feature of a thermal turbomachine, as opposed to a hydraulic turbomachine, is that the working fluid is compressible. The gas undergoes a marked change in volume with the density and temperature changes that occur as it passes through the machine. In a hydraulic machine, the fluid (usually cold water) is effectively incompressible and the density remains constant: the fluid then has the same volume, and very nearly the same temperature, at the inlet and the outlet of the machine. Thermodynamics is not relevant to the performance analysis in this case. A multistage pump has similar impellers in all of its stages as there is no difference in the volume flow at different positions in the machine. On the other hand, a multistage compressor requires that the flow channel of the stages is adapted to

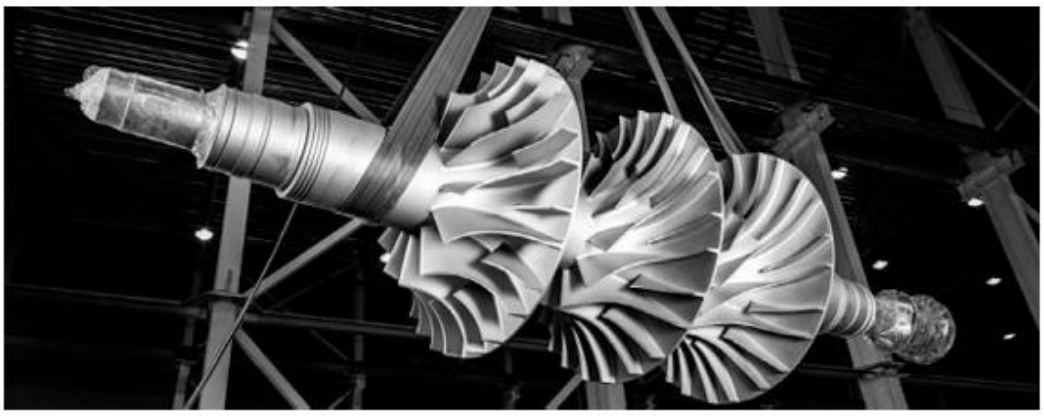

Figure 1-3 the shaft of a three-stage air compressor with open impellers manufactured by Entenmach RPC LCC, Saint Petersburg, Russia. (Image by courtesy of Entenmach)[9]

Account for the decrease in volume of the gas being compressed, which means that different impellers with narrower flow channels are needed on the passage through the machine. Figure (3) from Neverov and Liubimov (2018) shows this for a multistage machine with three different open impellers of the same diameter on the same shaft. The amount of volume compression for a given pressure rise is also a function of the gas properties of the fluid being compressed so that different impellers are also needed for different gases. The manufacturer of multistage pumps needs to develop a single stage that can be used at each position in a multistage machine

as the volume flow does not change through the machine, whereas the compressor manufacturer needs to develop or adapt separate stages for each location. A limiting case in respect of thermal turbomachinery is a low-speed ventilator where the density change is almost negligible and so these machines may be regarded as incompressible. The large changes in temperature and density in high-speed turbomachines can only be properly accounted for by the theory of compressible gas dynamics.

3- Acceleration and Deceleration of the Flow

The addition or extraction of energy is usually made at the expense of the fluid pressure; compressors generate a pressure rise, whereas turbines cause a pressure drop. Furthermore, whether the static pressure rises or falls through the machine is an important difference. In compressors and ventilators, the static pressure usually rises in the direction of flow, whereas it usually drops in the direction of flow in turbines. It is fundamentally difficult to persuade a fluid to move 'uphill' against rising pressure. This means that the basic aerodynamic design of compressors is generally more problematic and more affected by aerodynamic limits than that of turbines. Compressor blade rows generally experience decelerating flow as the flow gives up its kinetic energy to produce a static pressure rise. This tends to cause the slow moving fluid in the thin fluid boundary layers on the blades to become slower and, as a consequence, the boundary layers become thicker and are more liable to separate from the blade surface. The propensity for flow to separate means that the rate of reduction in velocity or the rise in pressure must be carefully managed, and this effectively results in a limit on the deceleration of the flow for compressor stages. Turbines, with accelerating flow in the direction of the pressure gradient, tend to have thin, stable boundary layers on the blades, and there is no limit to the amount of acceleration that the fluid encounters. This fundamental difference between the two types of machine is evident from the cross section of any industrial single-shaft gas turbine– where there are usually three to four times as many compressor stages as turbine stages, although both have the same rotational speed and nearly the same pressure ratio. Some turbomachines, such as a reversible pump-turbine for a pumped hydroelectric storage scheme, operate as both turbines and compressors. At times of low electrical demand, excess generation capacity is used to pump water into the higher reservoir. When there is higher demand, water is released into the lower reservoir through the same machine, which is now operating as a turbine and generating electricity. The design for pump operation takes priority; the machine will operate adequately as a turbine with accelerated flow when the water runs downhill, albeit no optimally.

4- Flow Direction

Another important criterion for the classification of turbomachinery is the flow direction relative to the axis of rotation. In purely axial rotors, the radius of the streamlines is approximately constant and the flow passes through the machine roughly parallel to the rotational axis. In purely radial machines, the radius changes significantly and the f low travels through the rotor perpendicular to the axis of rotation, as shown in Figure 1.4. In practice, axial machines tend to have some small radial velocity components as neither the inner nor the outer casing walls are perfectly cylindrical, and most radial machines have an axial component of velocity. Most radial flow compressors have axial flow at the inlet and are radial at the outlet (and vice versa for radial flow turbines), as shown in Figure 4. In some situations, these may qualify as mixed-flow machines because of the axial inlet and radial outlet. In the present text, the adjectives radial and centrifugal are used for all machines with a significant change of radius across the impeller and with a radial flow at exit. The name centrifugal impeller implies that the effect of centrifugal force (radius change) in generating a pressure rise across the impeller is significant. Defining the machine type based on the orientation of the leading and trailing edges can become confusing: for an axial inlet flow and radial outlet flow, the leading and trailing edges can also be designed with different sweeps with respect to the mean meridional flow. The term diagonal is sometimes used for rotors which have leading and trailing edges which are neither axial nor radial and are swept forwards or backwards in the flow channel. The term mixed flow can be linked to the direction

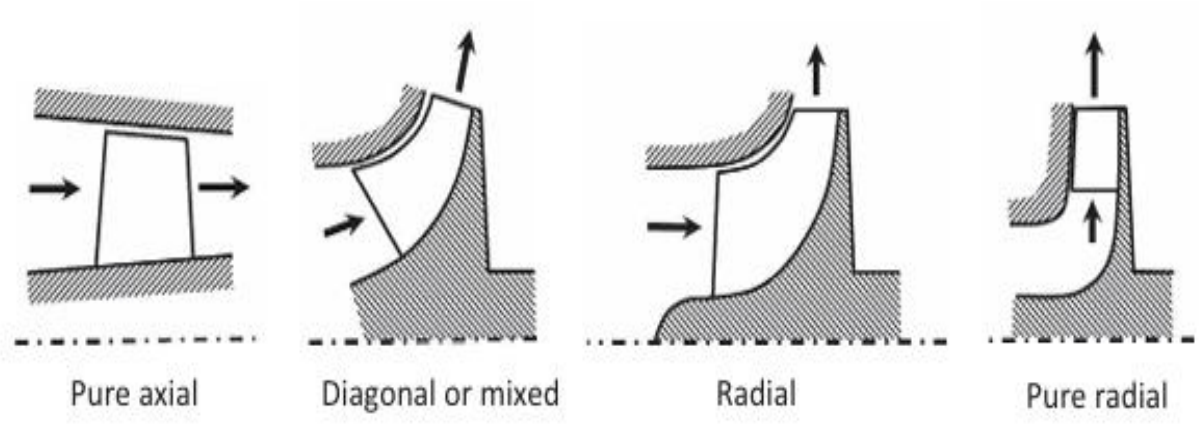

Figure 1-4 Sketches of axial, diagonal, mixed and radial flow compressors [9]

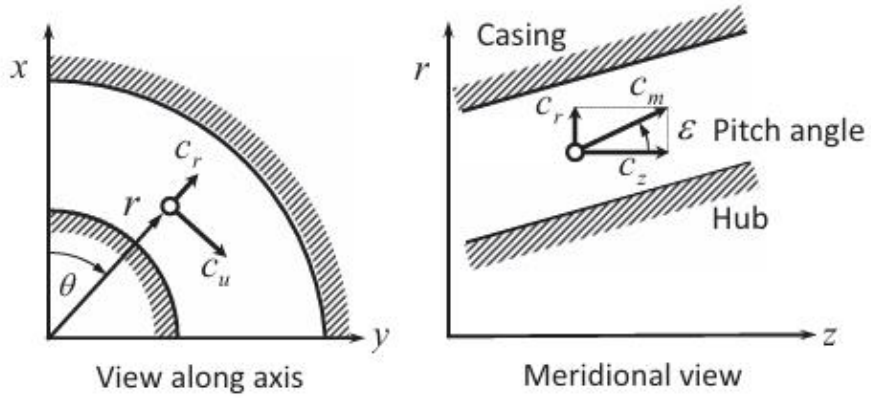

Figure 1-5 Axial, radial, circumferential and meridional velocity components [9]

Of the mean flow at the impeller outlet, which then has a large axial component of velocity. This naming convention is mainly relevant to the impeller and not to the entire machine, as turning the meridional flow downstream of the rotor to the axial direction does not change the type of the machine.

The term meridional direction is often used. This refers to the mean direction of the flow in a meridional plane through the axis of the rotor and can be axial, radial or something in between. This formulation has the advantage that it allows the same equations to be used for the analysis of axial and radial machines; see the notation in Figure 5. The key significance of the distinction between axial and radial flow arises owing to the centrifugal effect whereby an object travelling in a circle behaves as if it is experiencing an outward force. In an axial machine with swirling flow, this causes the static pressure to rise towards the casing to counteract the swirling motion of the fluid such that the pressure at the casing is higher than at the hub. This radial pressure gradient causes a natural pressure rise on a swirling fluid particle whenever its radius increases within a rotating blade row, and this pressure gradient accounts for 75% of the static pressure rise in centrifugal compressor impellers. This is sometimes considered to be a free pressure rise as it does not require flow deceleration and does not, in itself, result in any flow separations. The centrifugal effect makes centrifugal stages somewhat easier to design than axial stages for a given pressure rise. For this reason, the first effective gas turbine engines all made use of radial compressors.

As shown in Figure 6, compressor rotors increase the absolute velocity across the rotor blade rows by adding swirl to the circumferential flow, and they are equipped with a downstream diffuser or row of stator vanes to convert the rotor outlet kinetic energy into a useful pressure rise. Compressor rotors turn the flow from the meridional direction towards the circumferential

direction in the direction of rotation. In contrast, turbines are equipped with an upstream stator vane or a casing to provide swirl in the direction of rotation, and this leads to high inlet kinetic energy, which is then extracted by the rotor. The turbine rotor turns the absolute flow velocities from the circumferential direction against the direction of rotation back towards the meridional direction.

5-Degree of Reaction

The degree of reaction for a turbomachinery stage describes the relative pressure rise (or fall) in the rotor compared to that of the stage. This is often discussed in the context of steam turbines where reaction turbines and impulse designs with no reaction can be found. In the history of steam turbines, both types were invented independently, the reaction turbine by Sir Charles Parsons (1854–1931) and the impulse turbine by Gustaf de Laval (1845–1913). The reaction turbine, as the name implies, is turned by reactive force rather than by a direct push or impulse. An impulse turbine has fixed nozzles (stator blades) that orient the fluid flow into high speed jets. These jets contain significant kinetic energy, and the rotor blades, shaped symmetrically like buckets, convert this into shaft rotation as the jet changes direction. A pressure drop occurs in the nozzle, but the pressure is the same when the flow enters and leaves the rotor blade, and this gives rise to an impulse machine with zero degree of reaction. In a reaction turbine, the rotor makes use of the reaction force produced as the fluid accelerates through the rotor blades. The fluid is directed on to the rotor by the fixed vanes of the stator. It leaves the stator as a stream that fills the entire circumference of the rotor. In a reaction machine, the pressure change occurs across both the stator and the rotor. Centrifugal compressors with no inlet swirl are reaction machines and generally have a degree of reaction close to 0.6 indicating that about 60% of the overall static pressure rise of the stage takes place in the rotor

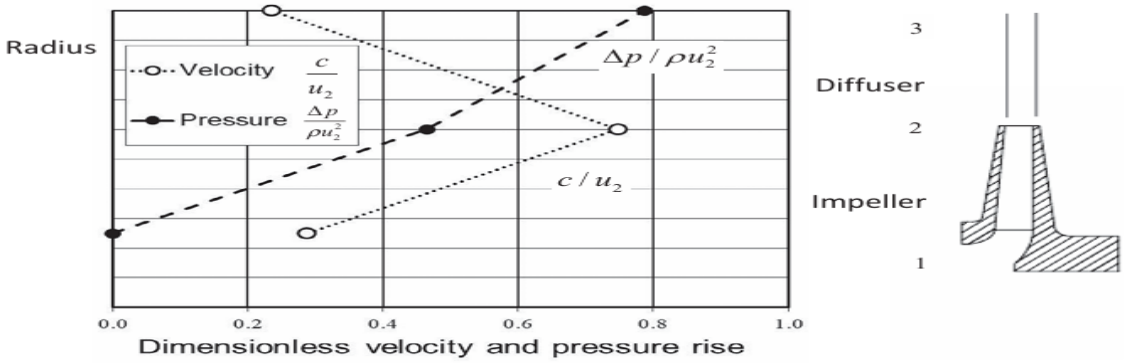

Figure 1-6 Dimensionless absolute gas velocity and pressure rise in a 2D compressor stage [9]

6- Boundary of the Flow Field

Turbomachines can also be classified with respect to configurations with and without a casing. In machines without a casing, such as windmills, wind turbines, propellers and some axial fans, where no walls exist to support a pressure difference against the ambient pressure, it is essentially the kinetic part of the change in the fluid energy which effects the energy transfer with no change in static pressure. [9]

2.COMRESSOR

A compressor is a device that pressurizes a working fluid. One of the basic aims of using a compressor is to compress the fluid and deliver it at a pressure higher than its original pressure. Compression is required for a variety of purposes, some of which are listed below:

- To provide air for combustion
- To transport process fluid through pipelines
- To provide compressed air for driving pneumatic tools
- To circulate process fluid through a certain process

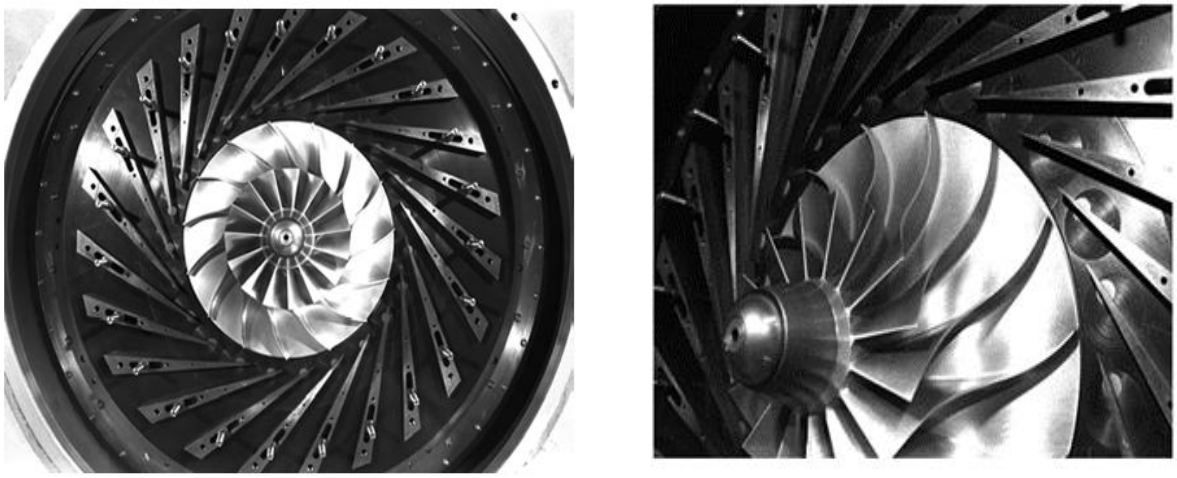

Figure 1.7 Centrifugal compressor stage - front wall removed [3]

2.1COMPRESSOR SELECTIONS

Centrifugal Axial Mixed Flow It is not always obvious what type of compressor is needed for an application. Of the many types of compressors mostly used in the process industry, some of the more significant are the centrifugal, axial, rotary, and the reciprocating compressors. They fall into three categories, as shown in Figure 7. For very high flows and low-pressure ratios, an axial-flow compressor is best. Axial-flow compressors usually have a higher efficiency, as seen in Figure 8, but a smaller operating region than a centrifugal machine. Centrifugal compressors operate most efficiently at medium flow rates and high-pressure ratios. Rotary and reciprocating compressors (positive-displacement machines) are best used for low flow rates and high-pressure ratios. The positive displacement compressors, more commonly known as the reciprocating compressor, were the most widely used compressors in the process and pipeline industries up to and through the 1960s.

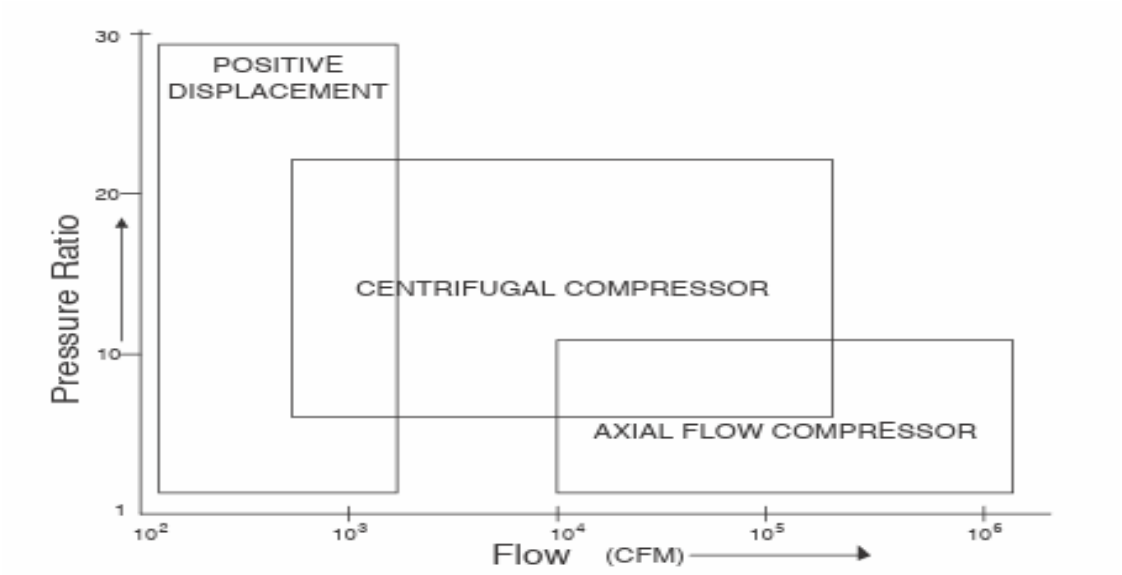

Figure 1.8 Performance characteristics of different types of compressors [10]

In the 1960s, the centrifugal flow compressors became popular because their efficiency was comparable to that of the reciprocating compressor, and because of its much lower maintenance costs. Today the centrifugal compressor is the main compressor in the process and pipeline industries. Due to its compact size and its comparable light weight, the centrifugal compressor is used extensively in the offshore industry. The centrifugal and axial flow compressors fall into the category known as the turbomachinery group of machines. The turbomachine group of machines mostly consists of high speed rotating machines, with steady flow characteristics.

Centrifugal compressors are an integral part of the chemical process industries. They are used extensively because of their smooth operation, large tolerance-to-process fluctuations, and higher reliability than other types of compressors. The centrifugal compressor may be known as a fan, blower, booster, or exhauster. Broadly speaking, fans are low-pressure compressors and blowers are medium-pressure compressors. Boosters and exhausters are named for their application. Before giving an in-depth discussion about centrifugal compressors, let us look at different types of compressors and their applications.

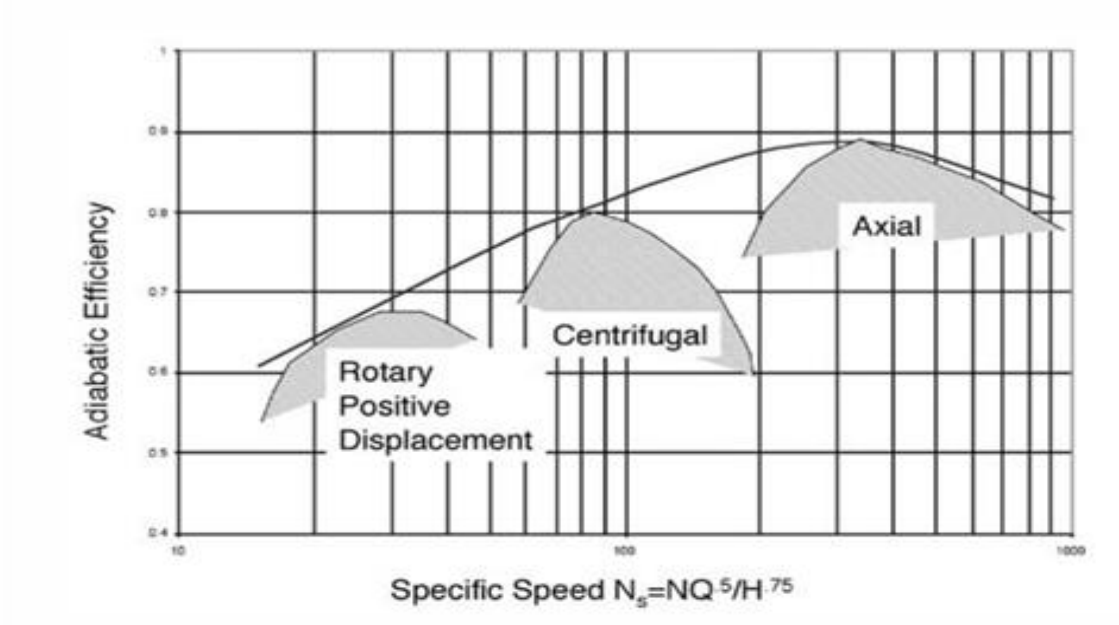

Figure 1.9 Variation of adiabatic efficiency with specific speed for three types of compressors [10]

In turbomachinery the centrifugal flow and axial flow compressors, which are continuous flow compressors, are the ones used for com pressing the air. Positive displacement compressors such as the, reciprocating, gear type, or lobe type to name just a few, are widely used in the industry for many applications. We are examining the centrifugal compressor in its many applications from the large lower pressure process compressor to the high-pressure centrifugal compressors used in small gas turbine applications. The characteristics of these compressors are given in Table 1. The pressure ratio of the axial and centrifugal compressors has been classified into three groups: industrial, aerospace, and research. The industrial pressure ratio is low for the reasons that the operating range needs to be large. The operating range is defined as the range between the surge point and the choke point. Figure 9 shows the operating characteristics of a compressor. The surge point is the point when the flow is reversed in the compressor. The choke point is the point when the flow has reached a Mach=1.0, the point

where no more flow can get through the unit, a “stone wall.” When surge occurs, the flow is reversed and so are all the forces acting on the compressor, especially the thrust forces, which can lead to total destruction of the compressor. Thus, surge is a region that must be avoided. Choke conditions cause a large drop in efficiency but do not lead to destruction of the unit. [10]

Table 1.1 Compressor characteristics. It is important to note that the operating range is narrowed with the increase in pressure ratio and the number of stages [10]

e	Pressure ratio			Efficiency	Operating range
	Industrial	Aerospace	Research		
Positive displacement	Up to 30	-	-	75% - 82%	-
Centrifugal	1.2 – 1.9	2.0 – 7.0	13	75% - 87%	Large 25%
Axial	1.05 – 1.3	1.1 – 1.45	2.1	80% - 91%	Narrow 3% - 10%

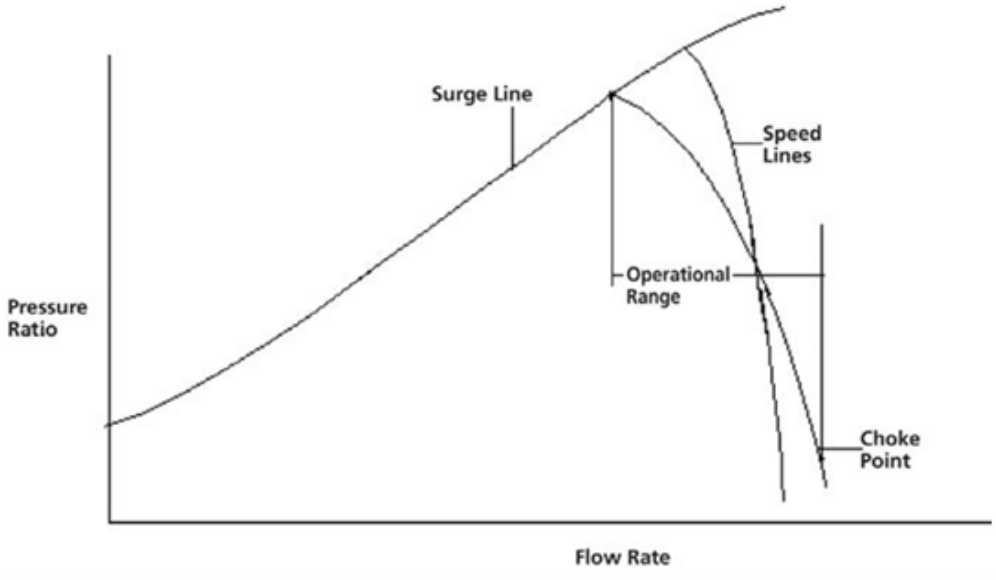

Figure 1.10 Operating characteristics of a compressor [10]

2.2The mechanical components of a centrifugal compressor

The mechanical components of a centrifugal compressor include an impeller (rotor), a stator (diffuser), a surrounding body (or casing), and an outlet collector. In certain aircraft engines, multiple centrifugal compressors can be arranged in series (one after the other) to enhance the overall compression ratio.

1-The inlet part of a compressor:

The inlet section of a compressor serves to efficiently direct the flow towards the rotor with minimal losses. Typically, this section is preceded by one or more elbows, depending on the motor installation and air filter configuration. However, these elbows may negatively impact the compressor's efficiency.

2-The rotor (impeller):

The impeller is the fundamental element of the compressor, as it ensures the exchange of work, being the only moving part of the stage.

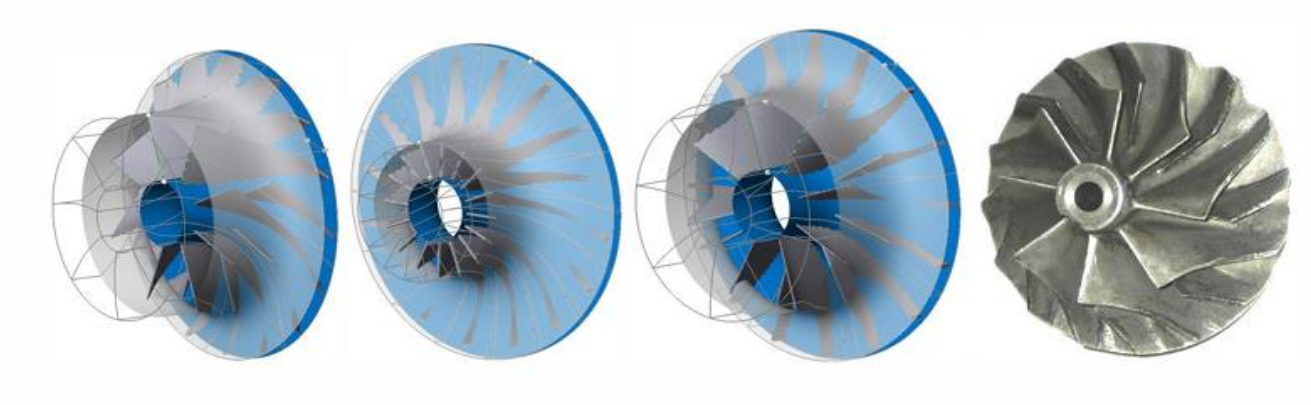

Figure 1.11 Different forms of the centrifugal compressor impellers

Figure (11) illustrates various geometric configurations of centrifugal compressor impellers, showcasing differences in blade count, blade height, and outlet backsweep angle. The intricate nature of these three-dimensional geometries necessitates the use of reference surfaces to facilitate flow analysis. Meridian surfaces are derived from projections onto the plane generating the impeller volume, while blade-to-blade surfaces typically conform to the mean plane and include orthogonal sections that approximate quasi-planes.

3-The diffuser:

The diffuser serves a critical role at the outlet of the rotor. As the flow exits the rotor, its static pressure increases, yet a portion of the total pressure delivered by the impeller remains as

kinetic energy. Consequently, the diffuser functions to decelerate the high-velocity air with minimal losses, resulting in an increase in static pressure. This is crucial because losses in downstream ducts are greatly influenced by the Mach number of the flow. Additionally, the deceleration process enables the conversion of some kinetic energy into static pressure energy.

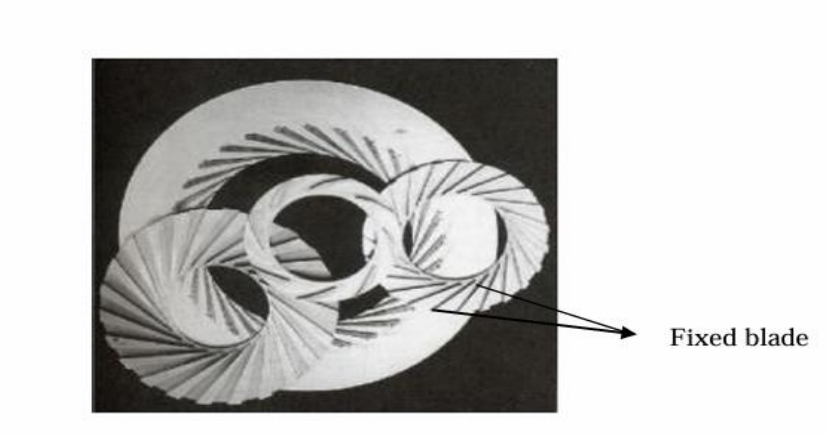

Figure 1.12 Different centrifugal compressor diffusers, Japkse and Baines (1997)

4-The volute:

The volute plays a crucial role in collecting and further decelerating the air before it reaches the compressor outlet, minimizing loss and ideally converting some kinetic energy into static pressure. Among its key geometrical characteristics are: (1) the presence of a nozzle, which significantly impacts compressor flow, and (2) the semicircular shape of the volute section, along with its azimuthal surface evolution. Despite its importance, the volute is often overlooked in centrifugal compressor design and research, with a significantly lower number of publications compared to other radial machine components (see Figure 13).

Figure 1.13 centrifugal compressor

When the impeller initiates rotation, it generates a flow at the outlet, which is then either collected by the volute (see Figure 14.b) or directed along the axis of rotation by a system, as seen in turbojets (see Figure 14.a).

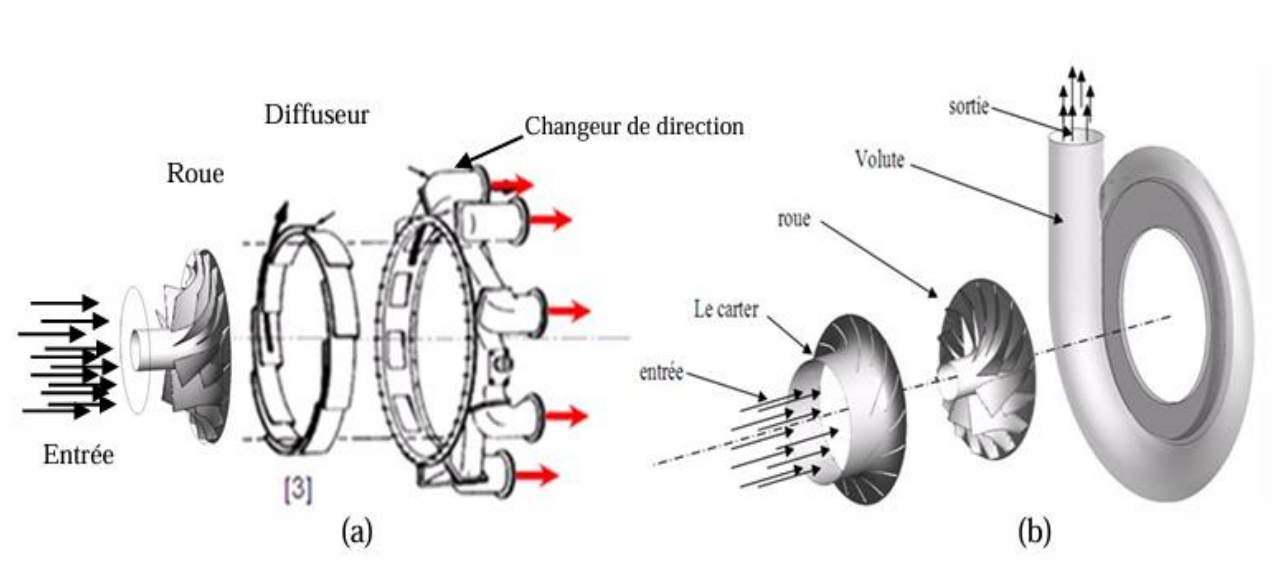

Figure 1.14 The centrifugal compressor in separate elements

2.3CENTRIFUGAL FLOW COMPRESSORS

Centrifugal compressors are an integral part of the petrochemical industry, finding extensive use because of their smooth operation, large tolerance of process fluctuations, and their higher reliability compared to other types of compressors. They are also used in small gas turbines. The centrifugal compressors range in size from pressure ratios of 1.3:1 per stage in the process industries, to 3-7:1 per stage in small gas turbines, and as high as 13:1 on experimental models. This means that the compressor pressure ratio must be between this is considered a highly loaded compressor.

With pressure ratios that exceed 5:1, flows entering the diffuser from the impeller are supersonic in their mach number (M>1.0). This requires special design of the diffuser. The centrifugal compressor has a limited stable operating range. The capacity varies from 45% to 90% of rated capacity. This may affect the economics of operating at partial load. The centrifugal type compressor should be selected for the worst possible conditions, but at the same time, meet other design requirements.

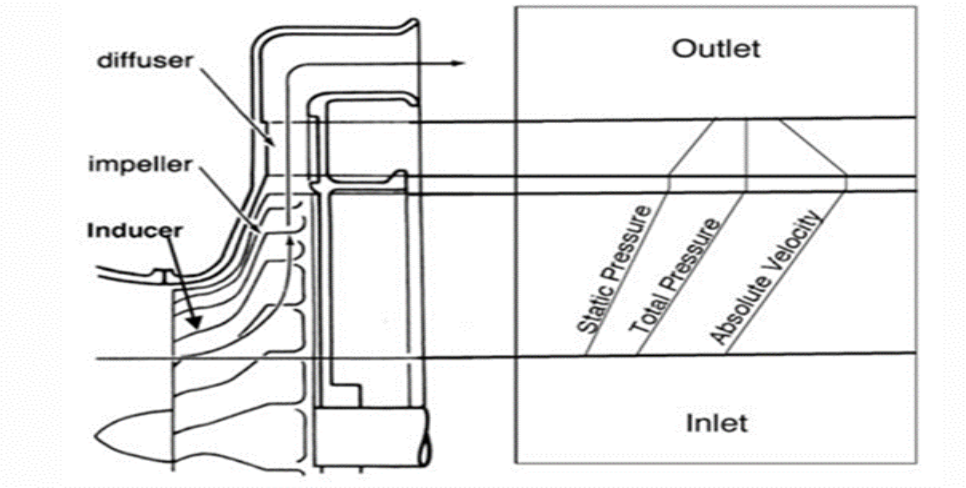

Figure 1.15 Aerodynamic and thermodynamic properties in a centrifugal compressor stage [10]

The operating speed of the centrifugal compressor is higher than that for other compressors. For aircraft and space applications, the rpm can range from 50,000 to 100,000. Most commercial units run below 20,000 rpm. With the trend toward increasing the rpm, problems due to bearing lubrication, vibration, and balancing are becoming more significant at higher speeds. Centrifugal compressors are well suited for direct connection to gas or steam turbine drives which have variable-speed control. Due to absence of inertia forces, centrifugal compressors require smaller and less expensive foundations. These machines have a high availability factor, frequently operate for 2 to 3 years without shutdown, and require less maintenance than the reciprocating type. In a typical centrifugal compressor, the fluid is forced through the impeller by rapidly rotating impeller blades. The velocity of the fluid is converted to pressure, partially in the impeller and partially in the stationary diffusers. Most of the velocity leaving the impeller is converted into pressure energy in the diffuser as shown in Figure 15. It is normal practice to design the compressor so that half the pressure rise takes place in the impeller and the other half in the diffuser. The diffuser consists essentially of vanes, which are tangential to the impeller. These vane passages diverge to convert the velocity head into pressure energy. The inner edge of the vanes is in line with the direction of the resultant airflow from the impeller, as shown in Figure 16. In the centrifugal or mixed-flow compressor, the air enters the compressor in an axial direction and exits in a radial direction into a diffuser. This combination of rotor (or impeller) and diffuser comprises a single stage. The air initially enters a centrifugal compressor at the inducer, as shown in Figure 15. The inducer, usually an integral

part of the impeller, is very much like an axial-flow compressor rotor. Many earlier designs kept the inducer separate. The air then goes through a 90º turn and exits into a diffuser, which usually consists of a vaneless space followed by a vaned diffuser. This is especially true if the compressor exit is supersonic, as is the case with high-pressure ratio compressors. The vaneless space is used to reduce the velocity leaving the rotor to a value lower than Mach number =1 (M<1). From the exit of the diffuser, the air enters a scroll or collector. The centrifugal compressor is slightly less efficient than the axial-flow compressor, but it has higher stability. A higher stability means that its operating range is greater (surge-to-choke margin).

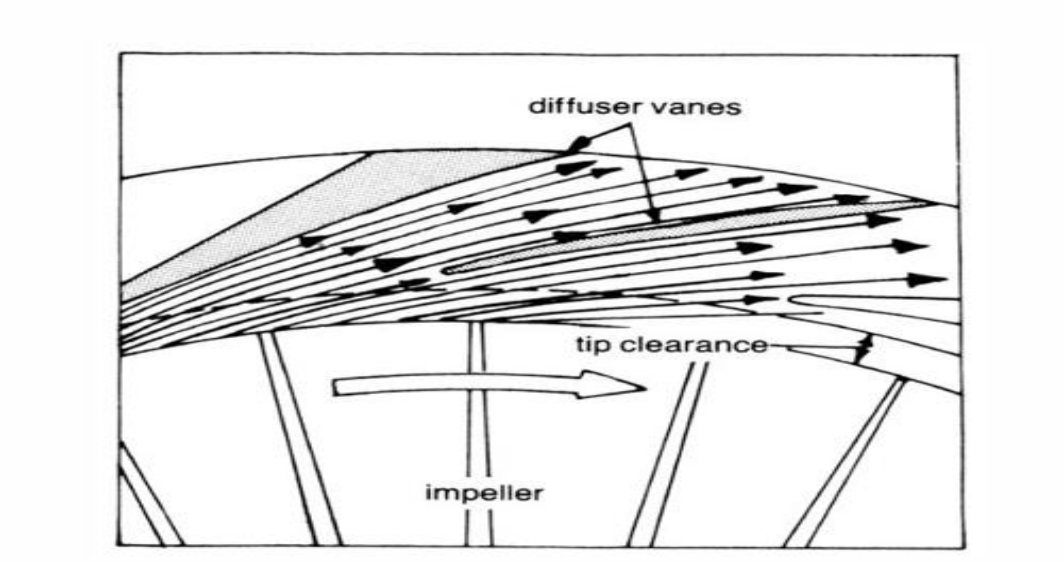

Figure 1.16 Flow in a vaned diffuser [10]

The fluid comes into the compressor through an intake duct and can be given a prewhirl by the IGVs. The inlet guide vanes give circumferential velocity to the fluid at the inducer inlet. IGVs are installed directly in front of the inducer or, where an axial entry is not possible, located radially in an intake duct. The purpose of installing the IGVs is usually to decrease the relative Mach number at the inducer-tip (impeller eye) inlet because the highest relative velocity at the inducer inlet is at the shroud. When the relative velocity is close to or greater than the sonic velocity, a shock wave takes place in the inducer section. A shock wave produces shock loss and chokes the inducer. The flow can enter the impeller axially, with a positive rotation (rotation of the flow in the direction of rotation of the impeller), or with a negative rotation (rotation of the flow in the direction opposite to the rotation of the impeller). It then flows into an inducer with a minimal incidence angle, and its flow direction is changed from axial to radial.

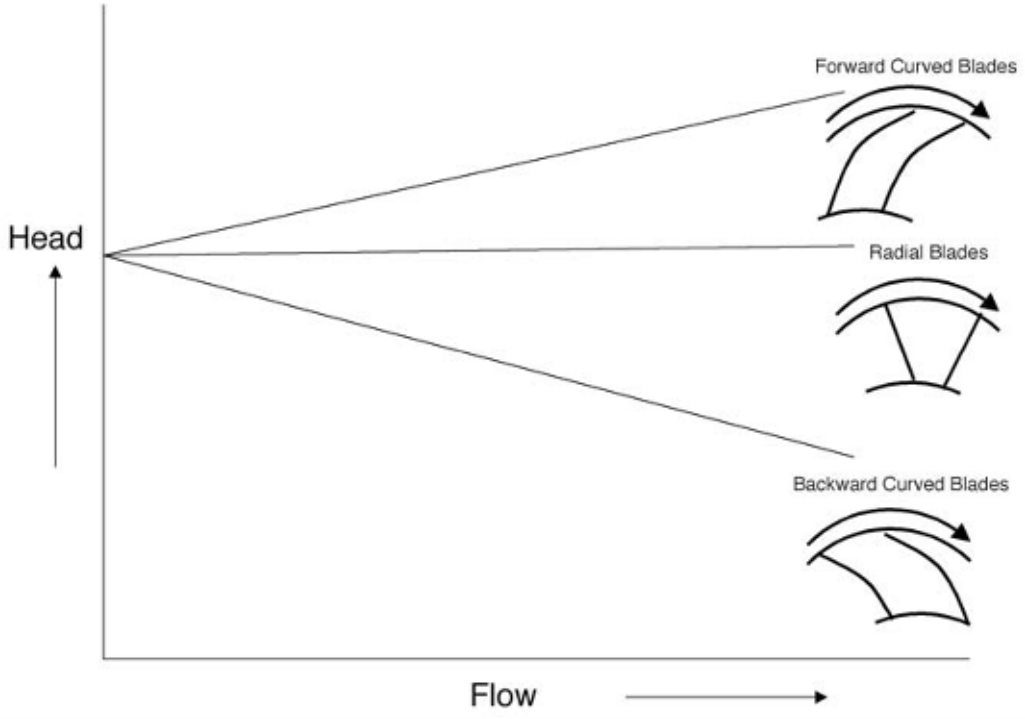

Figure 1.17 Theoretical head characteristics as a function of the flow in a centrifugal impeller [10]

An impeller in a centrifugal compressor imparts energy to a fluid. The impeller consists of two basic components: (1) an inducer such as an axial-flow rotor, and (2) the blades in the radial direction where energy is imparted by centrifugal force. Flow enters the impeller in the axial direction and leaves in the radial direction. The velocity variations from hub to shroud resulting from these changes in flow directions complicate the design procedure for centrifugal compressors. The fluid is given energy at this stage by the rotor as it goes through the impeller while compressing. It is then discharged into a diffuser, where the kinetic energy is converted into static pressure. The flow enters the scroll from which the compressor discharge is taken. There are three impeller vane types, as shown in Figure 16. These are defined according to the exit blade angles. Impellers with exit blade angle $\beta 2 = 90°$ are radial vanes. Impellers with $\beta 2 < 90°$ are backward curved or backward-swept vanes, and for $\beta 2 > 90°$, the vanes are forward curved or forward-swept. They have different characteristics of theoretical head-flow relationship to each other. In Figure 16, the forward-curved blade has the highest theoretical head. In actual practice, the head characteristics of all the impellers are similar to the backward curved impeller. Most applications use backward curved blades since they have the lowest velocity leaving the impeller, thus the diffuser has a much smaller dynamic head to convert. Also, backward curved blades have a much larger operational margin. Table 2 shows the advantages and disadvantages of various impeller designs.

Table 1.2 Impeller designs—advantages and disadvantages [10]

Types of impellers	Advantages	Disadvantages
Radial blades	1-Reasonable compromise between low energy transfer and high absolute outlet velocity 2-No complex bending stress 3-Ease in manufacturing	Surge margin is narrow
Backward curved blades	1- Low outlet kinetic energy 2-Low diffuser inlet mach number 3-Surge margin is widest of the three	1-Low energy transfer 2-Complex bending stress 3-Difficulty in manufacturing
Forward curved blades	High energy transfer	1-High-outlet kinetic energy 2-High diffuser inlet mach number 3-Complex bending stress 4-Difficulty in manufacturing

Diffusers form an important part of a centrifugal compressor, and usually are the most difficult to design. The function of the diffuser in a compressor is the conversion of dynamic or kinetic head generated by the impeller to pressure energy. This conversion is essential for obtaining the required pressure rise of the compressor and also for achieving good efficiency in the gas transmission along the supply pipe. In a gas turbine engine using a centrifugal compressor, the air is required to negotiate through several narrow passages and bends before arriving at the combustion chamber. The bends in these narrow passages will reduce the total energy of airflow; this energy loss can be reduced when an efficient diffuser, and hence low velocities, occur in these passages and bends. A low velocity is also essential in the combustion chamber for achieving high combustion efficiencies. A diffuser is, hence, a component of critical importance when optimum efficiency is a requirement in turbomachinery. Figure I.14 shows the static pressure and velocity changes in a centrifugal compressor and diffuser.

The diffuser assembly may be an integral part of the compressor casing or a separately attached assembly. In each instance, it consists of a number of vanes formed tangentially to the impeller as seen in Figure 15. The vane passages are divergent to convert the kinetic energy into pressure energy, and the inner edges of the vanes are in line with the direction of the resultant airflow from the impeller. The clearance between the impeller and the diffuser is an important factor, as too small a clearance will set up aerodynamic buffeting impulses that could be transferred to the impeller and create unsteady airflow and vibration. [10]

2.4APPLICATION OF CENTRIFUGAL COMPRESSORS

The centrifugal compressor has many applications, requiring it to have many performance characteristics. Centrifugal compressors used in gas turbines are required to have a high-pressure ratio and have a narrow operating range. Centrifugal compressors operating in the process industry have a need for a large operating range and thus operate at a small pressure ratio. Table (3) summarizes some important applications of centrifugal compressors. [10]

Table 1.3 Applications of centrifugal compressors [10]

Industry or application		Service or process	Typical gas handled
Gas turbines	Power	Compression	Air
	Drive	Compression	Air
Iron and steel	Blast furnace	Combustion	Air
		Off gas	Blast furnace gas
	Bessemer converter	Oxidation	Air
	Cupola	Combustion	Air
	Coke oven	Compression	Coke oven gas

Mining and metallurgy	Power Furnaces	For tools and machinery Copper and nickel Purification Pelletizing (iron ore concentration)	Air Air Air
Natural gas	Production Distribution Processing	Re-pressuring oil wells Transmission Natural gasoline separation Refrigeration	Natural gas Natural gas Natural gas Propane and methane
Refrigeration	Chemical Industrial and commercial	Various processes Air conditioning	Butane,propane, ethylene, ammonia Special refrigerants Special refrigerants
Utilities	steam generators City gas	Soot blowing Combustion Cyclone furnaces Manufacturing Distribution	Air Air Air Fuel gas Fuel gas
Miscellaneous	Sewage treatment Industrial power Paper making Material handling Gas engines	Agitation Power for tools and machines Fourdrinier vaccum Conveying Supercharging	Air Air Air and water vapor Air

2.5The pumping and the anti-pumping system

Pumping is this aerodynamic instability of the compressor assembly during operation at low flow when the delivery network has become sufficiently empty in suction, this phenomenon known from the origin of compressors manifests itself when the flow volume of a machine drops below a certain limit, being connected to two different pressure networks. The high pressure capacity of the discharge is emptied into the low pressure capacity of suction by counter-current flow in the compressor.

Compressors are equipped with surge protection devices. To prevent this phenomenon centrifugal compressors are equipped with an automatic system of flow regulation called anti-pumping circuit.

Centrifugal compressor pumping and anti-surge systems have made the subject of numerous writings. One of the important aspects of the anti-pumping system is the design of the compression system, in particular the pipes upstream and downstream of the compressor. Most anti-pumping systems are capable of preventing pumping in normal operating conditions.

2.6Performance of centrifugal compressors

Centrifugal compressor performance is highly data dependent geometry of the impellers and volutes. Unlike volumetric compressors, predicting machine performance from geometric data alone is very difficult. This is why, as with centrifugal pumps, compressors are delivered with performance curves determined by tests with a reference fluid. Basically the performances of a centrifugal compressor of given geometry are described by three curves as a function of the inlet gas volume flow.

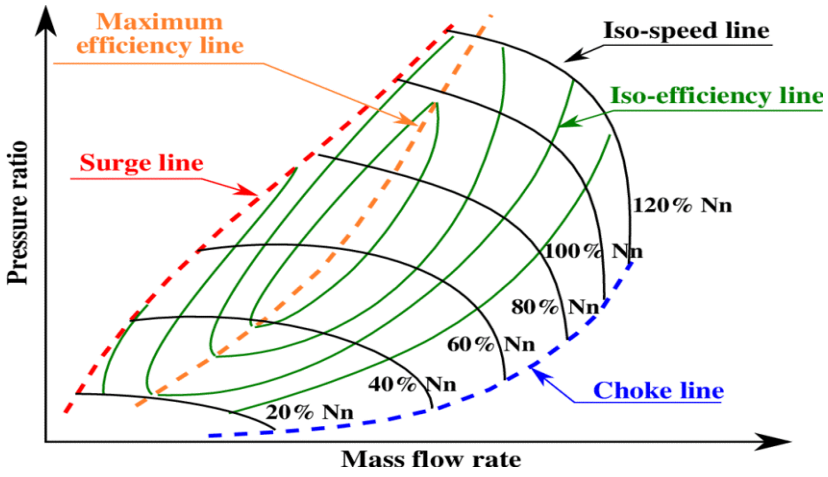

Figure 1.18 Performance curves

CHAPTER 2

MATHEMATICAL MODEL

Introduction

The mathematical model is derived based on the physical phenomena described in the problem statement. Fluid flow equations are constructed primarily from differential equations that illustrate the connections between flow parameters and their corresponding spatial and temporal coordinates. The equations governing fluid flow are essentially derived from differential equations that illustrate the connection between flow variables and their corresponding spatial and temporal coordinates.

1 Governing equations

The fundamental equations governing fluid mechanics consist of the conservation laws for mass, momentum, and energy. The Navier-Stokes equations, which stem from the momentum equations, play a pivotal role in this framework. These equations encapsulate the behavior of fluid flow variables such as density, pressure, and velocity. Given their nonlinear nature, the differential forms of these equations are most suitable for comprehensive analyses, especially when detailed field information is required. During their derivation, the number of equations is carefully matched with the number of unknown dependent fields to establish a solvable system. These equations are rooted in the dynamic nature of fluids, as delineated by the principles of mass conservation, momentum conservation, and energy conservation.

1.1 Mass conservation

Mathematical modeling of the physical principle for the conservation of mass results in an integral or differential equation known as the equation of continuity. This equation demonstrates that mass remains conserved within a flow. It asserts that the total mass of fluid flowing in and out of a control volume per unit time per unit volume must be equal to the rate of change of mass within the control volume. The continuity equation for compressible flow is expressed as follows:

$$-\frac{\partial \rho}{\partial t} = \frac{\partial (\rho u)}{\partial x} + \frac{\partial (\rho v)}{\partial y} + \frac{\partial (\rho w)}{\partial z} \qquad (2.1)$$

u, v, w : Velocity components in the x ,y ,and z directions.

ρ: Fluid density.

The continuity equation is applicable to all fluids, regardless of whether they exhibit compressible or incompressible flow, and regardless of whether they are Newtonian or non-Newtonian fluids. It embodies the law of conservation of mass at every point within a fluid and thus must be upheld at all points within a flow field. In the case of incompressible flow, where density remains constant, the rate of change of density of a fluid particle per unit time will be zero. The continuity equation for incompressible flow can be simplified as:

$$\frac{\partial u}{\partial x}+\frac{\partial v}{\partial y}+\frac{\partial w}{\partial z}=0 \qquad (2.2)$$

1.2 Momentum conservation

The momentum conservation equation is derived from Newton's second law, which is the fundamental principle governing fluid momentum.. The Navier–Stokes equations for 3D viscous compressible flow are presented next:

. x-momentum equation:

$$\underbrace{\left(\frac{\partial \rho u}{\partial t}+u\frac{\partial \rho u}{\partial x}+v\frac{\partial \rho u}{\partial y}+w\frac{\partial \rho u}{\partial z}\right)}_{\text{Inertial terms}} = \underbrace{-\frac{\partial p}{\partial x}}_{\text{Pressure Gradient}} + \underbrace{\mu\left(\frac{\partial^2 u}{\partial x^2}+\frac{\partial^2 u}{\partial y^2}+\frac{\partial^2 u}{\partial z^2}\right)}_{\text{Viscous Terms}} + \underbrace{F_x}_{\text{Body Force Terms}} \qquad (2.3)$$

. y-momentum equation:

$$\left(\frac{\partial \rho v}{\partial t}+u\frac{\partial \rho v}{\partial x}+v\frac{\partial \rho v}{\partial y}+w\frac{\partial \rho v}{\partial z}\right)=-\frac{\partial p}{\partial y}+\mu\left(\frac{\partial^2 v}{\partial x^2}+\frac{\partial^2 v}{\partial y^2}+\frac{\partial^2 v}{\partial z^2}\right)+F_y \quad (2.4)$$

. z-momentum equation:

$$\left(\frac{\partial \rho w}{\partial t}+u\frac{\partial \rho w}{\partial x}+v\frac{\partial \rho w}{\partial y}+w\frac{\partial \rho w}{\partial z}\right)=-\frac{\partial p}{\partial z}+\mu\left(\frac{\partial^2 w}{\partial x^2}+\frac{\partial^2 w}{\partial y^2}+\frac{\partial^2 w}{\partial z^2}\right)+F_z \quad (2.5)$$

p: fluid pressure

μ: the dynamic viscosity of the fluid

The terms on the left-hand side are represented as advective terms and stem from momentum fluctuations. These advective terms are countered by the pressure gradient term (∂p/∂x), followed by viscous forces that continuously act to decelerate the flow. Fx, Fy, and Fz denote the body forces along the x, y, and z coordinates, respectively.

The advective terms quantify the change in velocity of a fluid component as it moves through space. The ∂/∂t term, known as the local derivative, indicates the rate of change of fluid velocity at a fixed point within the flow field. The remaining three terms, given in the inertial terms, are combined and referred to as the convective terms.

1.3 Energy conservation

The fundamental principle utilized in deriving the energy equation is the first law of thermodynamics, which asserts that any increase in energy within a system is equivalent to the heat added to that system plus the work done on it. The conservation of energy equation shares some similarities with the momentum equations and is expressed as follows:

$$C_p\left(\frac{\partial \rho T}{\partial t}+u\frac{\partial \rho T}{\partial x}+v\frac{\partial \rho T}{\partial y}+w\frac{\partial \rho T}{\partial z}\right) = \emptyset+\frac{\partial}{\partial x}\left[k\frac{\partial T}{\partial x}\right]+\frac{\partial}{\partial y}\left[k\frac{\partial T}{\partial y}\right]+\frac{\partial}{\partial z}\left[k\frac{\partial T}{\partial z}\right]+\left(u\frac{\partial p}{\partial x}+v\frac{\partial p}{\partial y}+w\frac{\partial w}{\partial z}\right) \quad (2.6)$$

Where:

$$\emptyset = 2\mu\left[\left(\frac{\partial u}{\partial x}\right)^2+\left(\frac{\partial v}{\partial y}\right)^2+\left(\frac{\partial w}{\partial z}\right)^2+0.5\left(\frac{\partial u}{\partial y}+\frac{\partial v}{\partial x}\right)^2+0.5\left(\frac{\partial v}{\partial z}+\frac{\partial w}{\partial y}\right)+0.5\left(\frac{\partial w}{\partial x}+\frac{\partial w}{\partial y}\right)^2\right] -\frac{2}{3}\mu\left(\frac{\partial u}{\partial x}+\frac{\partial v}{\partial y}+\frac{\partial w}{\partial z}\right)^2 \quad (2.7)$$

T: the temperature of the fluid.

C_p: the specific heat at constant pressure.

K: the thermal conductivity coefficient.

The terms on the left-hand side of Equation (2.6) represent the rate of change of total energy per unit volume within the control volume and the rate of depletion of total energy by convection per unit volume through the control volume. On the right-hand side of the equation, the terms encapsulate the heat generated per unit volume by external sources, followed by the rate of heat lost by conduction per unit volume through the control volume. The next two terms signify the work done on the control volume per unit volume by the surface forces and body forces, respectively.

2.Turbulence modelling

Turbulence stands as a prominent area of focus in contemporary fluid dynamics research, drawing contributions from esteemed physicists over the past century. Notable figures such as

G. I. Taylor, Kolmogorov, Reynolds, Prandtl, von Karman, Heisenberg, Landau, Millikan, and Onsagar have made significant strides in this domain. The systematic exploration of turbulence traces back to Osborne Reynolds in 1883. His pioneering investigation into flow through pipes revealed a critical threshold, wherein the dimensionless Reynolds number ($Re = \rho VD/\mu$) dictates the transition from laminar to turbulent flow. Named in honor of Reynolds by Sommerfeld, this dimensionless parameter emerged as pivotal in discerning the behavior of viscous flows.

As the Reynolds number increases, a transition to turbulent flow occurs, characterized by three-dimensional vorticity fluctuations and a mix of dissipative, diffusive, and random flow behaviors. In turbulent flow, velocity and other flow properties exhibit chaotic and unpredictable variations. This phenomenon arises naturally in fluid systems with high velocity gradients, manifesting as temporal and spatial perturbations in the flow field. Examples abound in nature, from smoke dispersing in the air to ocean waves, condensation on surfaces, planetary atmospheres, and stormy weather. Turbulent flows are commonly encountered in various engineering applications such as turbine operation, engine combustion, compressor dynamics, and within combustion chambers.

Turbulence modeling involves the development and application of models to forecast the impacts of turbulence. Given that turbulent flows are prevalent in engineering scenarios, understanding turbulent flow regimes is not only theoretically significant but also essential in practical terms. Fluid dynamic engineers rely on effective tools capable of addressing a range of turbulence effects to navigate the challenges posed by turbulent flows in engineering applications.

2.1 Direct Numerical Simulation (DNS)

In DNS, the Navier-Stokes equations are directly solved using finely refined meshes capable of resolving all turbulent length scales. These simulations provide both the mean flow and all turbulent velocity fluctuations. While DNS holds promise for simulating complex turbulent flows, the algorithms for solving the 3D continuity and Navier-Stokes equations are well established. However, due to the high computational costs involved, DNS is not commonly used for industrial flow computations.

DNS is anticipated to assume a progressively significant role in turbulence research in the near future. However, DNS methods require extremely fine, fully 3D meshes, powerful computers,

and a substantial amount of CPU time. Given current computational capabilities, DNS results are not yet feasible for highly turbulent flows in engineering applications.

2.2 Large Eddy Simulation (LES)

LES offers an alternative method for achieving more sophisticated turbulent flow simulations. Unlike the RANS system of equations, LES employs a much finer mesh. Its precision falls between RANS and Direct Numerical Simulation (DNS)

. Turbulent flows are characterized by eddies of various length and time scales. The largest eddies are typically comparable in size to the characteristic length of the average flow, while the smallest scales are responsible for turbulence kinetic energy dissipation.

LES analysis involves two primary steps: filtering and subgrid scale (SGS) modeling. Filtering addresses the resolution of large eddies, while the SGS model deals with unresolved small eddies. While LES captures large unsteady turbulent eddies, it models small-scale dissipative turbulent eddies. The underlying theory is that smaller turbulent eddies exhibit statistically parallel and predictable behavior, irrespective of the turbulent flow field's orientation.

One major limitation of LES lies in wall boundary layers, which necessitate high-resolution grids. Even large eddies near the wall transition into smaller eddies and require resolution dependent on Reynolds number.

2.3 Reynolds-Averaged Navier–Stokes Equations "RANS equations"

Turbulent flows are often described by averaging the Navier–Stokes equations over both space and time. In 1895, Reynolds introduced the initial mathematical framework for predicting turbulent flows. This method involves breaking down flow variables into two components: a mean component and a fluctuating component. The conservation equations (Eqs. (2.3)–(2.4)) are subsequently solved for the mean values. Specifically, the velocity components:

$$u_i = \bar{u}_i + \dot{u}_i \quad (2.8)$$

$\bar{u}_i, \dot{u}_i$: the mean and fluctuating velocity components(i =1,2,3).

Likewise, for pressure and other scalar quantities:

$$\emptyset = \overline{\emptyset} + \acute{\emptyset} \quad (2.9)$$

$\emptyset$: a scalar such as pressure, energy, or species concentration.

Mean values are obtained through an averaging process, which can be executed in various manners including time averages, ensemble averages, spatial averages, and mass averages. However, this discussion will focus solely on the time averaging method for flow variables.

Let's consider a variable f, which can be expressed as the sum of its mean quantity $\overline{f}$ and a fluctuating part $\acute{f}$. In this context, f can be represented as:

$$f(\mathrm{x},\mathrm{t}) = \overline{f}(x,t) + \acute{f}(x,t) \qquad (2.10)$$

Where $\overline{f}$ is coined the time average of f:

$$\overline{f}(x,t) = \frac{1}{\Delta t}\int_t^{t+\Delta t} f\,(x,t)dt \qquad (2.11)$$

With:

$$\overline{\acute{f}} = \frac{1}{\Delta t}\int_t^{t+\Delta t} \acute{f}\,dt = 0 \qquad (2.12)$$

In equations (2.11) and (2.12), the time interval Δt is chosen to be consistent with the timescale of turbulent fluctuations for variable f and other variables present in the physical domain. When employing time averaging for compressible flows, the conservation equations can be expressed as follows:

$$\frac{\partial \overline{u_i}}{\partial x_i} = 0 \qquad (2.13)$$

In Equation (2.13), the tensor notation u_i represents a velocity component$(u_i = [u_1 + u_2 + u_3]^{\mathrm{T}})$, and x_i denotes a coordinate direction. The momentum equation for x-momentum can be formulated as:

$$\left(\frac{\partial \rho\overline{u}_i}{\partial t} + \overline{u}_j\frac{\partial \overline{\rho u}_i}{\partial x_j}\right) = -\frac{\partial \overline{p}}{\partial x_{\mathrm{i}}} + \frac{\partial}{\partial x_{\mathrm{j}}}\left(\overline{\tau}_{ij} - \rho\overline{\acute{u}_i\acute{u}_j}\right) \qquad (2.14)$$

The set of equations described here is referred to as the Reynolds-averaged Navier–Stokes (RANS) equations. These equations, governing turbulent flows, bear resemblance to the Navier–Stokes equations (Eqs. (a)–(c)), except for the absence of an additional term.

$$\tau_{ij}^{\mathrm{R}} = -\rho\overline{\acute{u}_i\acute{u}_j} = -\rho\left(\overline{u_i u_j} - \overline{u}_i\overline{u}_j\right) \qquad (2.15)$$

which constitutes the Reynolds Stress Tensor,τ_{ij} , symbolizing the transfer of momentum due to turbulent fluctuations. The laminar viscous stresses are expressed as:

$$\overline{\tau}_{ij} = 2\mu\overline{S}_{ij} = \mu\left(\frac{\partial\overline{u}_i}{\partial x_j} + \frac{\partial\overline{u}_j}{\partial x_j}\right) \qquad (2.16)$$

2.4 Turbulence closure models

To analyze turbulent flows using the Reynolds-Averaged Navier-Stokes (RANS) equations, it is imperative to employ turbulence closure models for predicting Reynolds stresses and scalar transport terms. First-order closures represent the simplest approach to approximate Reynolds stress terms within the RANS equations. For a turbulence model to be viable within a general Computational Fluid Dynamics (CFD) framework, it should possess broad applicability, reasonable accuracy, and simplicity. Among the array of first-order closure models available, the commonly utilized ones in contemporary simulations are delineated below. All three models are adaptable to both structured and unstructured meshes. Firstly, we discuss the well-known k-epsilon two-equation model is introduced. Lastly, the k-omega SST (Shear Stress Transport) two-equation model is elucidated.

- **Two-Equation Model**

Two-equation turbulence models ascertain both a turbulent length scale and a turbulent time scale through the solution of two transport equations.

The k-$\boldsymbol{\varepsilon}$ Model: The k-epsilon or k-ε turbulence model stands as one of the most commonly employed two-equation turbulence models across both industry and academia. It revolves around solving two fundamental equations: the turbulent kinetic energy equation and the turbulent dissipation rate equation. Initially proposed by Launder and Spalding in 1974, it has since served as a cornerstone in turbulent flow calculations in engineering. The standard k-ε model encompasses two distinct equations, one dedicated to k (turbulence kinetic energy) and the other to ε (turbulence dissipation rate), outlined below:

k equation:

$$\frac{\partial}{\partial t}(\rho k) + \frac{\partial}{\partial x_i}(\rho k u_i) = \frac{\partial}{\partial x_j}\left[\left(\mu + \frac{\mu_t}{\sigma_k}\right)\frac{\partial k}{\partial x_j}\right] + G_k + G_b - \rho\varepsilon - Y_M + S_k \qquad (2.17)$$

ε equation:

$$\frac{\partial}{\partial t}(\rho\varepsilon) + \frac{\partial}{\partial x_i}(\rho\varepsilon u_i) = \frac{\partial}{\partial x_j}\left[\left(\mu + \frac{\mu_t}{\sigma_\varepsilon}\right)\frac{\partial\varepsilon}{\partial x_j}\right] + C_{1\varepsilon}\frac{\varepsilon}{k}(G_k + C_{3\varepsilon}G_b) - C_{2\varepsilon}\rho\frac{\varepsilon^2}{k} + S_\varepsilon \qquad (2.18)$$

These equations can be expressed as:

Rate of change of k orε +Transport of k or ε by convection = Transport of k orε by diffusion + Rate of production of k or ε–Rate of destruction of k or ε + user − defined source terms

In this context, G_k represents the generation rate of turbulent kinetic energy arising from mean velocity gradients, while G_b signifies the generation rate of turbulence kinetic energy due to buoyancy effects. Y_M denotes the impact of fluctuating dilatation in compressible turbulence on the overall dissipation rate. Constants $C_{1\varepsilon}$, $C_{2\varepsilon}$, and $C_{3\varepsilon}$ are model parameters, whereas S_k and S_ε represent user-defined source terms. Additionally, σ_k and σ_ε denote turbulent Prandtl numbers for k and ε, respectively.

The turbulent viscosity term (μ_t) is calculated as follows:

$$\mu_t = \rho C_\mu \frac{k^2}{\varepsilon} \qquad (2.19)$$

where the model constants have the values: C_μ= 0.09, $C_{1\varepsilon}$= 1.44, $C_{2\varepsilon}$= 1.92, σ_k= 1.0, and σ_ε=1.3.

The k-$\boldsymbol{\omega}$ Model: In the k-ε model, the kinematic eddy viscosity μt is defined as the product of the velocity scale $\mu = \sqrt{k}$ and the length scale $1 = k^{3/2}/\varepsilon$. It's worth noting that the rate of turbulence kinetic energy dissipation (ε) isn't the sole potential length scale defining a variable. In reality, numerous other two-equation models have been suggested, each with its own distinct characteristics and length scale definitions.

A notable alternative to consider is the k-ω model, introduced by Wilcox in 1988. This model employs the turbulence frequency omega $\omega = \varepsilon/k$ (dimension s-1) as its second variable. Consequently, the length scale is defined as $l = \sqrt{k}/\omega$. The turbulence kinetic energy and the specific dissipation rate are derived from the following transport equations:

k equation:

$$\frac{\partial}{\partial t}(\rho k) + \frac{\partial}{\partial x_i}(\rho k u_i) = \frac{\partial}{\partial x_j}\left[\Gamma_k \frac{\partial k}{\partial x_j}\right] + G_k - Y_k + S_k \qquad (2.20)$$

ω equation:

$$\frac{\partial}{\partial t}(\rho \omega) + \frac{\partial}{\partial x_i}(\rho \omega u_i) = \frac{\partial}{\partial x_j}[\Gamma_\omega \frac{\partial \omega}{\partial x_j}] + G_\omega - Y_\omega + S_\omega \qquad (2.21)$$

the equations represent:

Rate of change of k or ω +Transport of k or ω by convection = Transport of k or ω by turbulent diffusion + Rate of production of k or ω −Rate of dissipation of k or ω + user − defined source terms.

In this context, G_ω represents the generation rate of ω, while Y_k and $Y_\omega$indicate the dissipation of k and ω attributed to turbulence. Γ_k and $\Gamma_\omega$represent the effective diffusivity of k and ω, respectively, and S_k and $S_\omega$are user-defined source terms.

The effective diffusivities are defined as follows:

$$\Gamma_k = \mu + \frac{\mu_t}{\sigma_k} \text{ and : } \Gamma_\omega = \mu + \frac{\mu_t}{\sigma_\omega} \qquad (2.22)$$

In this case, σ_k and σ_ω represent the turbulent Prandtl numbers for k and ω, respectively. Additionally, the turbulent viscosity μ_t can be computed by combining k and ω as $\mu_t = \alpha^* \frac{\rho k}{\omega}$, where α^*denotes the damping coefficient of turbulent viscosity, which initiates a modification at low Reynolds numbers.

Shear Stress Transport (SST) Model**:** Menter (1994) introduced the SST model to effectively combine the free-stream objectivity of the k-ε model in the far field with the robust and accurate prediction capabilities of the k-ω model in the near-wall region. In the SST model, the k equation remains the same as in Wilcox's original k-ω model, while the ε equation is transformed into a ω equation by substituting ε = kω. Additionally, the SST model incorporates a damped cross-diffusion derivative term in the ω equation. Consequently, the transport equations for the k-ω SST model can be expressed as:

k equation:

$$\frac{\partial}{\partial t}(\rho k) + \frac{\partial}{\partial x_i}(\rho k u_i) = \frac{\partial}{\partial x_j}\left[\Gamma_k \frac{\partial k}{\partial x_j}\right] + \widetilde{G_k} - Y_k + S_k \qquad (2.23)$$

ω equation:

$$\frac{\partial}{\partial t}(\rho \omega) + \frac{\partial}{\partial x_i}(\rho \omega u_i) = \frac{\partial}{\partial x_j}[\Gamma_\omega \frac{\partial \omega}{\partial x_j}] + G_\omega - Y_\omega + D_w + S_\omega \qquad (2.24)$$

$\widetilde{G_k}$: the generation rate of turbulence kinetic energy due to mean velocity gradients, calculated from G_k,and $D_w$represents the cross-diffusion term.

The turbulent viscosity μ_t is defined in terms of k and ω as follows:

$$\mu_t = \frac{\rho k}{\omega} \frac{1}{max\left[\frac{1}{\alpha^*}, \frac{SF_2}{a_1 \omega}\right]} \qquad (2.25)$$

CHAPTER 3

Simulation steps

Introduction

Nowadays, with the advancement of digital simulation tools and the increased power of computing resources, numerous software codes are available for addressing complex three-dimensional problems, especially in the fields of fluid mechanics and turbomachinery. Among the most well-known computational codes are ANSYS CFX, GAMBIT, FLUENT, STAR-CD, and others. In this work, ANSYS-CFX is used to model the compressible flow in a centrifugal compressor.

1. Numerical discretization methods

Numerical discretization methods involve transforming the resolution of the system of differential equations in the study domain, with appropriate boundary conditions, into a system of algebraic equations. The solution of this system provides the potential energy.

1.1 Finite element method

The finite element method is a numerical procedure for analysing structures and continua. Usually the problem addressed is too complicated to be solved satisfactorily by classical analytical methods. The problem may concern stress analysis, heat conduction, or any of several other areas. The finite element procedure produces many simultaneous algebraic equations, which are generated and solved on a digital computer. Finite element calculations are performed on personal computers, mainframes, and all sizes in between. Results are rarely exact. However, errors are decreased by processing more equations, and results accurate enough for engineering purposes are obtainable at reasonable cost.

The finite element method originated as a method of stress analysis. Today finite elements are also used to analyse problems of heat transfer, fluid flow, lubrication, electric and magnetic fields, and many others. Problems that previously were utterly intractable are now solved routinely. Finite elements procedures are used in the design of buildings, electric motors, heat engines, ships, airframes, and spacecraft. Manufacturing companies and large design offices typically have one or more large finite element programs in –house. Smaller companies usually have acces to a large program though a commercial computing center or use a smaller program on a personal computer. [12]

This method involves transforming differential equations into integral forms based on the concept of minimizing a quantity (such as energy), leading to an exact solution. In other words, it involves finding a global function that represents the mathematical model in the studied

domain. The fundamental principle of the finite element method (FEM) consists of the following steps:

- Define a partition of the study domain, i.e., subdivide the study domain into elementary regions (finite elements).
- Represent the unknown function on each of these elements by a polynomial approximation.
- Construct the integral forms.
- Minimize the integral.
- Organize the calculations in a matrix form.
- Solve the algebraic system.

The FEM is a very powerful method for solving partial differential equations, especially in complex geometries. However, its implementation is quite complicated and requires a significant amount of memory.

1.2Finite difference method

The method involves replacing partial derivatives with divided differences or combinations of point values of the function at a finite number of discrete points or mesh nodes.

Advantages: Great simplicity in writing and low computational cost.

Disadvantages: Limitation in the geometry of the calculation domains (simple, non-complex), difficulties in accounting for boundary conditions, and generally, the absence of error bound results.

The finite difference method presents a technique for solving partial differential equations by approximating derivatives with finite differences. This method involves subdividing the study domain into a determined number of nodes and representing the sought function at each node of the domain by a truncated Taylor series expansion. Thus, the differential equation is transformed into an algebraic equation for each node. Solving the system of algebraic equations provides the distribution of the studied function within the study domain. The finite difference method does not account for the transition conditions from one physical medium to another and nonlinearities, which require specific handling. Moreover, it is poorly suited to objects with complex geometries due to the rigidity of the mesh.

1.3Finite volume method

The finite volume method is a special version of the weighted residual method where the projection function equals one. This method involves subdividing the study domain into

elementary volumes in such a way that each volume surrounds a main node P. Each volume is bounded by: two interfaces in the one-dimensional case denoted (e,w), four interfaces in the two-dimensional case (e,w,s,n), and six interfaces in the three-dimensional case (e,w,s,n,t,b). Each main node P is limited by neighboring nodes (E,W) in the one-dimensional case, (E,W,S,N) in the two-dimensional case, and (E,W,S,N,T,B) in the three-dimensional case. The differential equation is integrated within each finite elementary volume. To calculate the integral within this elementary volume, the unknown is represented using an approximation function (linear, parabolic, exponential, power, etc.) between two consecutive nodes. Then, the integral form is discretized within the study domain. The result of discretization yields an algebraic equation composed of the nodal values. [12]

2. Software Presentation CFX-23

CFX is a generic name for a set of CFD (Computational Fluid Dynamics) tools developed by ATA Technologies. This software offers numerous multiphase models and numerical schemes that allow users to model a wide range of fluid mechanics problems. Like many software programs, CFX-23 includes various tools and modules for:

- Geometry creation
- Mesh generation (structured or unstructured)
- Calculation

The study of the different parts of the turbomachine using CFX-23 is conducted step by step. In each step, the software utilizes specific tools or components. This process is illustrated in the following flowchart:

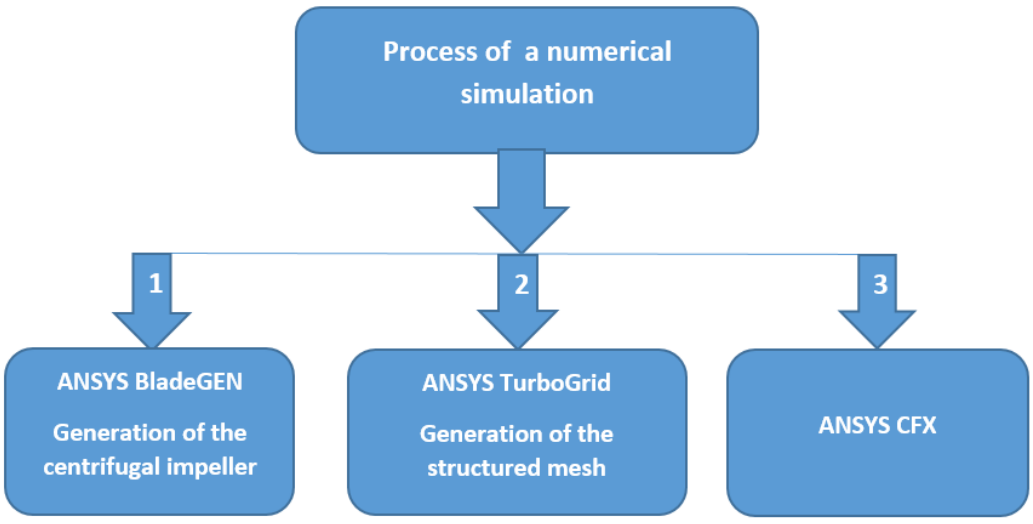

Figure 3.1 The different modules in CFX-23

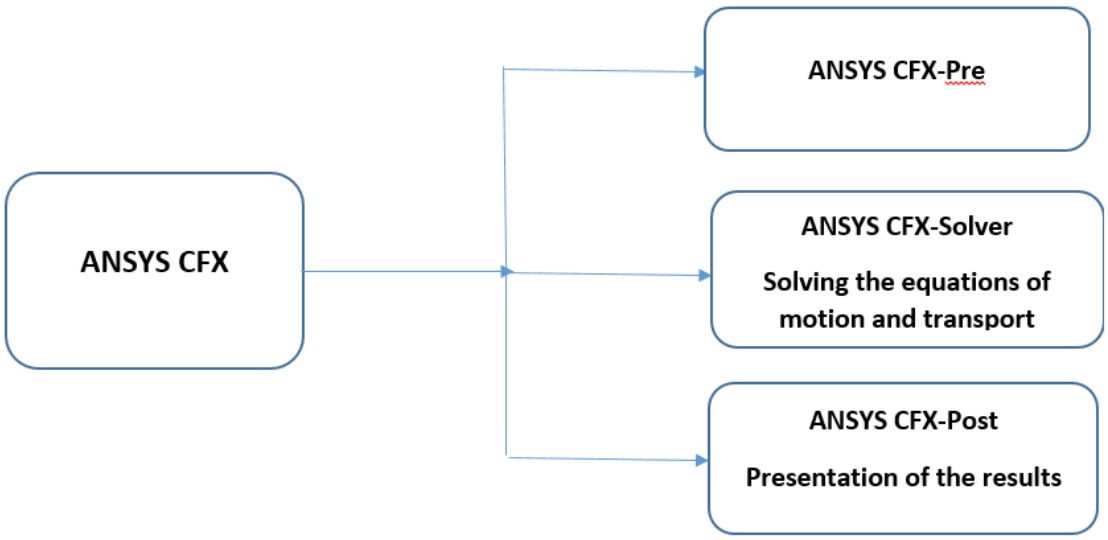

Figure 3.2 the different modules in ANSYS CFX

- **Simulation Assumptions**

The assumptions for studying the compressible flow in a stage of a centrifugal compressor are:

- The flow regime is steady;
- The fluid is compressible;
- The flow is three-dimensional;
- The thermodynamic properties of the fluid are assumed to be those of an ideal gas;
- The heat source term is zero;
- External body forces are negligible.

- **CENTRIFUGAL COMPRESSOR STAGE**

The centrifugal compressor stage used for the assessment of turbulence model predictions was the exemplar open CFD test case, entitled 'Radiver'. The compressor stage consists of an unshrouded impeller with 15 backswept blades and 23-vane wedge type diffuser. Numerical simulations were carried at 80% design speed due to the increased amount of experiment data available at this speed. Details of the impeller and diffuser geometry are shown in Table1.

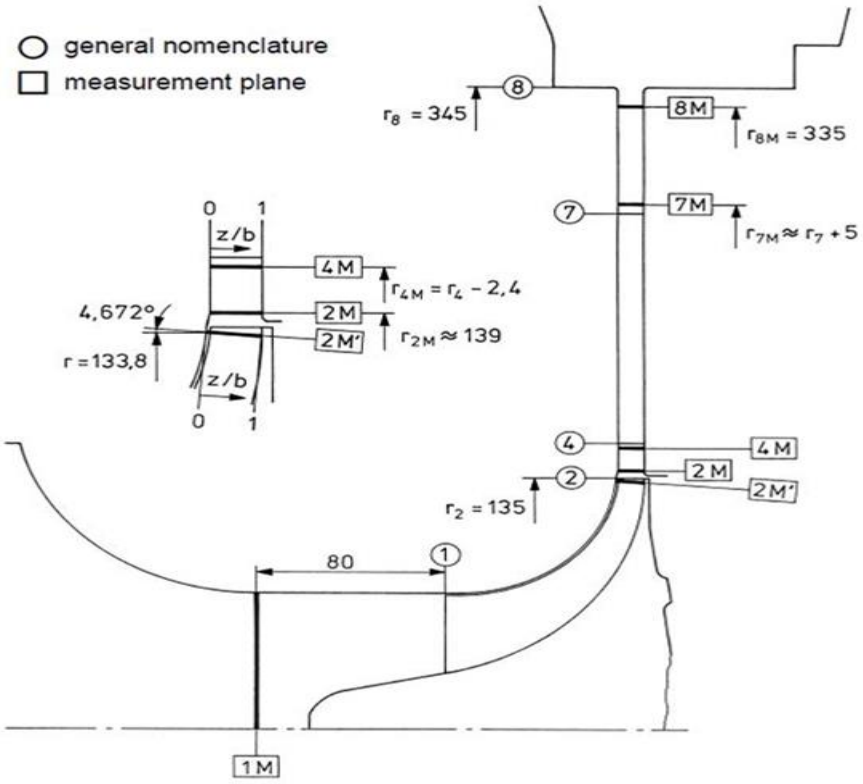

Figure 3-1 Measurement plans of the experimental tests – meridian section [3]

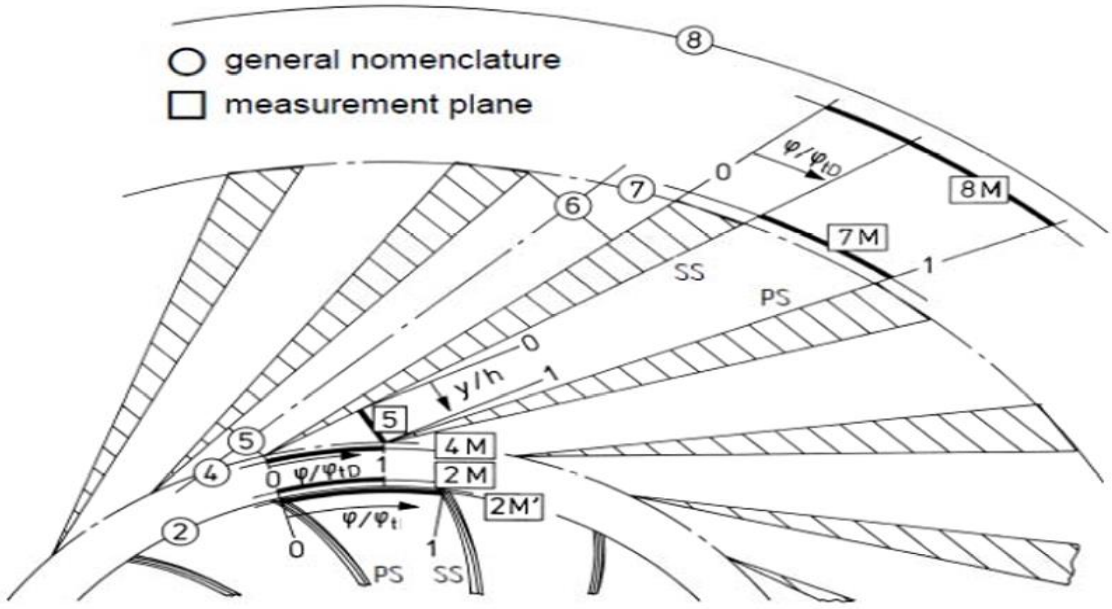

Figure 3-2 Measurement plans of the experimental tests – circumferential view [3]

Table 3.1 compressor details for R4/R2=1.14 at 80% speed [3]

Shaft speed (80%)	28541 rpm
Tip radius	135 mm
Number of impeller blades	15
Blade backsweep angle at impeller exit	38°
Impeller leading edge tip clearance	0.70 mm
Impeller trailing edge tip clearance	0.48 mm
Number of diffuser vanes	23
Diffuser vane angle	16.50°
Diffuser channel height	11.10 mm
Diffuser leading edge radius	140.40 mm
Plane 2M radius	138.10 mm
Plane 8M radius	335 mm

2.1 ANASYS CFX –BladeGen -23

BladeGen is part of the ANSYS suite of software, which is widely used in engineering for simulation and design optimization. By utilizing BladeGen, engineers can efficiently design and analyze the aerodynamic and mechanical aspects of these components, ensuring optimal performance and efficiency. Additionally, the tool allows for the integration with other ANSYS modules for comprehensive simulations, including fluid dynamics (CFD) and structural analysis. [13]

The first step in solving this problem is to define the geometry of the impeller and diffuser of the Centrifugal Compressor using CFX-BladeGen. This is a three-dimensional tool, quick to use for creating geometry, and specialized in the field of turbomachinery. This includes devices such as centrifugal and axial compressors, pumps, fans, turbines, and more.

2.1.1 Impeller and Diffuser Design

The process of designing the geometry of a centrifugal compressor, specifically the impeller and diffuser, is carried out in four steps. This is illustrated in the image of the ANSYS TurbGen software interface, which is used for designing these parts.

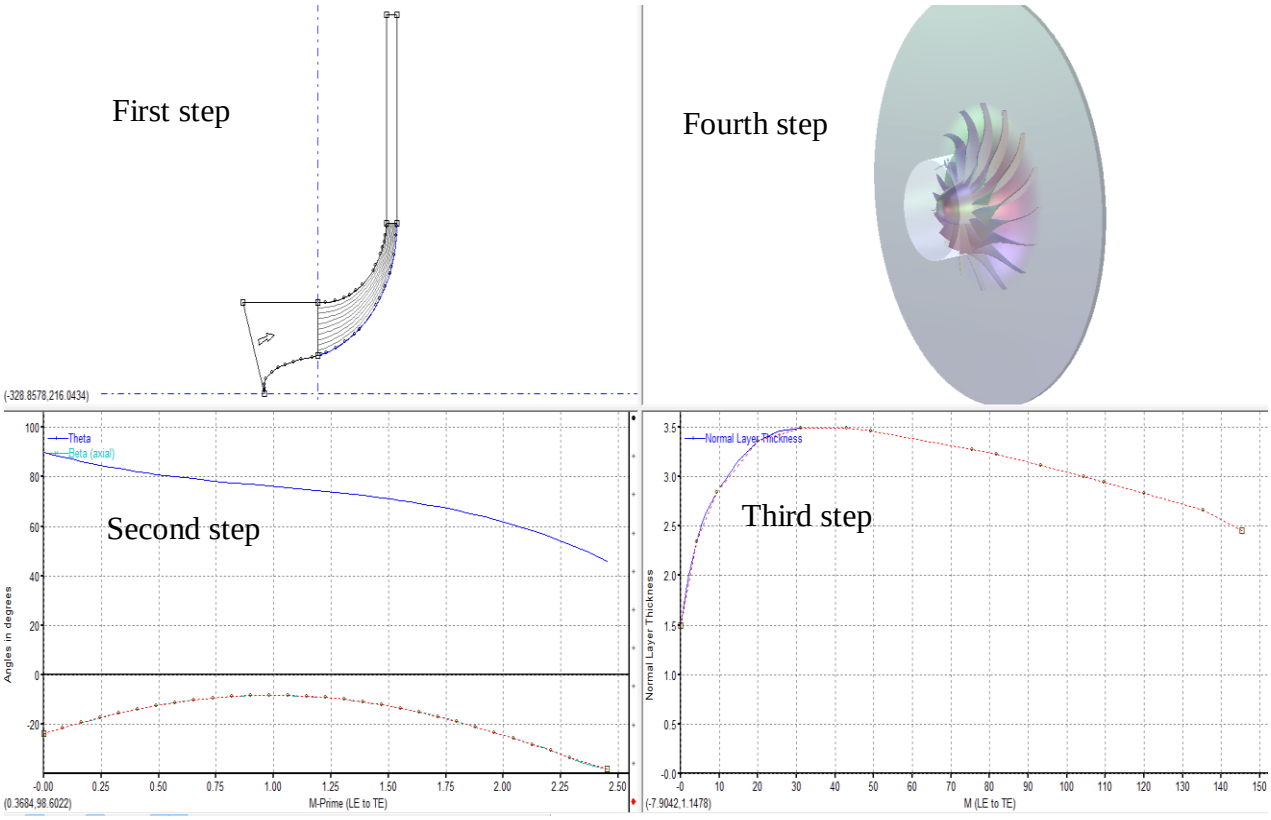

Figure 3.5 steps for designing impeller with BladeGen

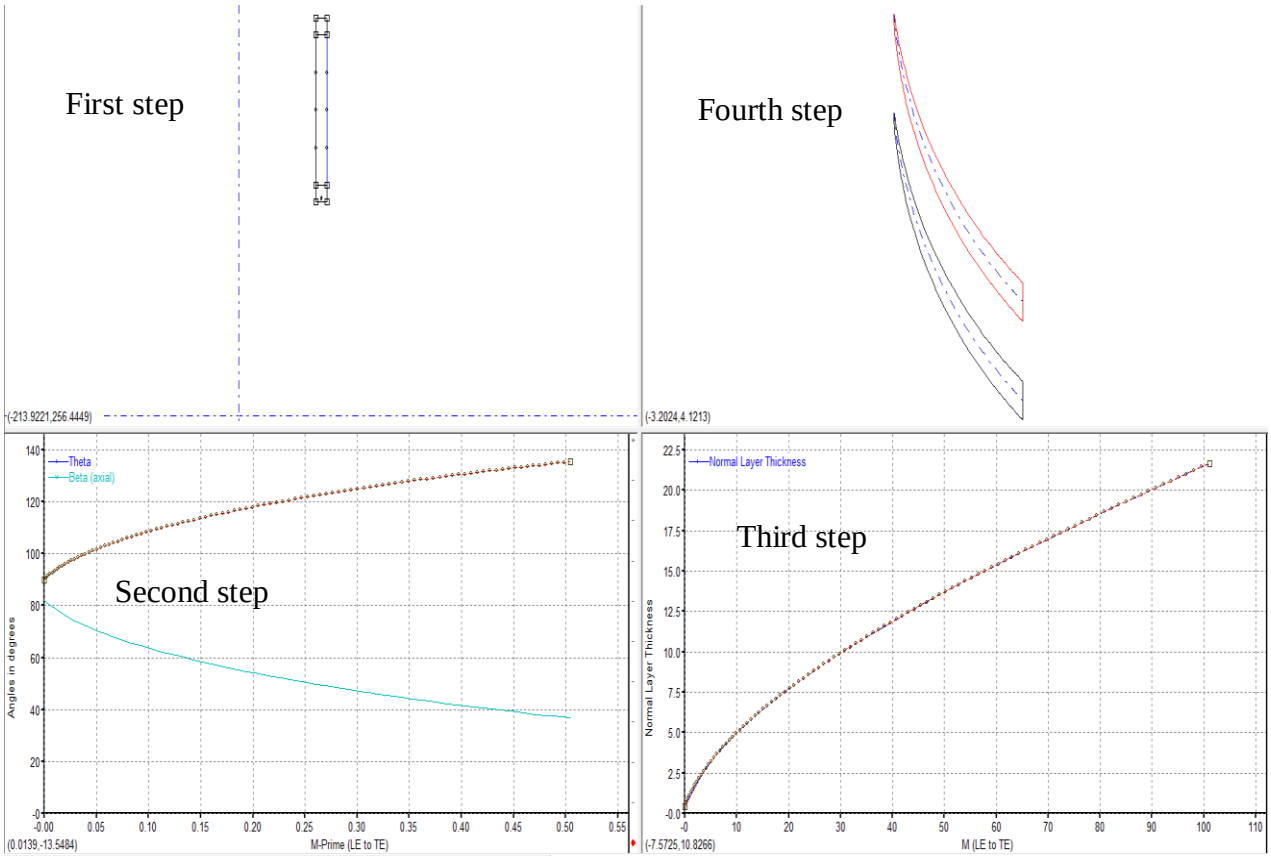

Figure 3.6 steps for designing Stator with BladeGen

► **First step**

The meridional channel is designed using a predefined model tailored to radial impellers, encompassing the hub and casing surfaces. These surfaces are characterized by two curves in the z-plane (r; θ), where z and r represent the axial and radial directions, respectively. The hub and casing surface curves are defined using three types of polynomial functions:

a) A Bézier curve with four control points.

b) A Bézier curve with (N) control points.

c) A B-spline curve with (N) control points.

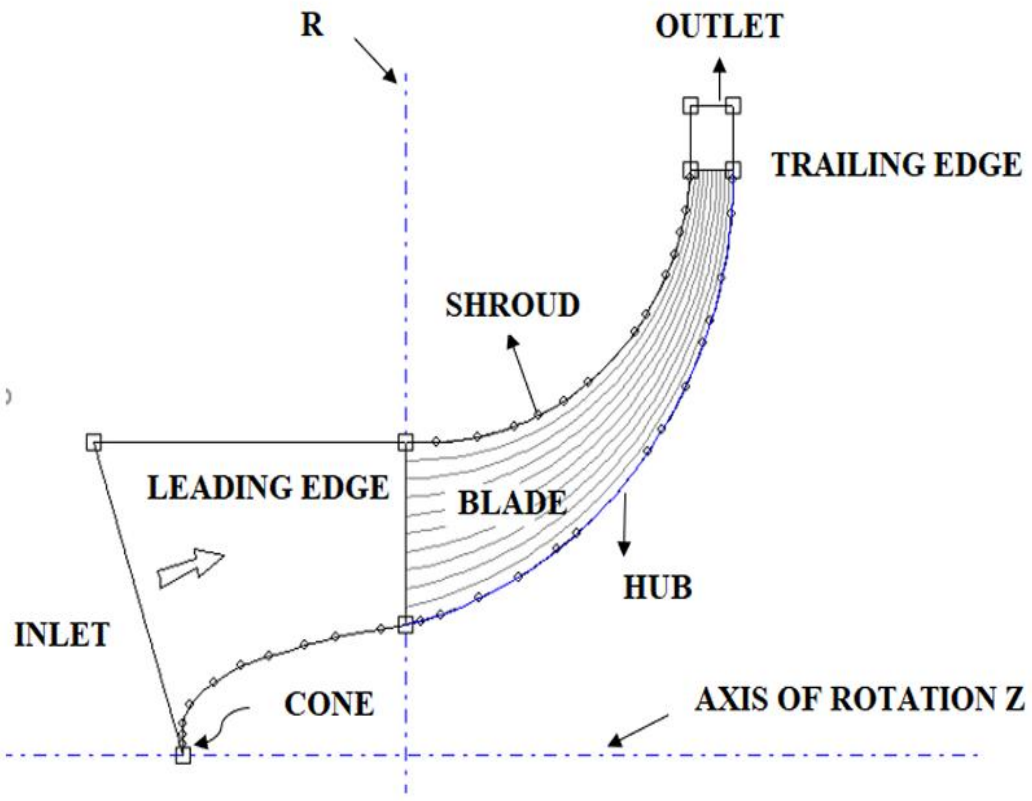

Figure 3.7 Meridian plane of rotor

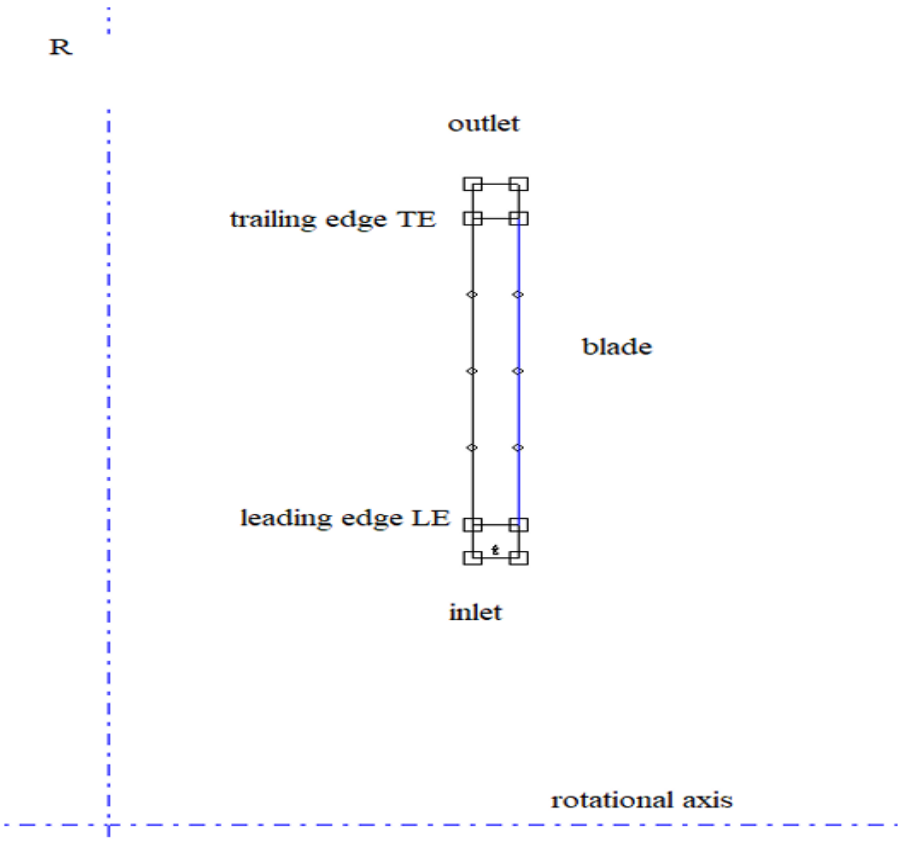

Figure 3.8 Meridian plane of stator

Location of meridian streamlines: Span is the standard position between the shroud and the hub (figure 4)

► **Second step**

This entails defining the angles of incidence (β) and the wrap angle (θ) as functions of the meridional distance through a conformal transformation of coordinates from the M frame to the M' frame. The equation for determining the new coordinates is as follows:

$$\delta M = \sqrt{(\delta R \,.\, \delta R + \delta Z \,.\, \delta Z)} \qquad (3.1)$$

Where:

M: represents the meridional distance

R: denotes the radius.

Z: signifies the axial position

M': stands for the meridional distance as a function of the radius

$$\delta M' = \delta M / R \tag{3.2}$$

The angle θ is determined by the following equation:

$$\delta\theta = \tan(\beta).\delta M' \tag{3.3}$$

►Third step

Involves determining the blade thickness based on the meridional distance. (Figure 3)

►Fourth step

Involves creating the three-dimensional (3D) geometric shape as shown in the following two figures:

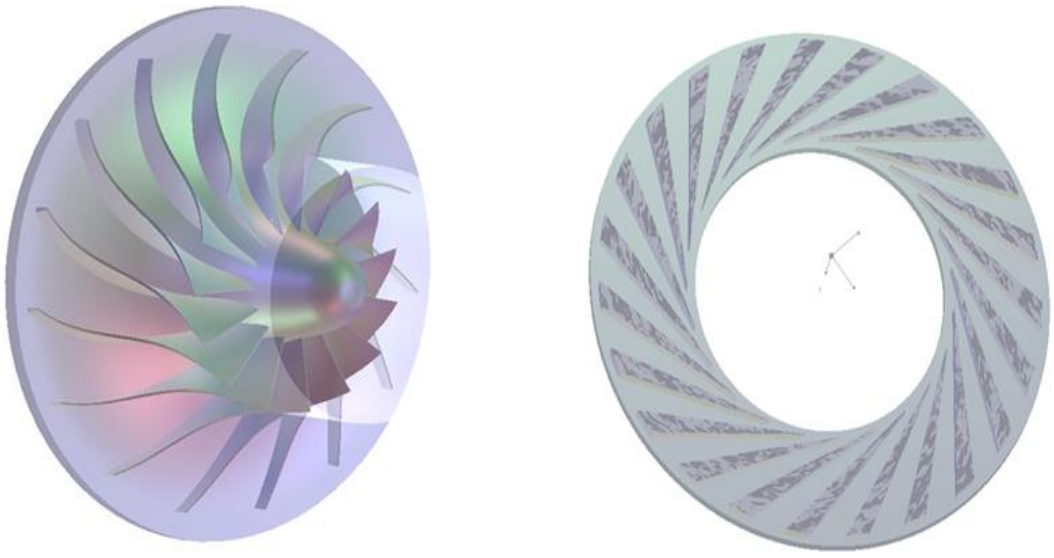

Figure 3.9 Presentation of rotor and stator in 3D

During this stage, the geometry is constructed in either a Cartesian coordinate system (x, y, z) or a cylindrical one. This involves defining all the components of the centrifugal compressor: the blade count, casing, hub, rotation axis, and periodic surfaces. After obtaining the geometry, it is exported to TurboGrid.

2.2 ANSYS CFX –Turbo Grid

This tool enables the generation of a structured mesh suitable for applications across different types of machines. However, there is no precise rule for achieving good mesh quality for certain complex geometries, such as the centrifugal compressor impeller.

Mesh generation for a structure is easier when using a multi-block geometry. This technique involves dividing the computational domains into several compartments with simple geometric shapes and meshing them separately.

Advantages:

- Economical in terms of the number of elements and reduces the risk of numerical errors.

Disadvantages:

- For complex geometries such as the centrifugal compressor impeller, meshing using this technique is not only difficult to generate but also results in poor quality.

Before ANSYS TurboGrid can generate a mesh, you need to provide several key pieces of information. This includes the locations of the geometry files (hub, shroud, and blades), the mesh topology type, and the distribution of mesh nodes. All this data is stored in a set of data objects known as CCL objects. Once you have properly specified the CCL objects, you can command ANSYS TurboGrid to create the mesh.

ANSYS TurboGrid is a powerful tool that produces high-quality meshes using an automatic topology method (ATM) that generates the mesh directly on the blade geometry. This results in a smooth, high-resolution mesh that ensures fast and accurate fluid dynamics analysis.

TurboGrid is used after the stator and rotor construction and utilizes the geometry created by BLADGEN. [13]

2.2.1 Mesh topology

In this section we have used an automatic topology which includes special topologies of the type H / J / C / and of the type ‘O ‘around the blade and the walls in the mesh creation see figure (III.11) below:

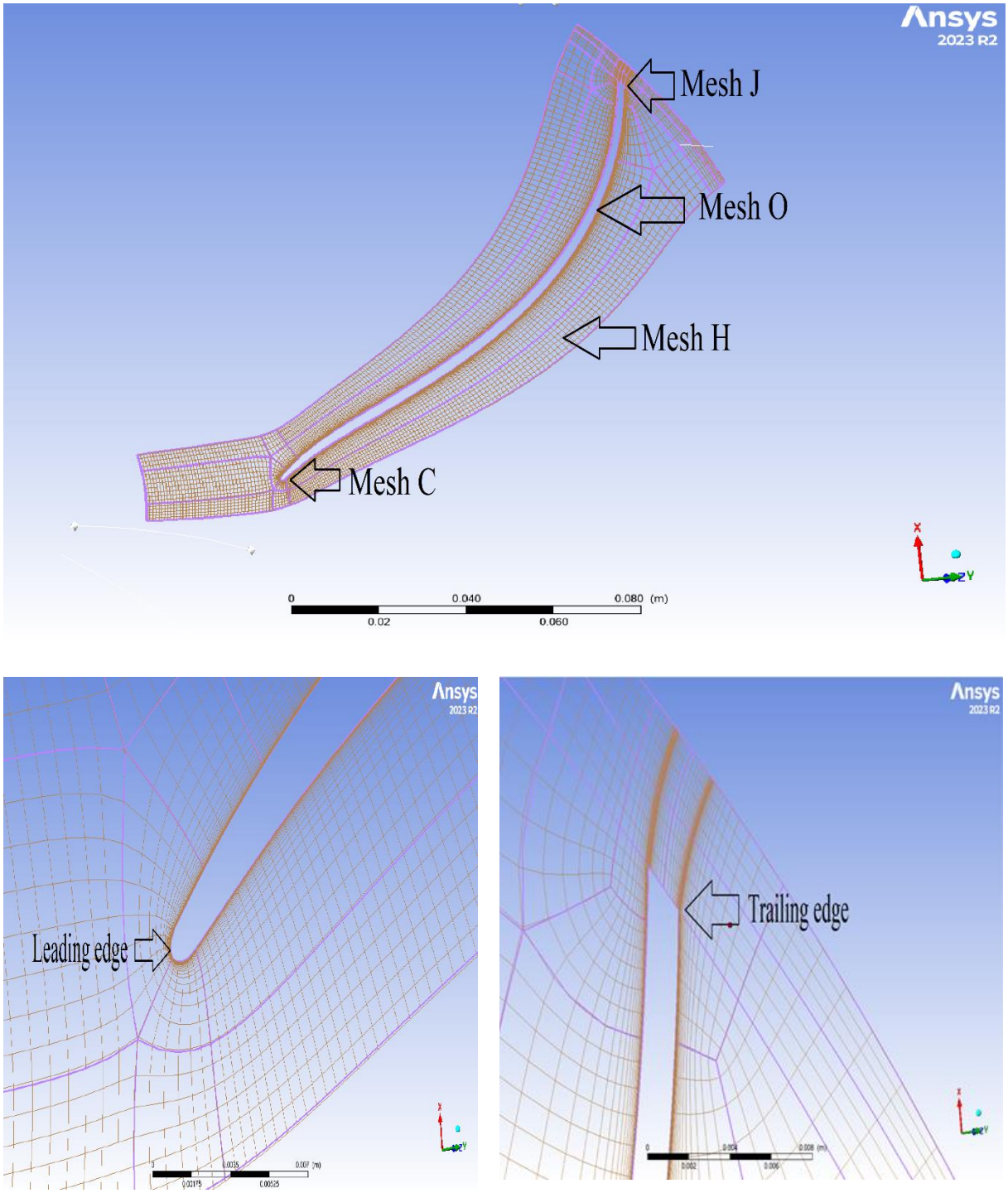

Figure 3.10 Mesh topology rotor

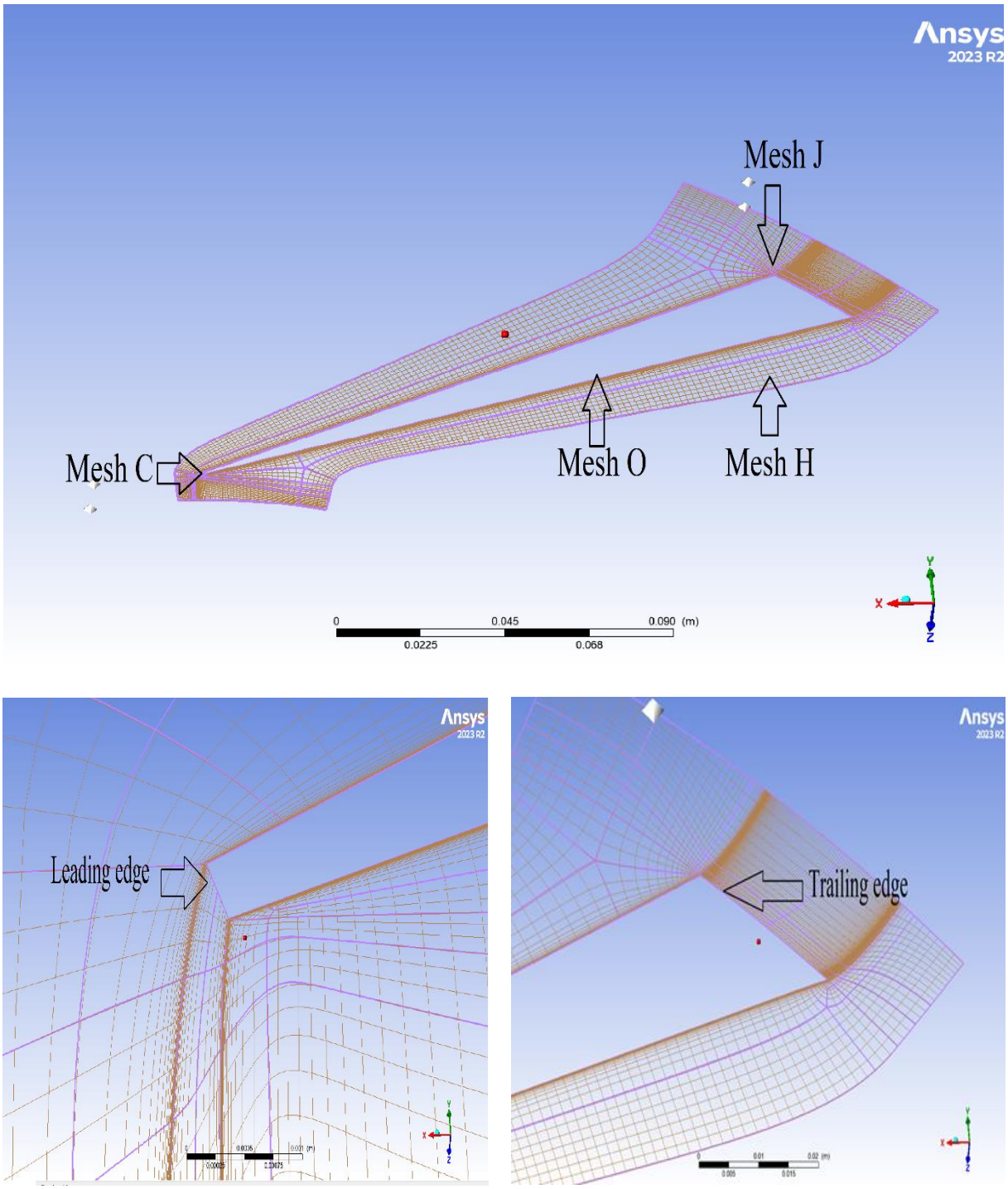

Figure 3.11 Mesh topology stator

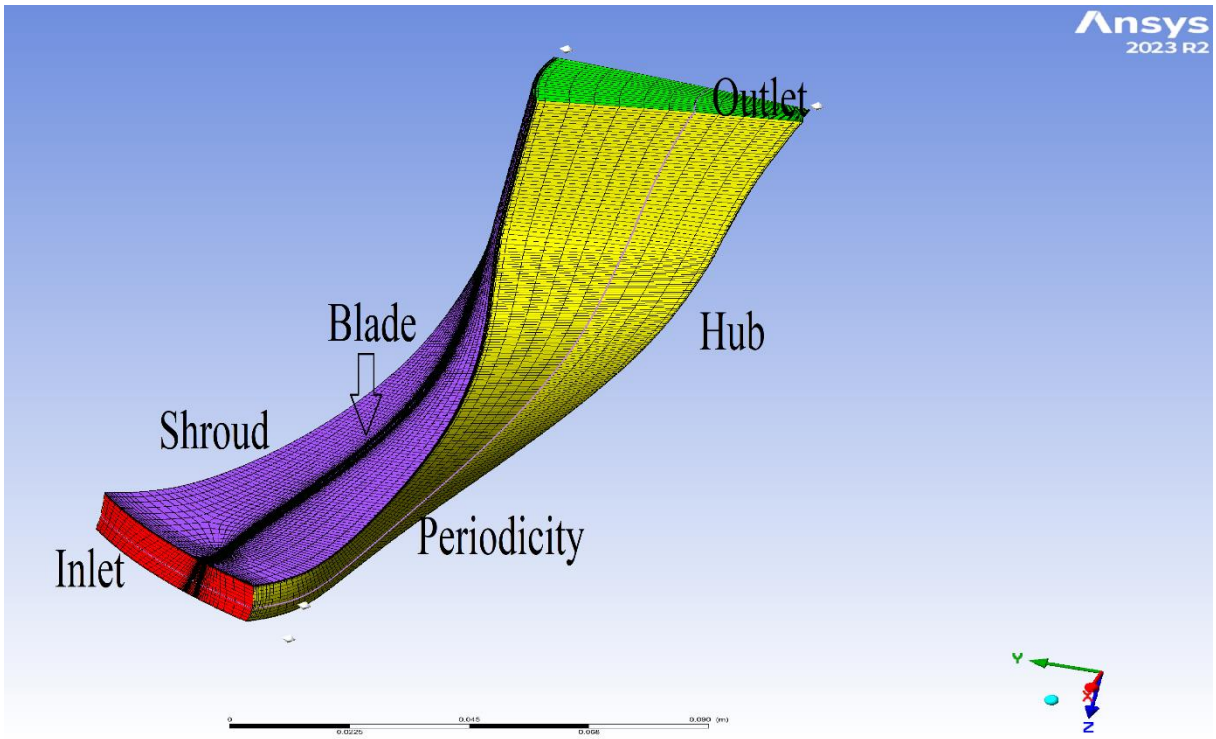

Figure 3.12 passage section rotor

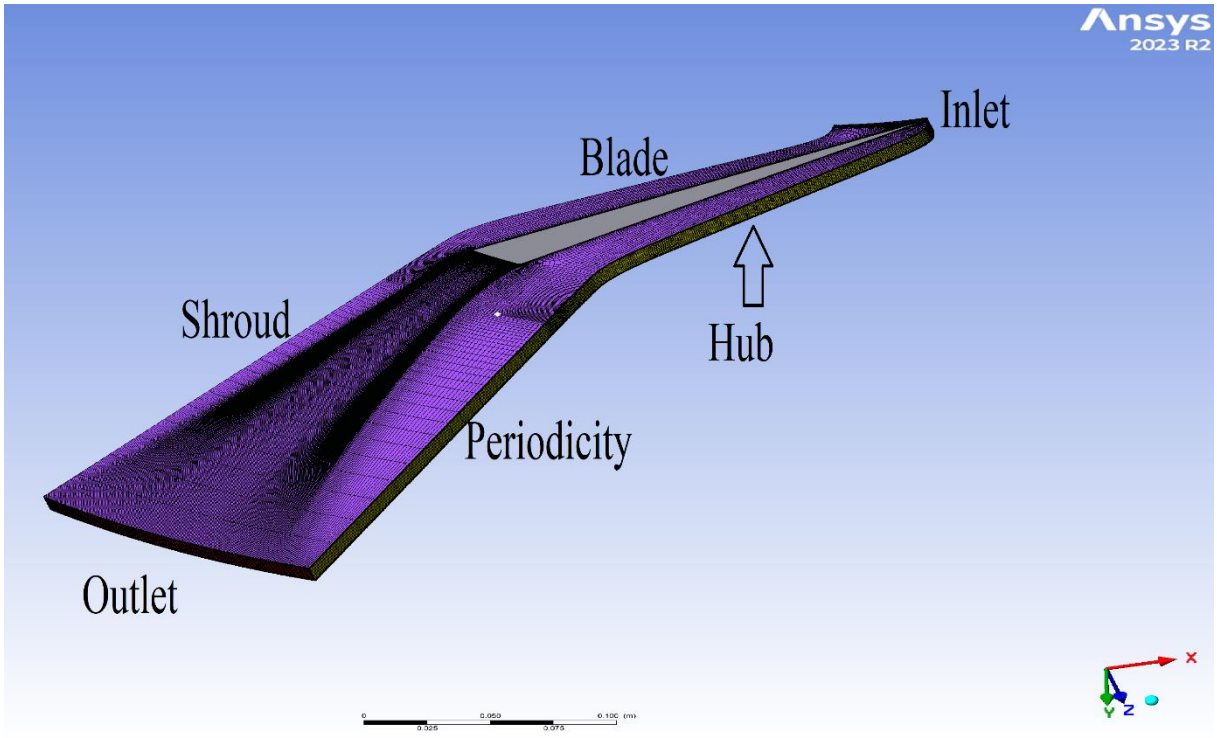

Figure 3.13 passage section stator

2.2.2 Create the mesh of the shroud parts and the hub

The meshing for a turbomachine depends on the following conditions:

1. **Maximum Face Angle**: This is the largest angle of all the faces touching the node, measuring distortion. The value of this angle is 165°.
2. **Minimum Face Angle**: This is the smallest angle between two edges touching the node, with a value of 15°.
3. **Connectivity Number**: This is the number of elements connected to a node. The maximum value is 12, and the minimum is 0.
4. **Element Volume Ratio**: This is the ratio between the largest volume and the smallest volume associated with a node. This ratio is positive.
5. **Edge Length Ratio**: This is the ratio of the distance of the longest edge to the shortest edge on the same face, with a maximum value of 10.
6. **Minimum Volume**: This is the positive volume of the mesh to ensure that no negative volumes exist in the fluid passage.

In order to obtain a very good quality mesh, the six conditions already mentioned must be met, mentioned above are met.

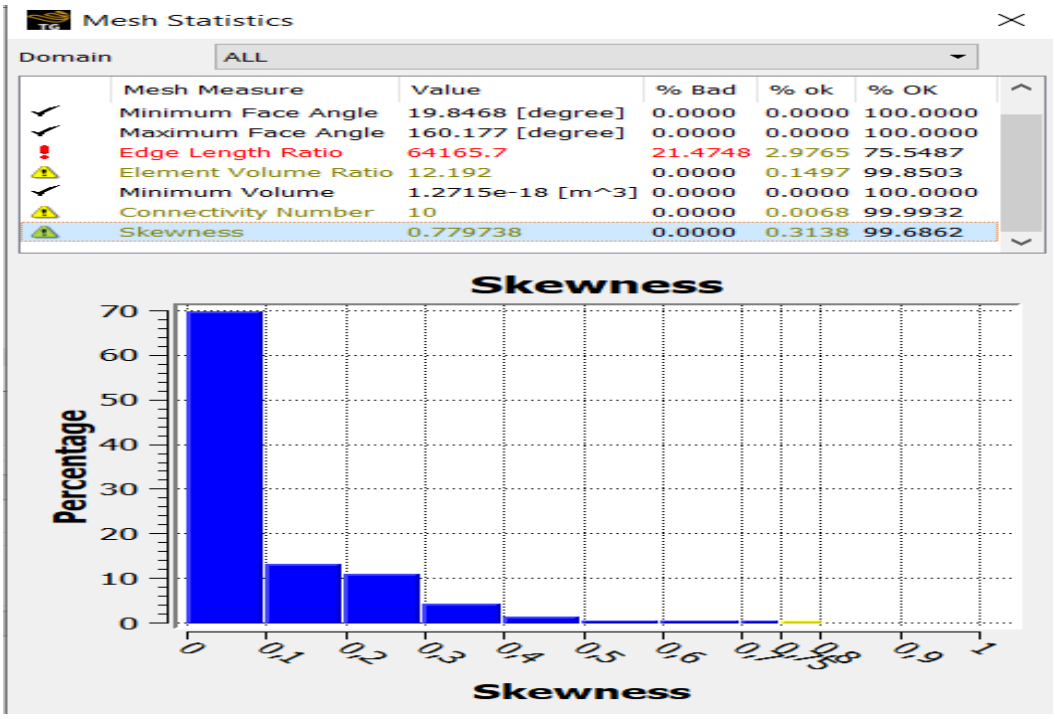

Figure 3.14 Mesh skewness

Skewness mesh metrics spectrum

Excellent	Very good	Good	Acceptable	Bad	Unacceptable
0-0.25	0.25-0.50	0.50-0.80	0.80-0.94	0.95-0.97	0.98-1.00

Figure 3.15 skewness mesh metrics spectrum

The quality of a mesh grid directly affects the stability and accuracy of calculations. The better the mesh quality, the more precise and robust the calculation results will be. Although there are no exact rules for achieving high-quality meshing, there are various techniques that can help us obtain an acceptable mesh:

a) Lack of element distortion
b) Ensures good resolution in the high gradient area
c) Ensures good smoothing in the transition zones between the fine mesh and rude

2.3 CFX Simulation

This component of the CFX .23 software enables the simulation of flows in complex geometries, such as in the assembly of a centrifugal compressor impeller and a radial diffuser. It provides designers with a robust and precise tool to analyze internal flows, which can be compressible or incompressible, steady or unsteady, laminar or turbulent, and the flow can be subsonic or supersonic.

After creating the stator and rotor mesh with TURBOGRID, the simulation process begins with ANSYS CFX to calculate the fluid dynamics in the compressor stage. This allows for the analysis of compressible fluid flow through the blade geometry. In addition to the mesh created by TURBOGRID, boundary conditions are specified, and CFX performs the calculations and displays the corresponding results. The simulation within CFX consists of three main components: [13]

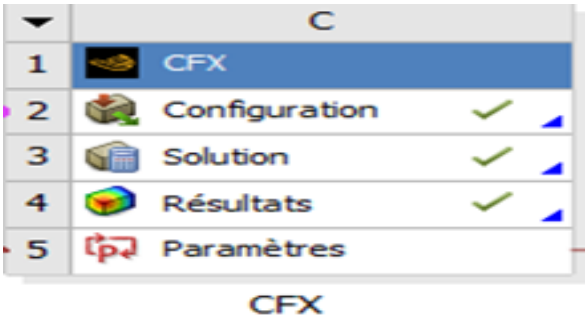

Figure 3.16 simulation steps

1. configuration
2. Solution
3. Results

2.3.1 Configuration

In this module, boundary and initial conditions corresponding to the flow regimes are defined. The numerical scheme is then selected, specifying the number of iterations, the convergence criteria, and the nature of the fluid. The computational domain consists of two meshes: one for the impeller and one for the diffuser. The interface between the impeller and the diffuser is simulated by a smooth diffuser attached to the impeller.

The simulation begins by selecting TURBO mode in the configuration, a specialized mode for setting up turbomachinery simulations. Each component of the stator-rotor is defined by importing their mesh from TURBOGRID, followed by identifying the basic parameters and boundary conditions. Utilizing the stage interface model included in CFX-Setup, where the flow field is repeated in multiple regions of identical rotation, only one region needs to be solved with the boundaries specified as periodic. Consequently, a single stator blade and a single rotor blade are presented for simulation. This method is efficient and significantly reduces computational requirements. [13]

2.3.1.1 Starting the turbo mode

First we have to define the basic parameters as machine type and analysis type

The machine type can be any one of Pump, Fan, Axial Compressor, Centrifugal Compressor, Axial Turbine, Radial Turbine, or Other. In all cases, as part of the Turbo System functionality, the machine type will be part of the data passed between CFX-Pre and CFD-Post in order to aid workflow.

In our case we choose centrifugal compressor.

The analysis type determines whether your problem is Steady State, Transient, or Transient Blade Row. In our case we choose steady state.

Steady-state simulations, by definition, are those whose characteristics do not change with time and whose steady conditions are assumed to have been reached after a relatively long time interval. They therefore require no real time information to describe them.[13]

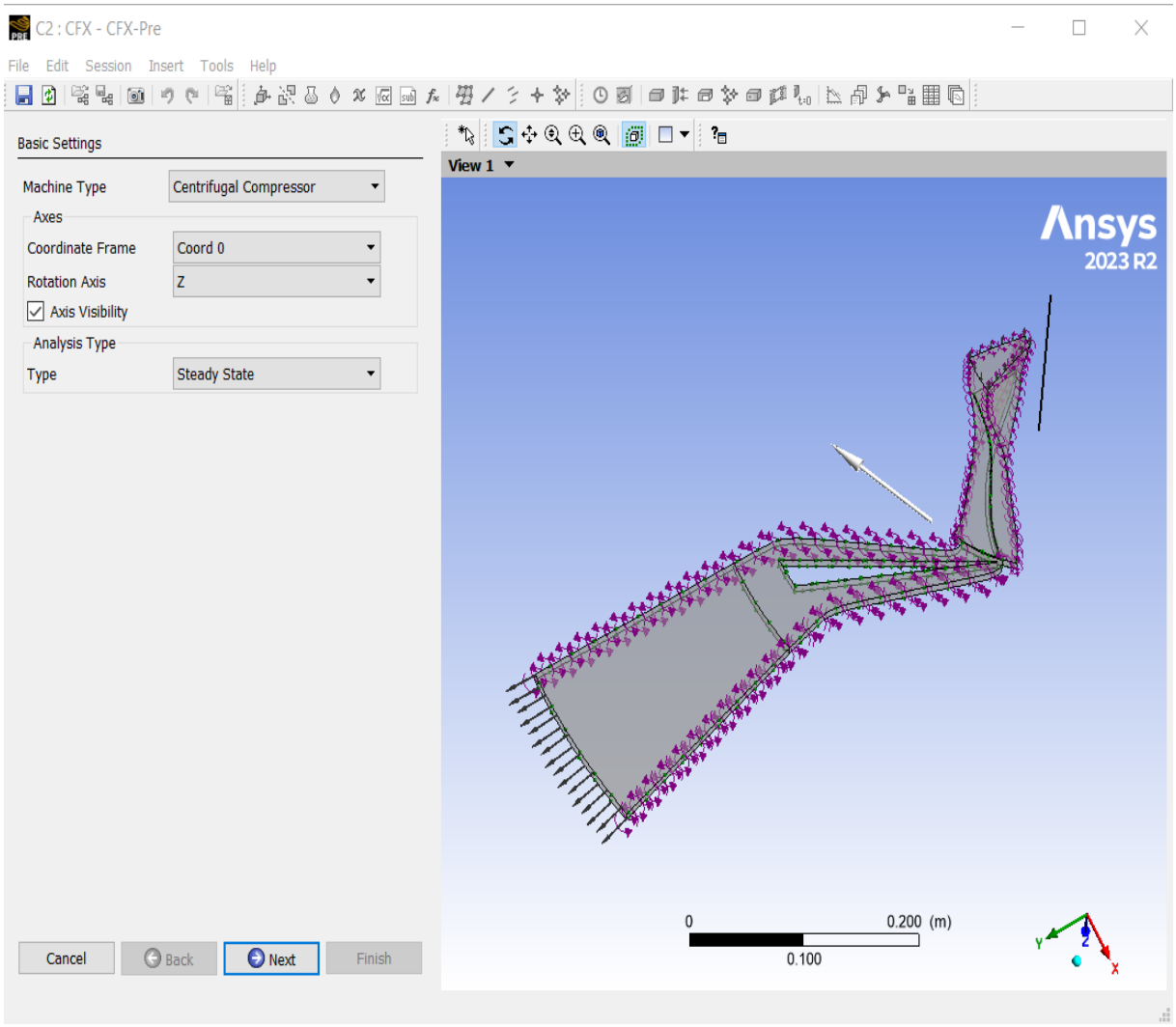

Figure 3.17 basic setting of stage (rotor-stator)

Second we have to define the components where:

- The first component 'the rotor' is added with a rotating status.
- The rotation speed is 28541 [rev ^min-1].
- The second component 'stator' is specified with a stationary status.

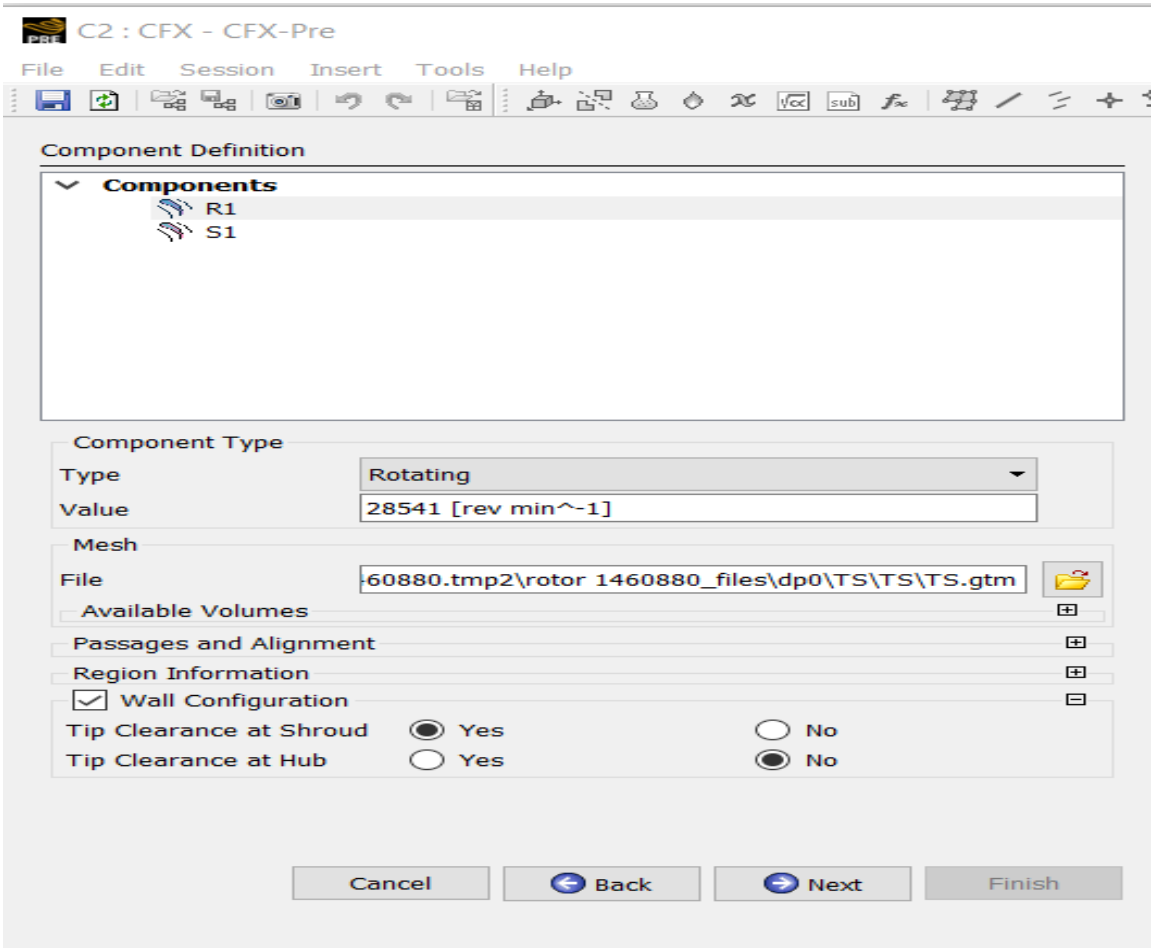

Figure 3.18 the creation of a system composed of stator and rotor

Third, Properties of the fluid domain and solver parameters are specified on the Physics Definition panel whereas, Our fluid is an ideal gas, For our model, we set the reference pressure to 0, which serves as the absolute pressure baseline against which all other relative pressures in the simulation are measured. In terms of heat transfer, we employ a model that predicts temperature distribution throughout the flow by using total energy. This approach models the transport of enthalpy and incorporates kinetic energy effects, which is essential when these effects become significant. For turbulence, we use the shear stress transport (SST) model to predict the impact of turbulence in the fluid flow without needing to resolve the smallest turbulent fluctuations. Regarding boundary conditions, we use P-Total Inlet and P-Static Outlet templates. The inflow conditions are set with a total pressure (P-Total) of 0.6 bar and a total temperature (T-Total) of 296 K, while the outflow is characterized by a static pressure (P-Static) of BP. [13]

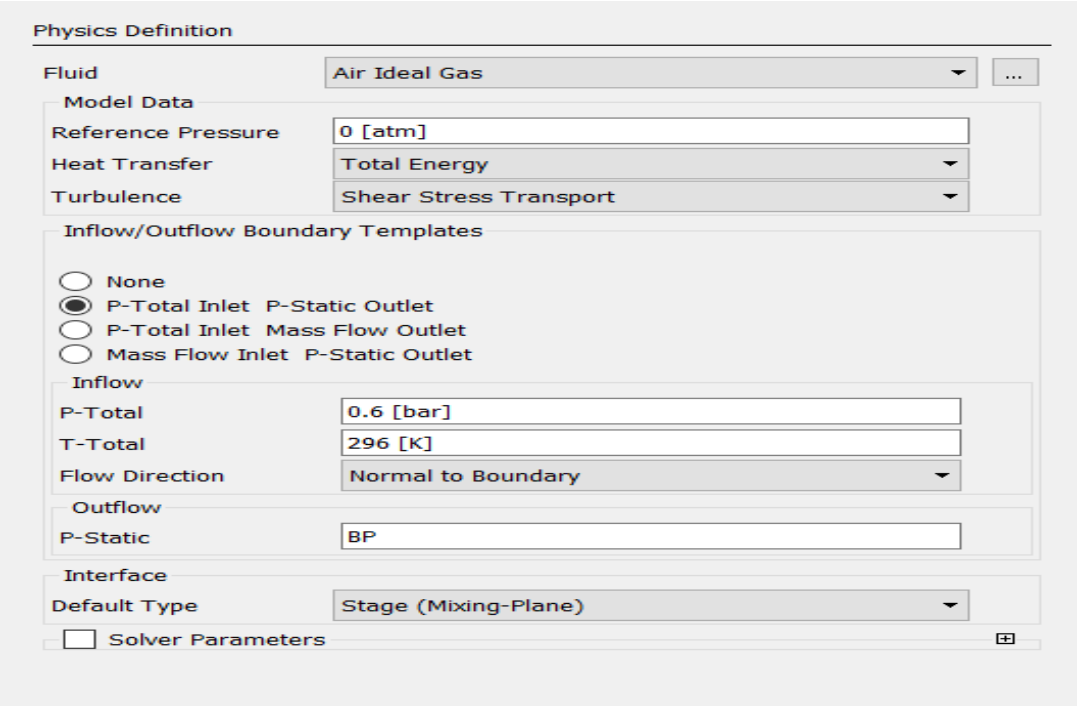

Figure 3.19 Physical definition

2.3.2 Solution (Solver)

This module performs the basic calculations to solve the equations of the given problem

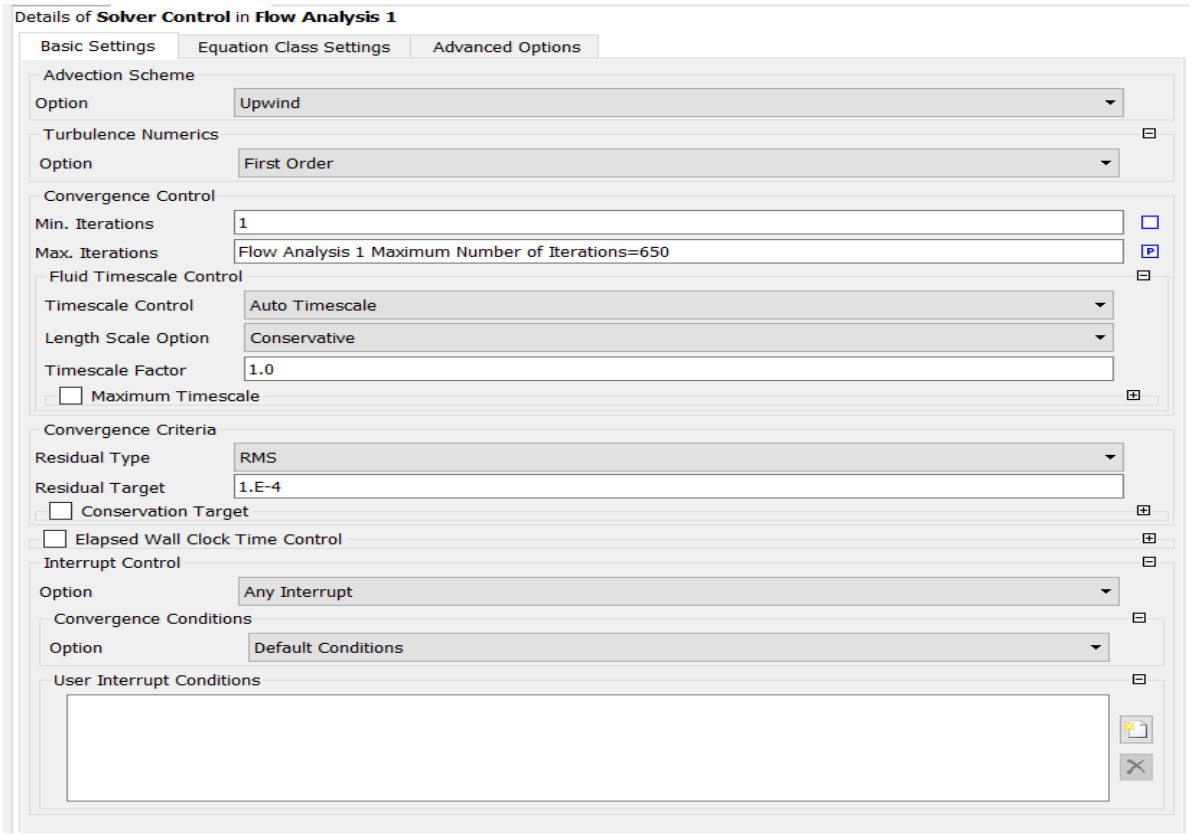

Figure 3.20 Solver Control

To solve the problem at hand, it is essential to calculate the isentropic efficiency and the corrected mass flow rate using the following equations:

- **Isentropic Efficiency for a Compressor**

The isentropic efficiency of a compressor can be determined using the relationship between the pressure ratio and the temperature ratio. The formula is given by:

$$\eta_c = \frac{\pi^{\frac{\gamma-1}{\gamma}} - 1}{\tau - 1} \qquad (3.4)$$

Where:

$\pi = \frac{P_{t2}}{Pt_1}$ is the pressure total ratio.

$\tau = \frac{Tt_2}{Tt_1}$ is the temperature total ratio.

γ is the specific heat ratio of the gas.

- **Corrected Mass Flow Rate**

The corrected mass flow rate can be calculated to account for variations in inlet conditions. The formula is:

$$\dot{m}_{\text{corr}} = \dot{m} \frac{\sqrt{\frac{T_{\text{ref}}}{T_1}}}{\frac{P_1}{P_{\text{ref}}}} \qquad (3.5)$$

Where:

$\dot{m}$ is the actual mass flow rate.

T_1 is the inlet temperature.

P_1 is the inlet pressure.

T_{ref} is the reference temperature .

P_{ref} is the reference pressure .

These calculations will enable us to accurately evaluate the performance of the compressor under varying operating conditions.

The CFX solution carries out several iterations to achieve the results, measuring the global residual error between successive iterations. Ideal convergence is attained when this global residual approaches zero, with lower residuals indicating a more accurate solution.

2.3.3 Post-Processing module (Results)

The Post-Processing module is a graphical tool used for handling and visualizing results, such as contour maps of iso-surfaces, streamlines, pressure fields, and more. The results can be exported in numerical format or as animations, among other options.

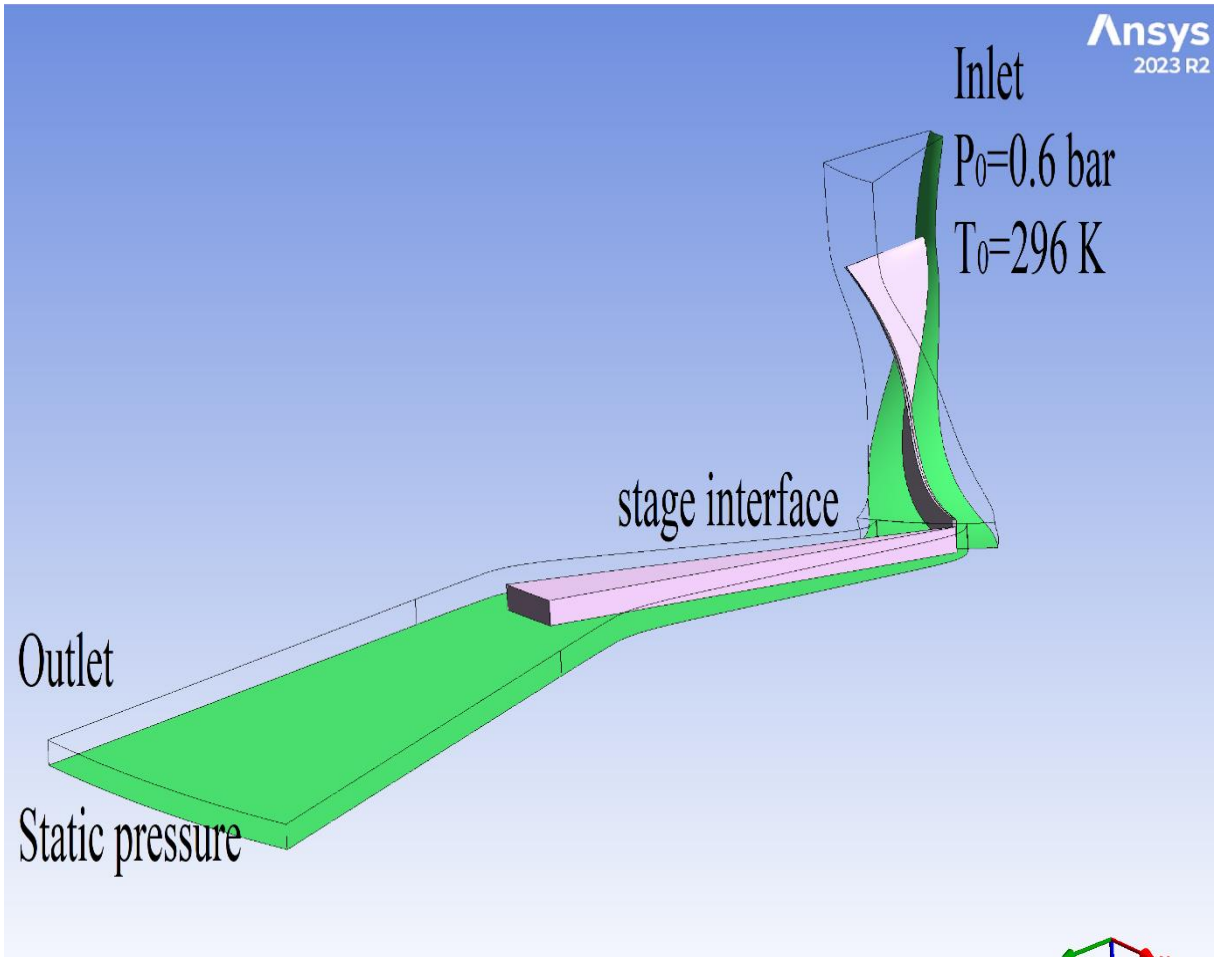

Figure 3.21 computational domain and boundary conditions

- **Calculation constraints**

The general calculation conditions are summarized in the following table:

Table 3.2 calculation constraints

Characteristics	ANSYS CFX R2.2023
Simulation domain	blade-to-blade channel (Periodic condition)
Simulation regime	Steady-state
Mesh (impeller and diffuser)	Structured
Fluid	Ideal gas (Compressible air)
Inlet boundary condition	Total pressure [Pa] Total temperature [K]
Outlet boundary condition	Static pressure [Pa]
Turbulence model	k−ω; SST
Numerical scheme	Second order
Residual Mean Square (RMS)	10^{-4}

- **Tools**

The simulations have been run on a computer with the following specifications:

Name of the device: DESKTOP-2L19DLH

Processor: 13th Gen Intel (R) Core (TM) i9-13900K 3.00GHz

Ram memory installed: 128 Go (128 Go usable)

Device ID: AC003C7C-9A12-4FF6-8676-FE8A34546AD1

Product ID: 00331-10000-00001-AA030

System type: 64-bit operating system, x64 processor

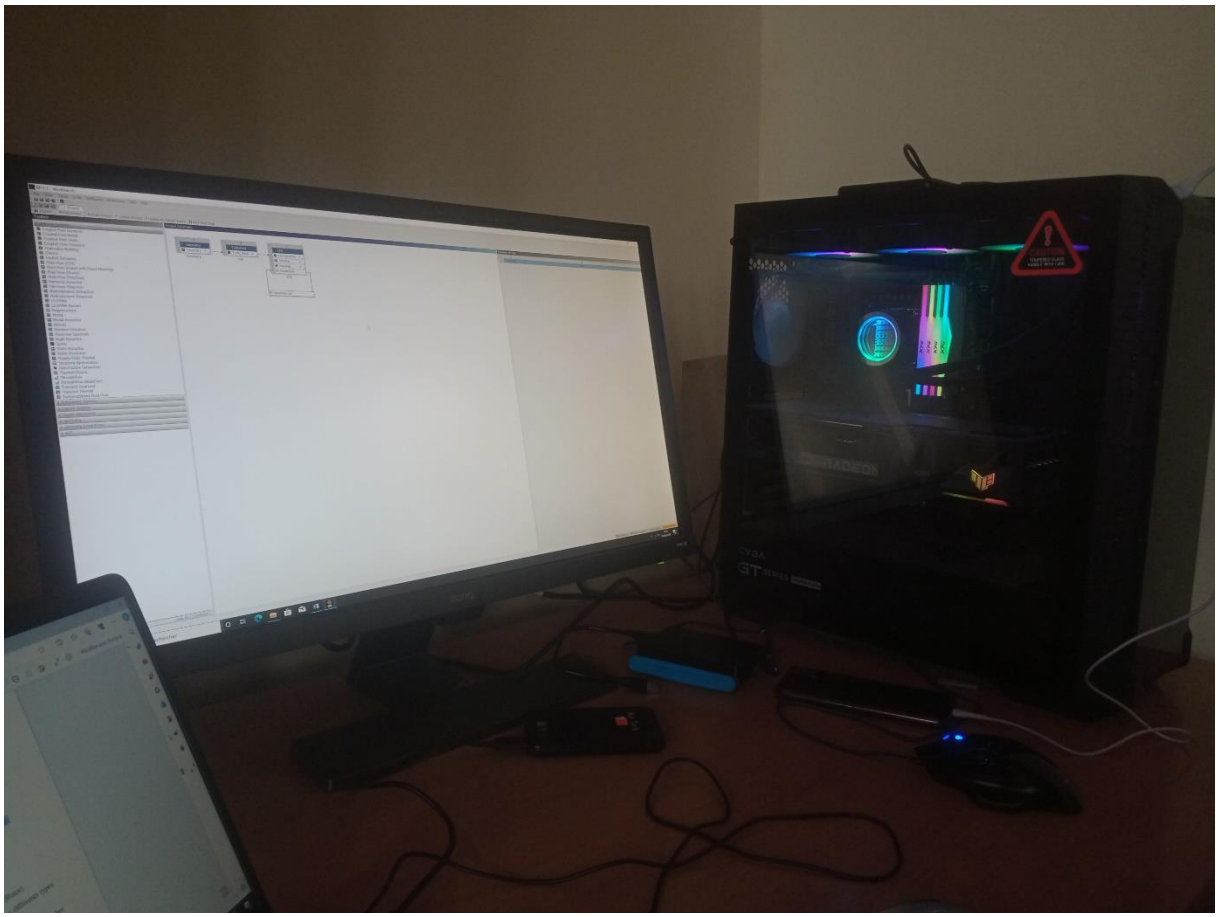

Figure 3.22 Simulation Computer Setup

Simulation Performed at the Laboratory of Aeronautical Sciences and Space Studies in Blida.

CHAPTER 4

Results and discussion

1.Introduction

In this chapter, we will discuss the results of our simulations for the compressor stage, examining four different diffuser-impeller radius ratios R_4/R_2. This analysis aims to observe the impeller-diffuser interaction and its impact on the aerothermodynamic parameters. We will begin with a mesh sensitivity study, evaluating the error between our simulations and the experimental data, and confirming that our results are mesh-independent. Subsequently, we will present the distribution of aerothermodynamic quantities throughout the fluid domain, illustrating the contours of these parameters and demonstrating the variations caused by different impeller-diffuser gap widths. Our discussion will highlight the performance differences and underlying mechanisms driving these changes, providing a comprehensive understanding of the impeller-diffuser interaction effects.

2. Mesh sensitivity an results validation

The impeller and diffuser fluid domains were meshed separately, and the two domains were subsequently joined in ANSYS CFX. In CFD simulations, the fluid domain is discretized into a mesh where quantities are calculated at the center of elements, edges, or nodes, depending on the solution scheme. A finer mesh typically yields more precise results until a certain mesh density is reached, beyond which further refinement does not improve accuracy. At this point, the solution is considered mesh-independent.

The initial set of simulations was conducted with a mesh of approximately 300,000 elements in each fluid domain, resulting in a total of roughly 600,000 elements. The mesh size was then increased to to 800,000 elements per domain, amounting to 2,500,000 elements in total.

A common practice is to reduce the number of elements to achieve the least dense mesh that still provides the same level of precision, known as the optimum mesh. However, due to time constraints, this procedure was not carried out in this dissertation.

Below is a graphical representation of the performance map of our compressor of every diffuser-impeller radius ratios R_4/R_2, obtained using two different meshes and the experimental data. This comparison helps validate the accuracy of our simulations and confirms the mesh independence of our results.

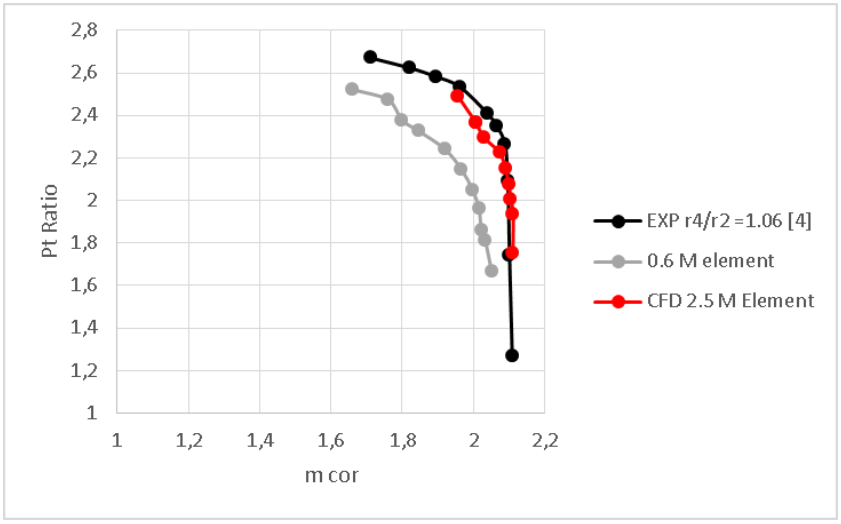

Fig 4.1: Mesh sensitivity analysis for $R_4/R_2 = 1.06$

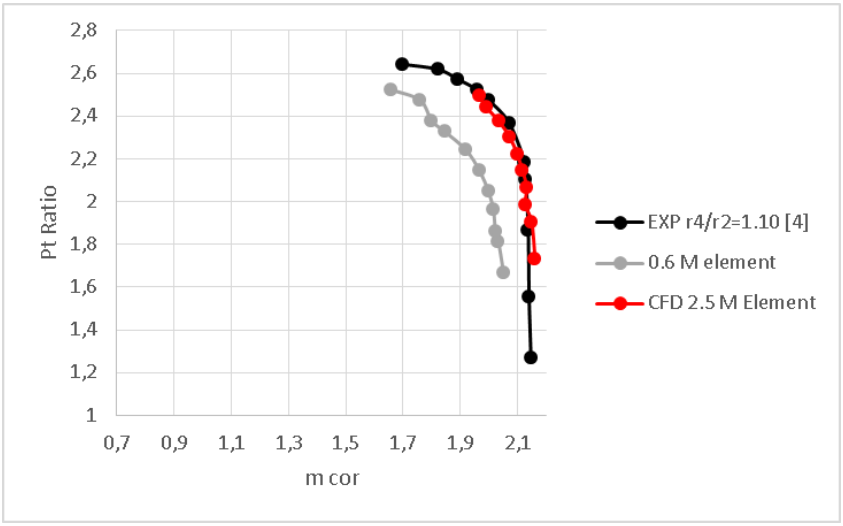

Fig 4.2: Mesh sensitivity analysis for $R_4/R_2 = 1.10$

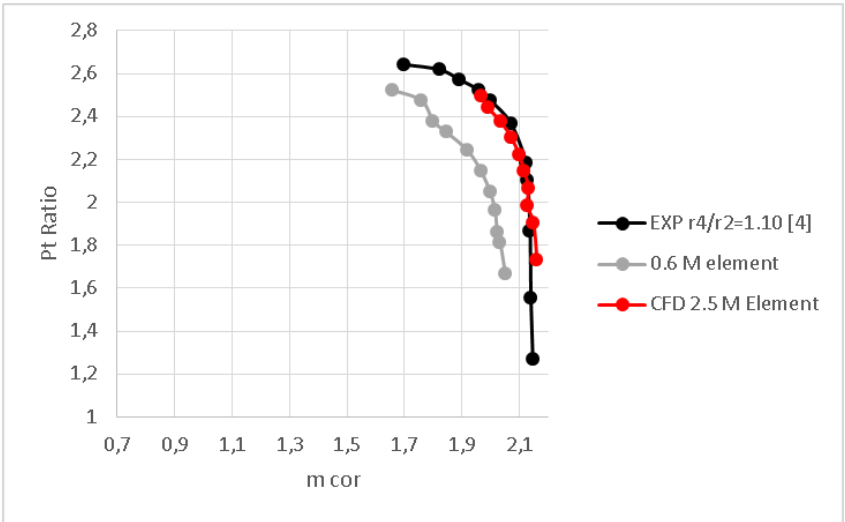

Fig 4.3: Mesh sensitivity analysis for $R_4/R_2 = 1.14$

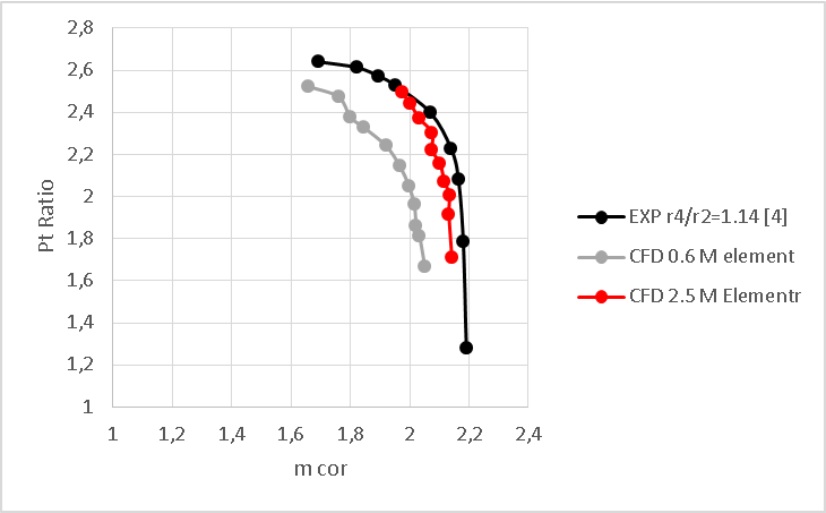

Fig 4.4: Mesh sensitivity analysis for $R_4/R_2 = 1.18$

Comparing the experimental data shown in these graphs, we observe a strong mesh sensitivity for 2.5 million elements (impeller and diffuser) in all R_4/R_2 configurations.

3. y^+validation

To achieve an accurate approximation of boundary layer properties, the mesh must yield an appropriate y^+ value, depending on the turbulence model used. For instance, the $k-\epsilon$ turbulence model requires a y^+ value between 30 and 300 for good precision in the boundary layer, whereas the $k-\omega-SST$ model needs a y^+ value of less than 5 to achieve similar accuracy.

Below are the y^+ contours for the impeller and diffuser blades, shroud, and hub. As illustrated, the y^+ values fall well within the acceptable range for our chosen turbulence model.

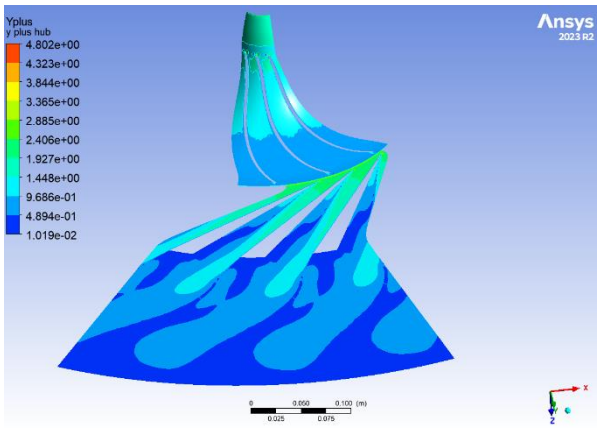

Fig 4.5: y^+contour for the hub

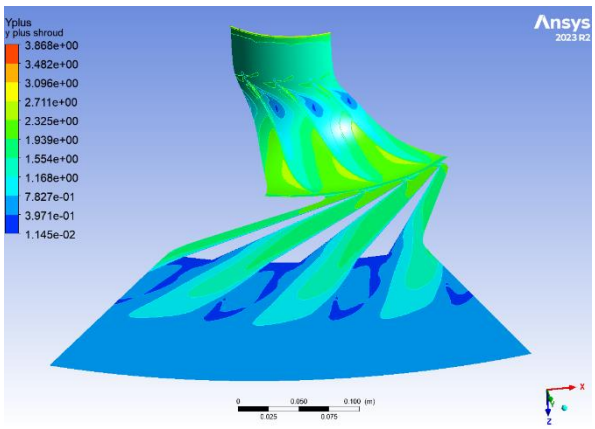

Fig 4.6: y^+contour for the shroud

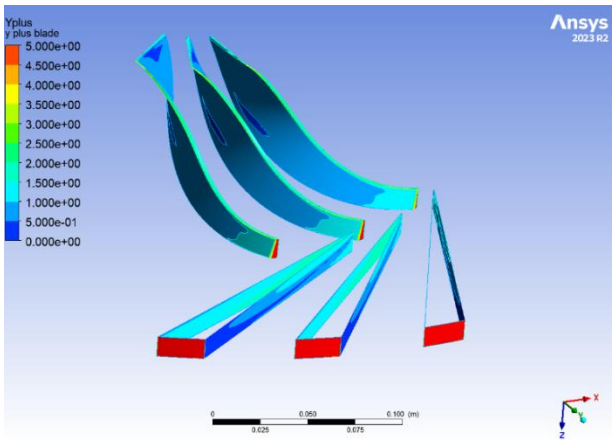

Fig 4.7: y^+contour for the impeller and diffuser blade

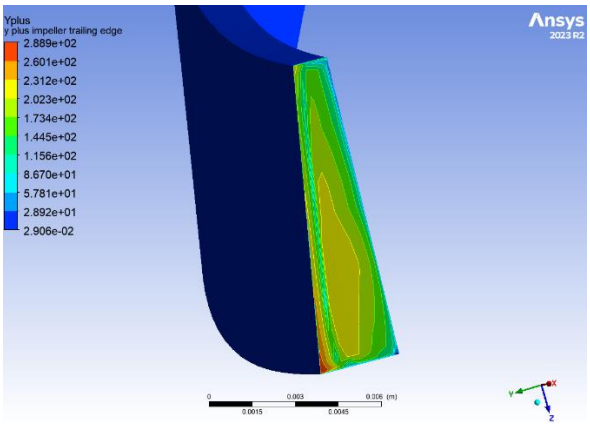

Fig 4.8: y^+contour for the impeller TE

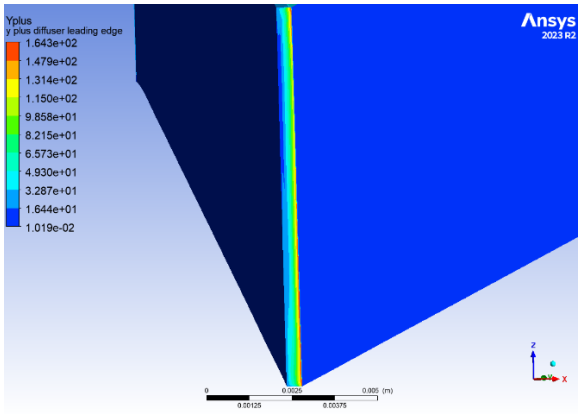

Fig 4.9: y^+contour for the diffuser LE

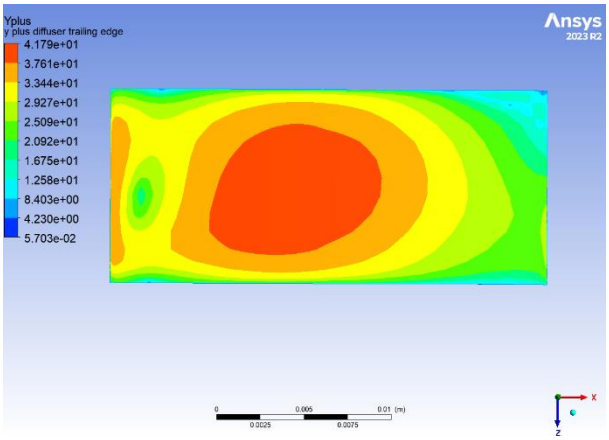

Fig 4.10: y^+contour for the impeller TE

Although the y^+ values exceed the limit set for the $k-\omega-SST$ turbulence model, they only affect a very small percentage of the total area, contributing minimally to the overall solution. Therefore, we can confidently consider this mesh suitable for our study. Similar observations have been previously noted by Andrew Lewis De Wet, who described the challenges of meshing such geometries.[14]

4. Simulation results and discussion

The CFX solver will provide the distribution of aerothermodynamic quantities throughout the fluid domain. Below, we present figures displaying the contours of these parameters, along with graphs illustrating the impact of varying the impeller-diffuser gap width.

First, we will present the overall performance table for the configurations with: R_4/R_2=1.06, R_4/R_2= 1.10, R_4/R_2=1.14, and R_4/R_2=1.18

Table 4.4 The overall performance table for all the configurations

R_4/R_2	Mass flow	Pt_{ratio}	Tt_{ratio}	η_{isen}	Power(W)
1.06	2,10482	2,00443	1,34889	0,629928	126986
1.10	2,09801	2,22356	1,34928	0,73428	126774
1.14	2,1021	2,15675	1,35111	0,6994	126076
1.18	2,09083	2,29008	1,34839	0,766651	126252

This table provides a comprehensive overview of how changing the R_4/R_2 ratio affects various performance metrics of the compressor. It shows that as the ratio varies, parameters such as mass flow, total pressure ratios, total temperature ratios, efficiency, and power fluctuate accordingly. This data is crucial for optimizing the design and operation of the compressor for desired performance characteristics.

We notice that for practically the same mass flow value, as the R_4/R_2 ratio increases, the total isentropic efficiency as well as total pressure ratio also generally increases. A higher total isentropic efficiency, and total pressure ratio signifies better compression performance. Which means that R_4/R_2= 1.18 configuration gave us the best performances.

4.1 Static pressure

Here we can see the distribution of static pressure in the three planes (meridional, blade to blade, and orthogonal). **. Meridional plane**

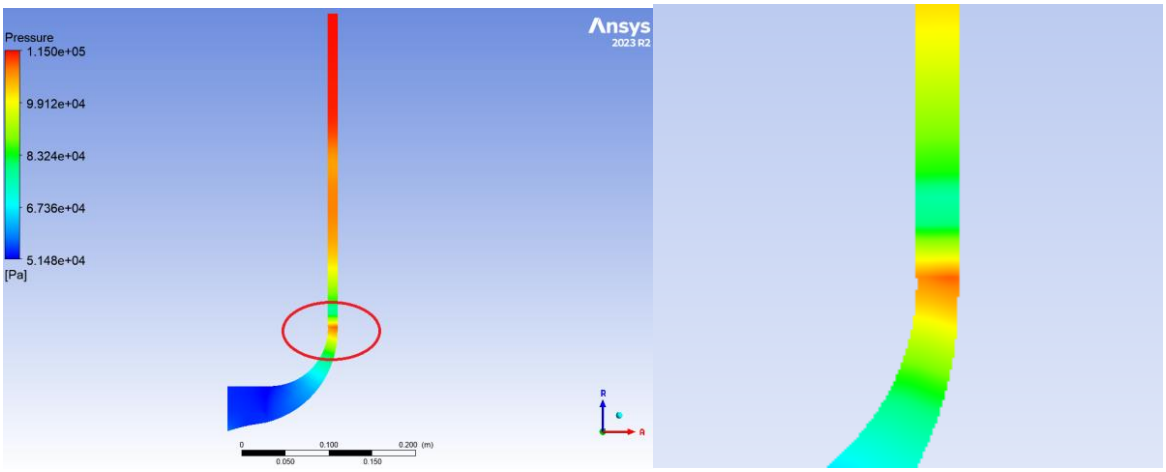

Figure 4.11: Static pressure contour
R_4/R_2= 1.06; $\dot{m}_{corr}$= 2,1048

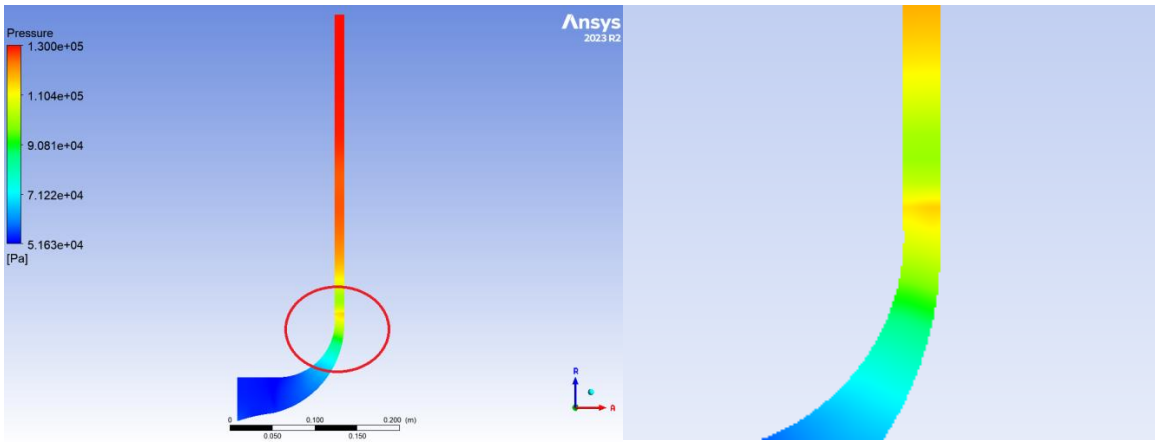

Figure 4.12: Static pressure contour
R_4/R_2= 1.10; $\dot{m}_{corr}$= 2,09801

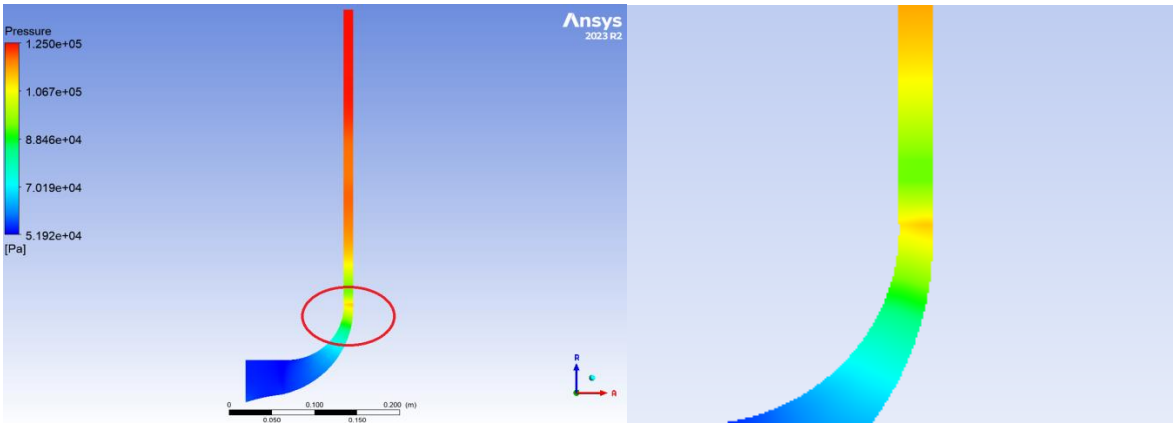

Figure 4.13: Static pressure contour
R_4/R_2= 1.14; $\dot{m}_{corr}$= 2,1021

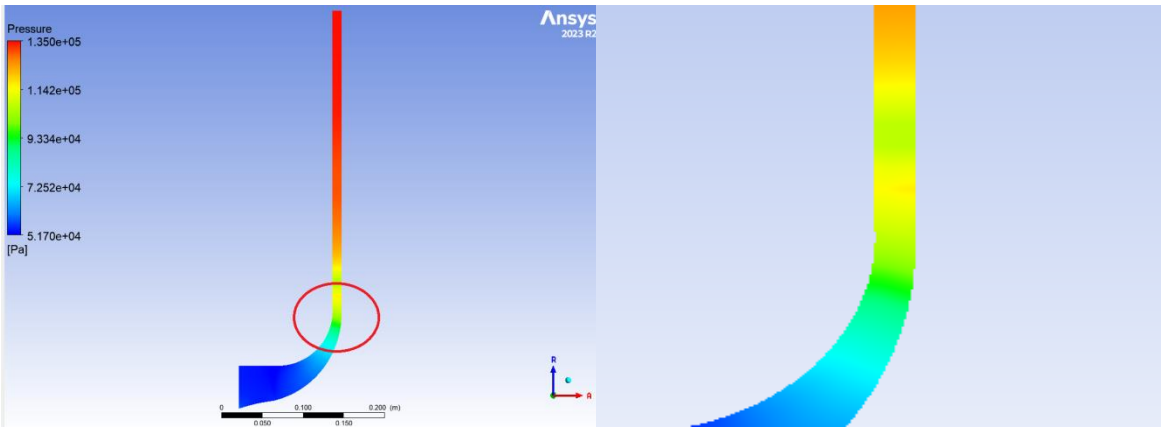

Figure 4.14: Static pressure contour
R_4/R_2= 1.18; $\dot{m}_{corr}$= 2,09083

. Blade to blade plane

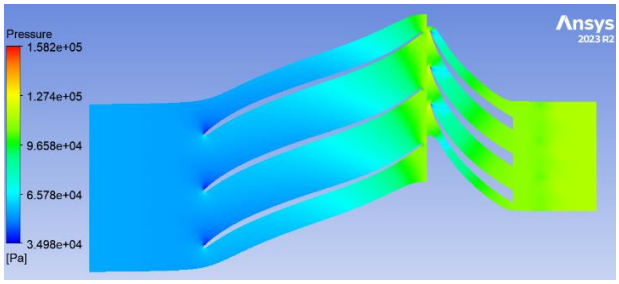

Figure 4.15: Static pressure contour R_4/R_2= 1.06; $\dot{m}_{corr}$= 2,10482

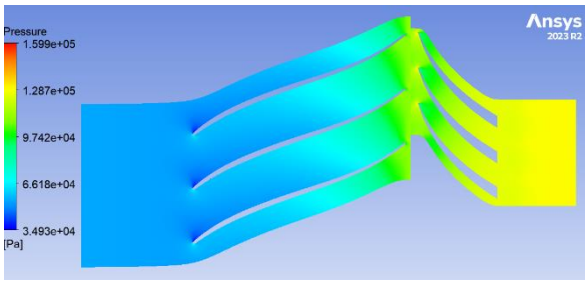

Figure 4.16: Static pressure contour R_4/R_2= 1.10; $\dot{m}_{corr}$= 2,09801

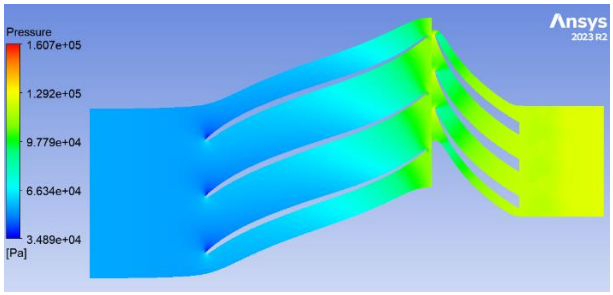

Figure 4.17: Static pressure contour R_4/R_2= 1.14; $\dot{m}_{corr}$= 2,1021

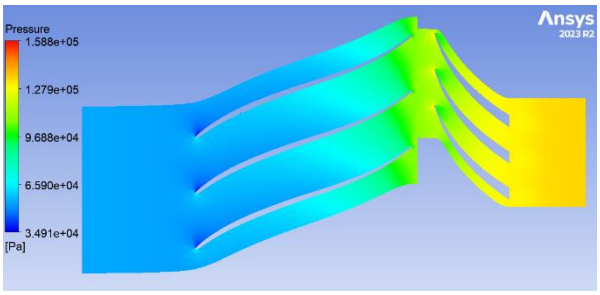

Figure 4.18: Static pressure contour R_4/R_2= 1.18; $\dot{m}_{corr}$= 2,09083

. Orthogonal plane

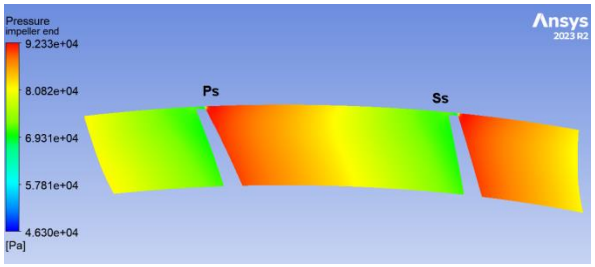

Figure 4.19: Static pressure contour R_4/R_2= 1.06; $\dot{m}_{corr}$= 2,10482

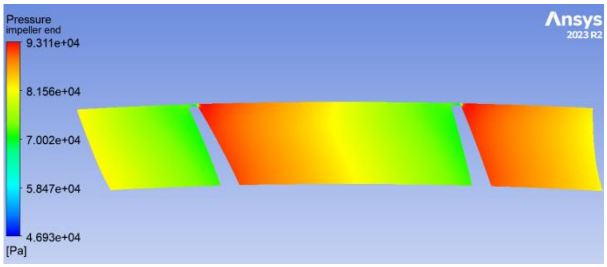

Figure 4.20: Static pressure contour R_4/R_2= 1.10; $\dot{m}_{corr}$= 2,09801

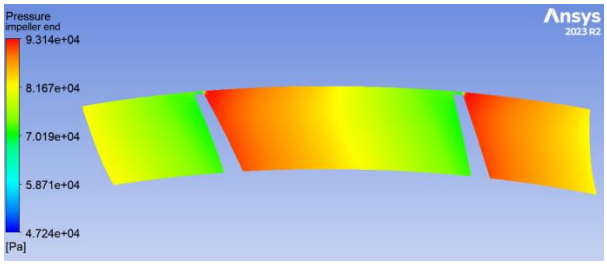

Figure 4.21: Static pressure contour R_4/R_2= 1.14; $\dot{m}_{corr}$= 2,1021

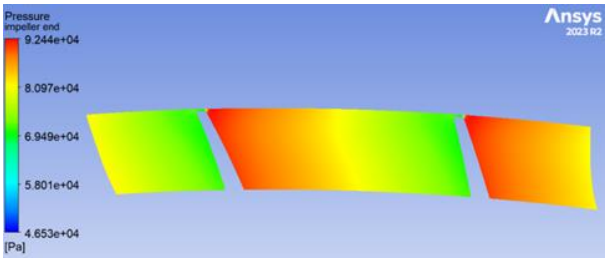

Figure 4.22: Static pressure contour R_4/R_2= 1.18; $\dot{m}_{corr}$= 2,09083

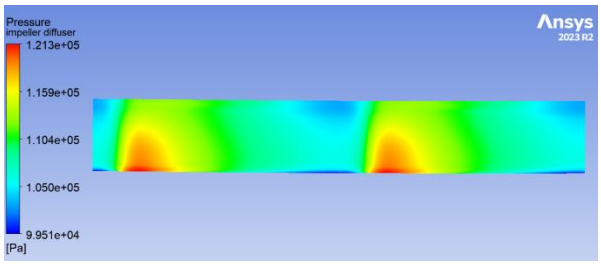

Figure 4.23: Static pressure contour R_4/R_2= 1.06; $\dot{m}_{corr}$= 2,10482

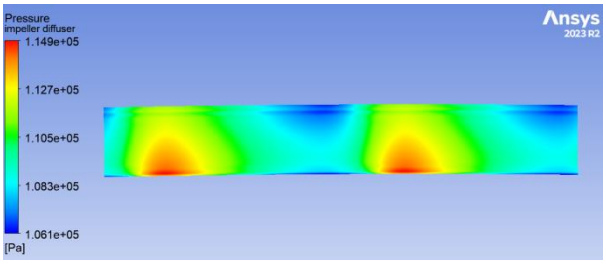

Figure 4.24: Static pressure contour R_4/R_2= 1.10; $\dot{m}_{corr}$= 2,09801

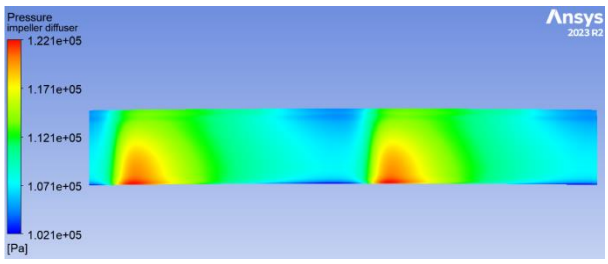

Figure 4.25: Static pressure contour R_4/R_2= 1.14; $\dot{m}_{corr}$= 2,1021

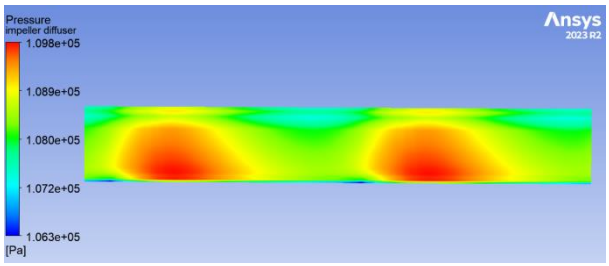

Figure 4.26: Static pressure contour R_4/R_2= 1.18; $\dot{m}_{corr}$= 2,09083

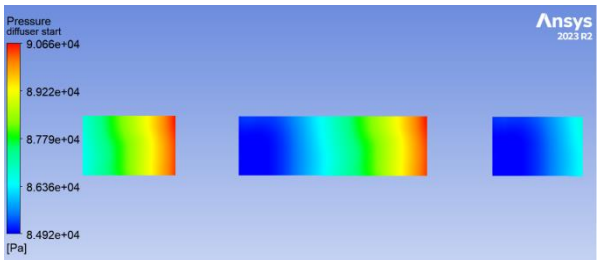

Figure 4.27: Static pressure contour R_4/R_2= 1.06; $\dot{m}_{corr}$= 2,10482

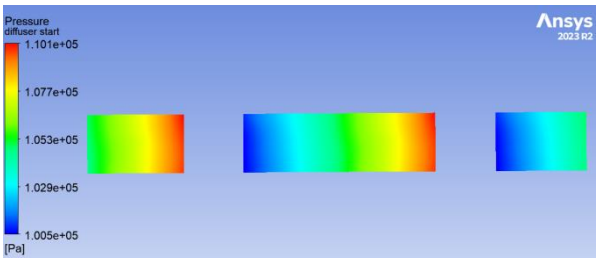

Figure 4.28: Static pressure contour R_4/R_2= 1.10; $\dot{m}_{corr}$= 2,09801

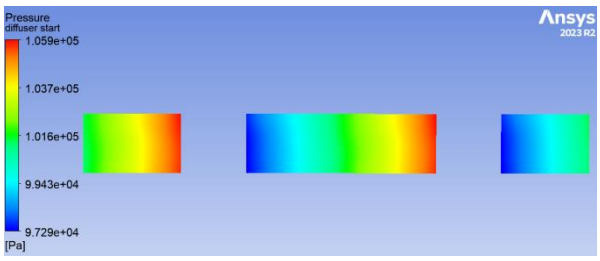

Figure 4.29: Static pressure contour R_4/R_2= 1.14; $\dot{m}_{corr}$= 2,1021

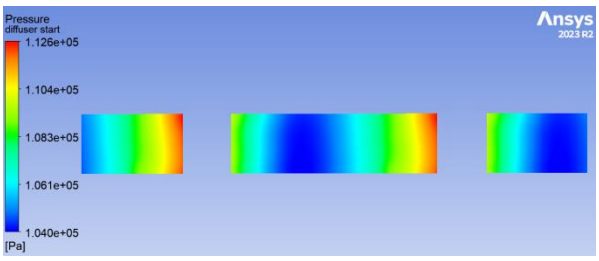

Figure 4.30: Static pressure contour R_4/R_2= 1.18; $\dot{m}_{corr}$= 2,09083

The static pressure contours show a consistent increase in pressure from the inlet to the outlet of the compressor, and from the pressure side to the suction side between two blades. The pressure gradient is highest at the inlet, indicating a strong compression effect. The contours also show a smooth pressure distribution across the flow path, suggesting that the flow is well-behaved and there are no significant flow separations or instabilities. The contour plots indicate that the compressor is operating efficiently and achieving the desired pressure increase. The

observed increase in static pressure in the figures above is primarily due to the convergence of the section in the streamwise direction.

4.4.2 Total pressure: Here we can see the distribution of static pressure in the three planes (meridional, blade to blade, and orthogonal).

. Meridional plane

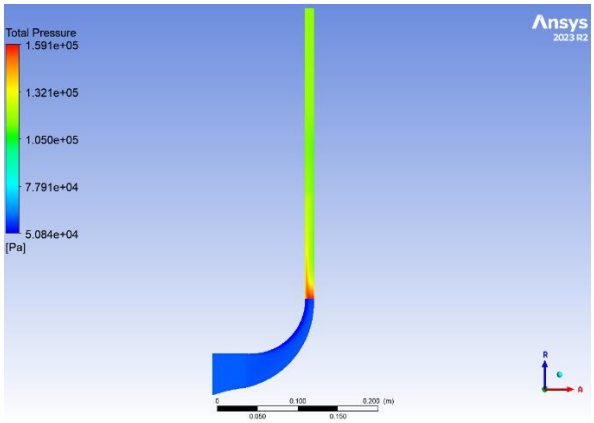

Figure 4.31: Total pressure contour
R_4/R_2= 1.06; $\dot{m}_{corr}$= 2,10482

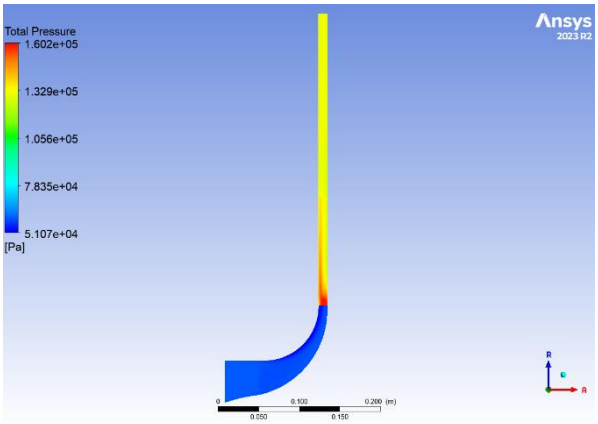

Figure 4.32: Total pressure contour
R_4/R_2= 1.10; $\dot{m}_{corr}$= 2,09801

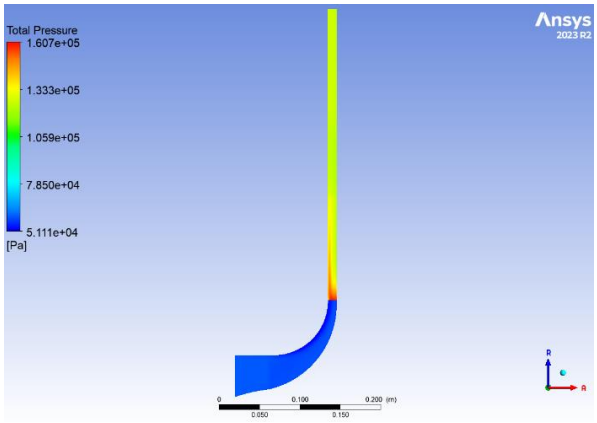

Figure 4.33: Total pressure contour
R_4/R_2= 1.14; $\dot{m}_{corr}$= 2,1021

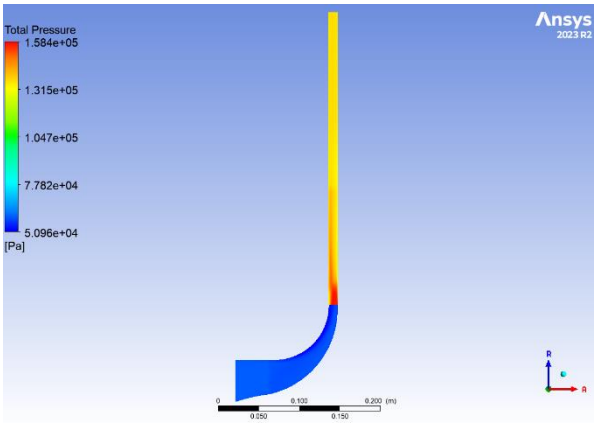

Figure 4.34: Total pressure contour
R_4/R_2= 1.18; $\dot{m}_{corr}$= 2,0908

. Blade to blade plane

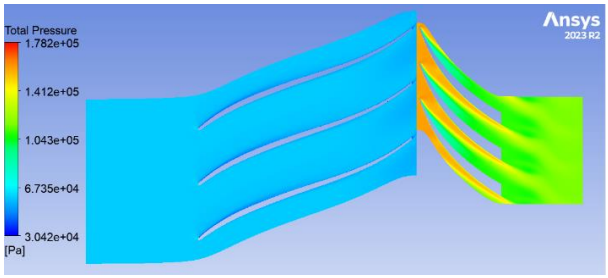

Figure 4.35: Total pressure contour
R_4/R_2= 1.06; $\dot{m}_{corr}$= 2,10482

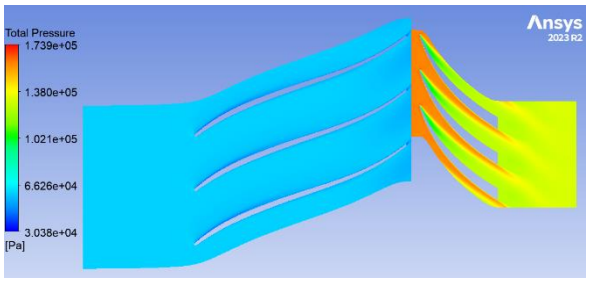

Figure 4.36: Total pressure contour
R_4/R_2= 1.10; $\dot{m}_{corr}$= 2,09801

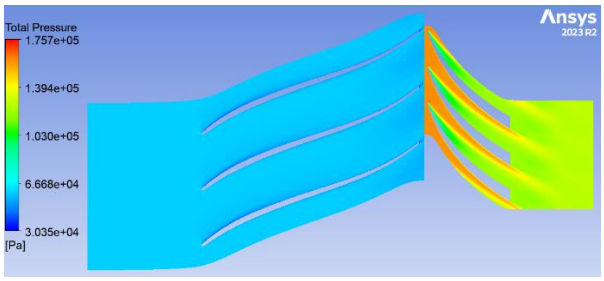

Figure 4.37: Total pressure contour
R_4/R_2= 1.14; $\dot{m}_{corr}$= 2,1021

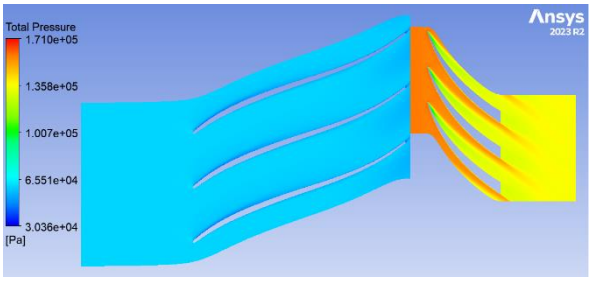

Figure 4.38: Total pressure contour
R_4/R_2= 1.18; $\dot{m}_{corr}$= 2,09083

The shock wave forms at the leading edge of the diffuser and is clearly visible in the blade-to-blade view of the total pressure contour. The discontinuity in total pressure arises because the impeller and diffuser meshes were created separately and then assembled in CFX. This assembly process creates an interface between the two meshes, which does not preserve the continuity of some quantities. Additionally, the sudden increase in total pressure can be explained by the fact that, upon exiting the impeller domain, the fluid enters a stationary domain, causing energy transfer from kinetic (velocity) to potential (pressure).

4.4.3 Static temperature: Here we can see the distribution of static temperature in the three planes (meridional, blade to blade, and orthogonal).

. Meridional plane

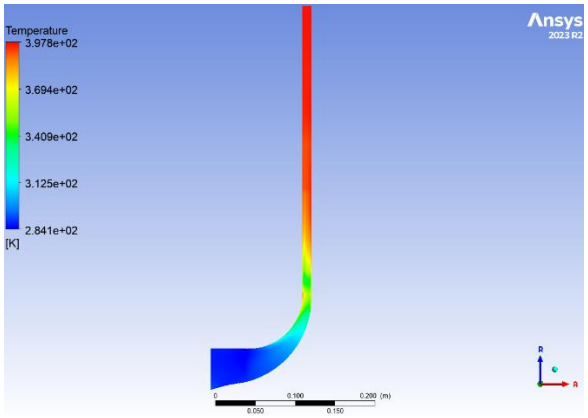

Figure 4.39: Static temperature contour
R_4/R_2= 1.06; $\dot{m}_{corr}$= 2,10482

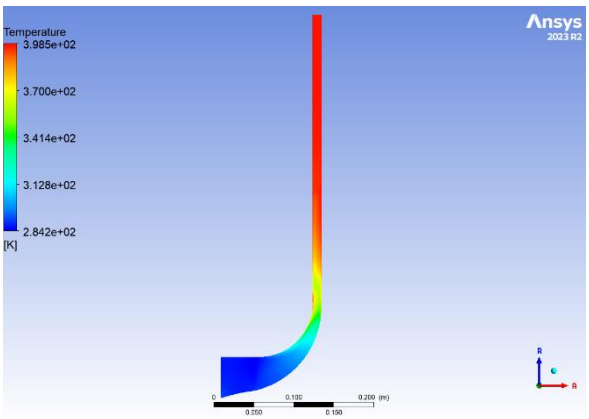

Figure 4.40: Static temperature contour
R_4/R_2= 1.10; $\dot{m}_{corr}$= 2,09801

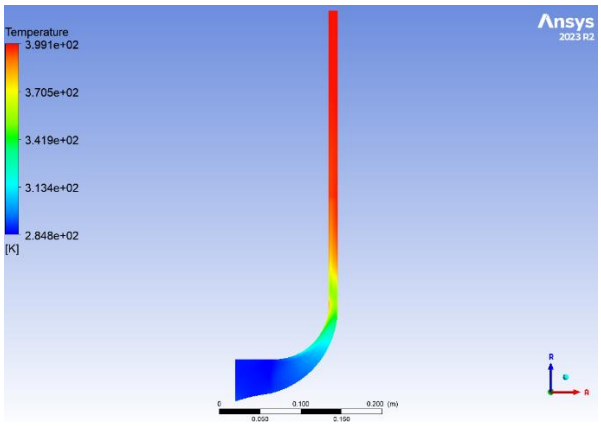

Figure 4.41: Static temperature contour R_4/R_2= 1.14; $\dot{m}_{corr}$= 2,1021

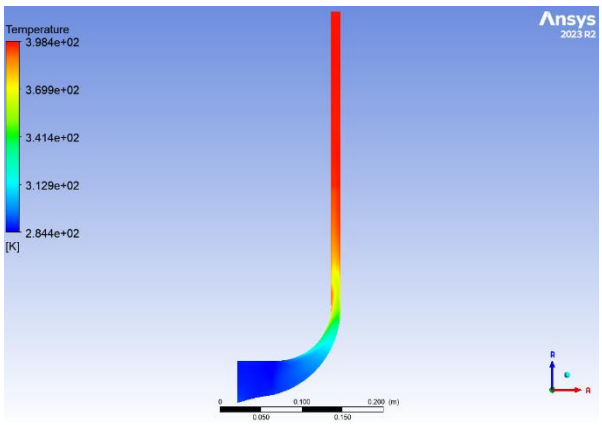

Figure 4.42: Static temperature contour R_4/R_2= 1.18; $\dot{m}_{corr}$= 2,09083

. Blade to blade plane

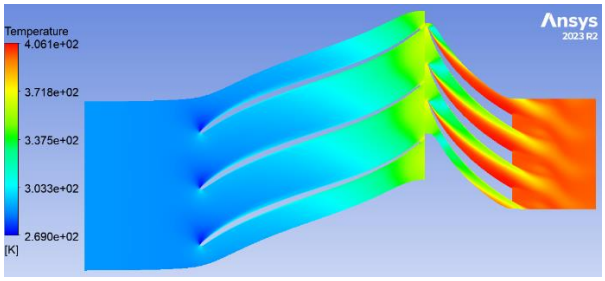

Figure 4.43: Static temperature contour R_4/R_2= 1.06; $\dot{m}_{corr}$= 2,10482

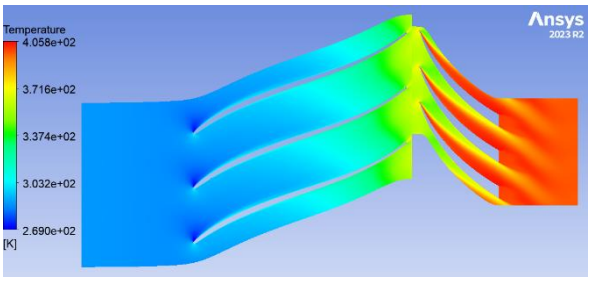

Figure 4.44: Static temperature contour R_4/R_2= 1.10; $\dot{m}_{corr}$= 2,09801

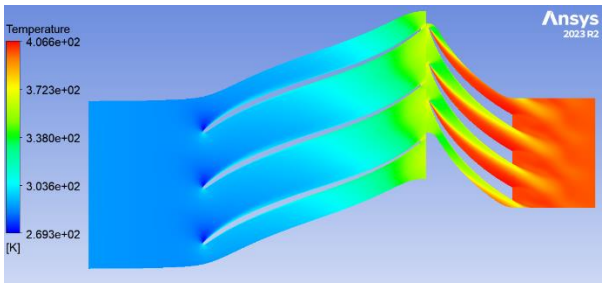

Figure 4.45: Static temperature contour R_4/R_2= 1.14; $\dot{m}_{corr}$= 2,1021

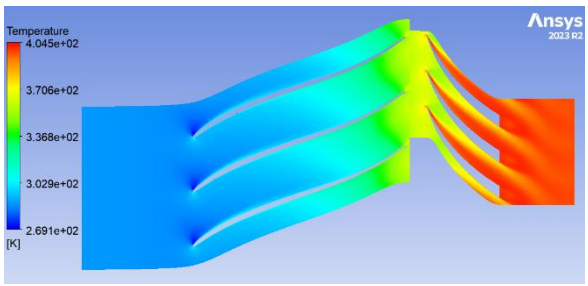

Figure 4.46: Static temperature contour R_4/R_2= 1.18; $\dot{m}_{corr}$= 2,09083

. Orthogonal plane

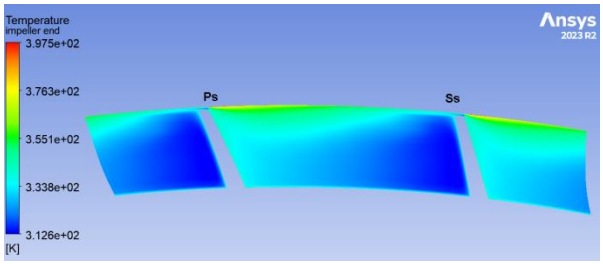

Figure 4.47: Static temperature contour R_4/R_2= 1.06; $\dot{m}_{corr}$= 2,10482

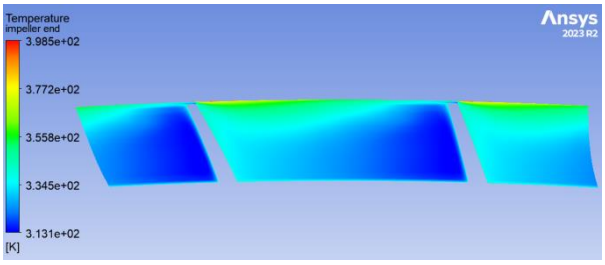

Figure 4.48: Static temperature contour R_4/R_2= 1.10; $\dot{m}_{corr}$= 2,09801

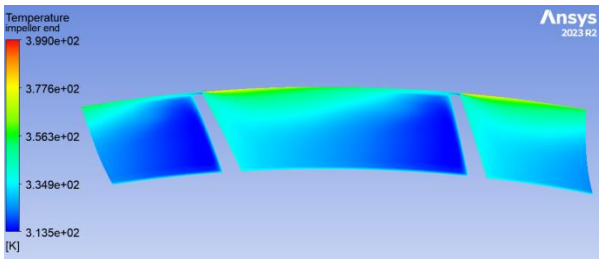

Figure 4.49: Static temperature contour
R_4/R_2= 1.14; $\dot{m}_{corr}$= 2,1021

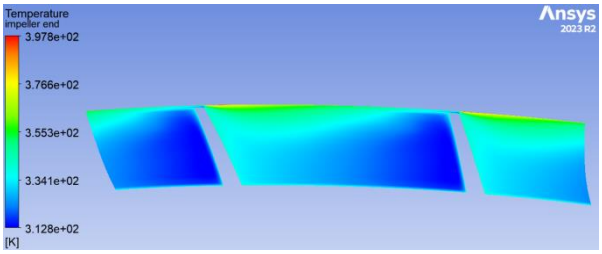

Figure 4.50: Static temperature contour
R_4/R_2= 1.18; $\dot{m}_{corr}$= 2,09083

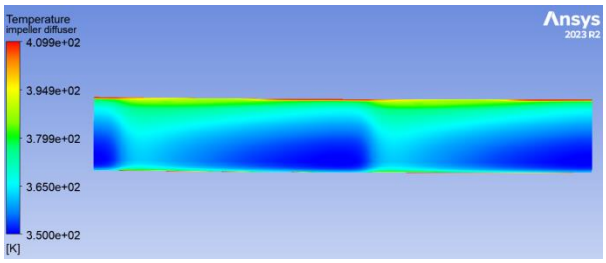

Figure 4.51: Static temperature contour
R_4/R_2= 1.06; $\dot{m}_{corr}$= 2,10482

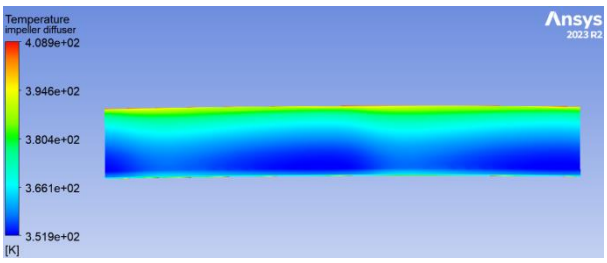

Figure 4.52: Static temperature contour
R_4/R_2= 1.10; $\dot{m}_{corr}$= 2,09801

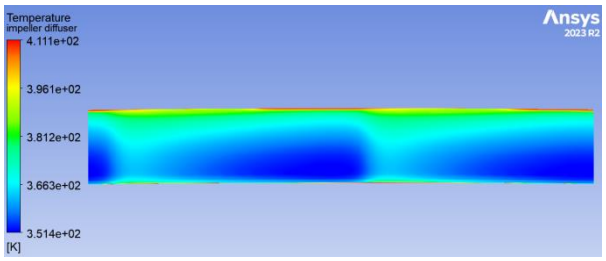

Figure 4.53: Static temperature contour
R_4/R_2= 1.14; $\dot{m}_{corr}$= 2,1021

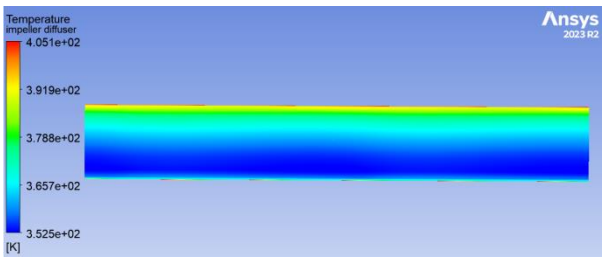

Figure 4.54: Static temperature contour
R_4/R_2= 1.18; $\dot{m}_{corr}$= 2,09083

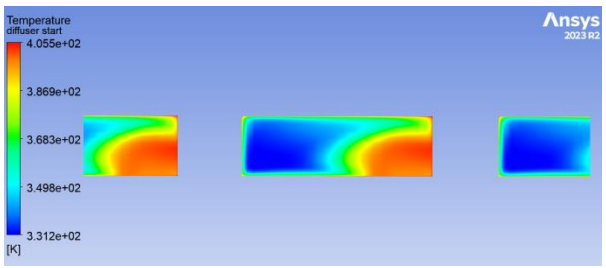

Figure 4.55: Static temperature contour
R_4/R_2= 1.06; $\dot{m}_{corr}$= 2,10482

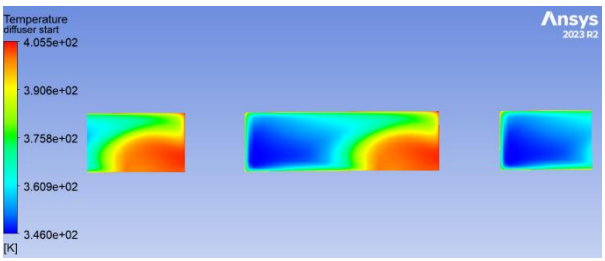

Figure 4.56: Static temperature contour
R_4/R_2= 1.10; $\dot{m}_{corr}$= 2,09801

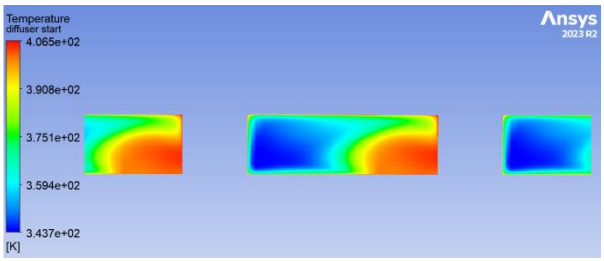

Figure 4.57: Static temperature contour R_4/R_2= 1.14; $\dot{m}_{corr}$= 2,1021

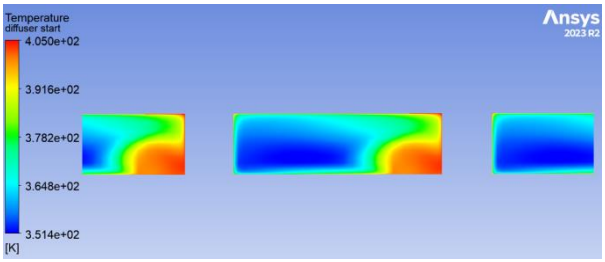

Figure 4.58: Static temperature contour R_4/R_2= 1.18; $\dot{m}_{corr}$= 2,09083

These figures represent the static temperature distribution in the compressor and show a comparable pattern with minor differences in maximum temperatures. This analysis can help in understanding the thermal behavior and performance of the compressor.

The static temperature increases from the inlet to the outlet, with a smooth transition between colors.

The overall distribution pattern is consistent between all R_4/R_2 configurations, indicating a similar performance in terms of static temperature rise within the compressor.

We can observe also in the orthogonal plane that the static temperature increases on pressure and decreases on the suction side. This can be explained by the fact that the static temperature is directly proportional to the static pressure.

4.4.4 Total temperature: Here we can see the distribution of total temperature in the three planes (meridional, blade to blade, and orthogonal).

. Meridional plane

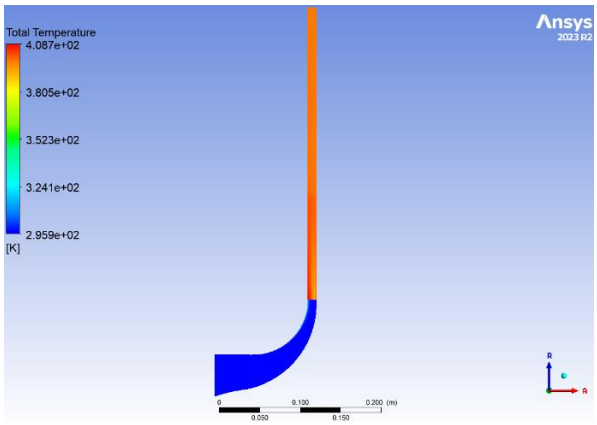

Figure 4.59: Total temperature contour R_4/R_2= 1.06; $\dot{m}_{corr}$= 2,10482

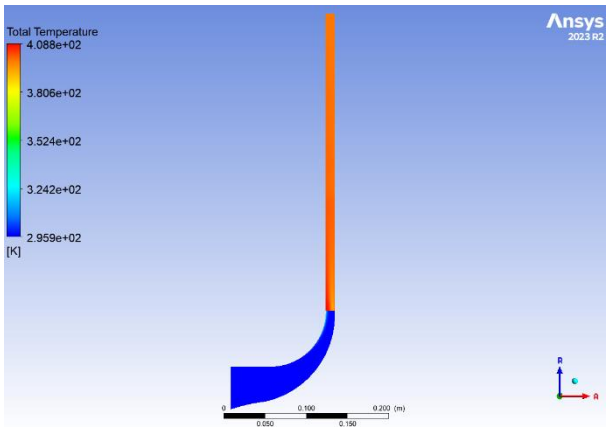

Figure 4.60: Total temperature contour R_4/R_2= 1.10; $\dot{m}_{corr}$= 2,09801

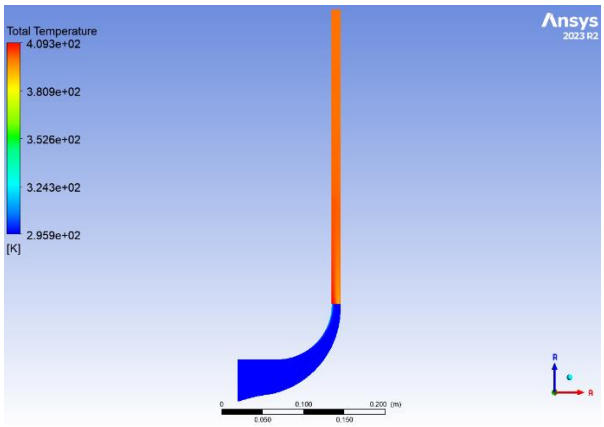

Figure 4.61: Total temperature contour
R_4/R_2= 1.14; $\dot{m}_{corr}$= 2,1021

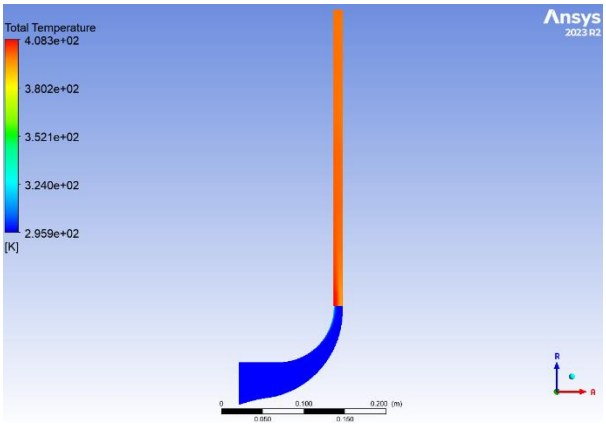

Figure 4.62: Total temperature contour
R_4/R_2= 1.18; $\dot{m}_{corr}$= 2,09083

. Blade to blade plane

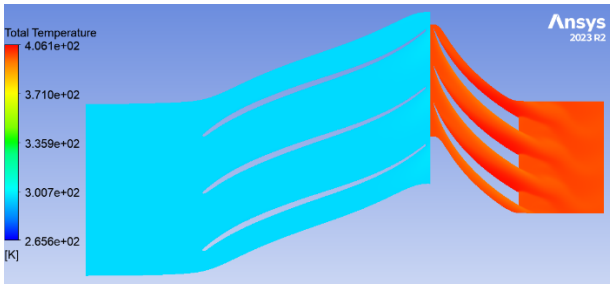

Figure 4.63: Total temperature contour
R_4/R_2= 1.06; $\dot{m}_{corr}$= 2,10482

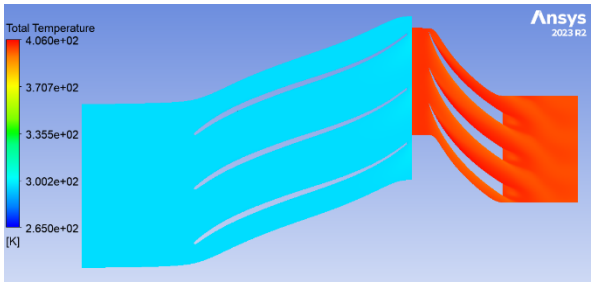

Figure 4.64: Total temperature contour
R_4/R_2= 1.10; $\dot{m}_{corr}$= 2,09801

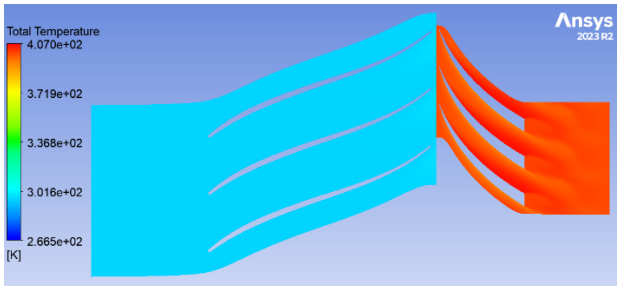

Figure 4.65: Total temperature contour
R_4/R_2= 1.14; $\dot{m}_{corr}$= 2,1021

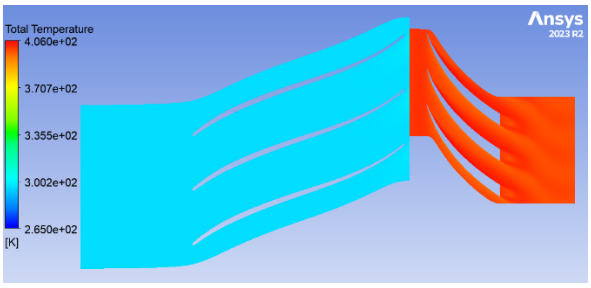

Figure 4.66: Total temperature contour
R_4/R_2= 1.18; $\dot{m}_{corr}$= 2,09083

4.4.5 Mach number: Here we can see the distribution of Mach number in the three planes (meridional, blade to blade, and orthogonal)

. Meridional plane

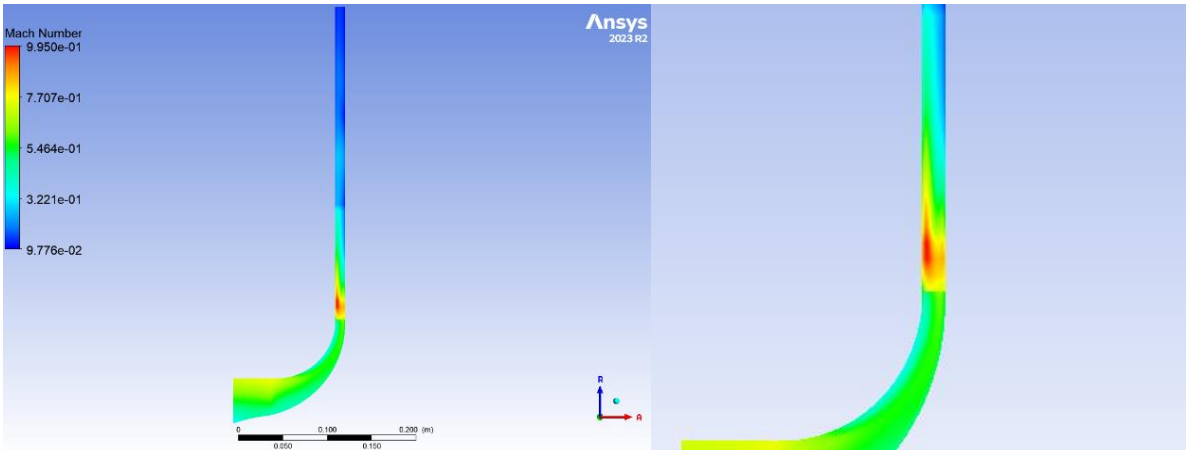

Figure 4.67: Mach number contour

R_4/R_2= 1.06; $\dot{m}_{corr}$= 2,10482

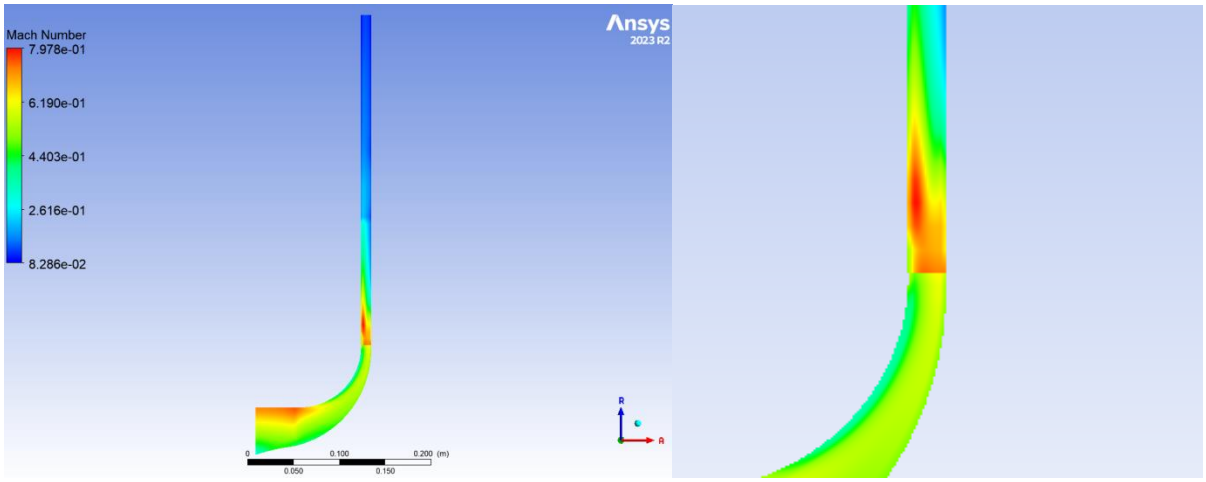

Figure 4.68: Mach number contour

R_4/R_2= 1.10; $\dot{m}_{corr}$= 2,09801

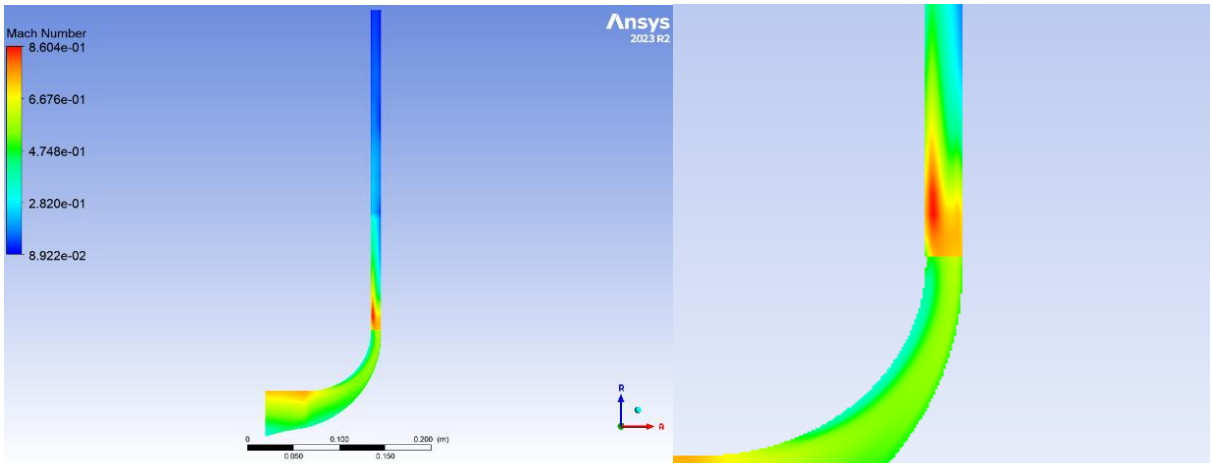

Figure 4.69: Mach number contour

R_4/R_2= 1.14; $\dot{m}_{corr}$= 2,1021

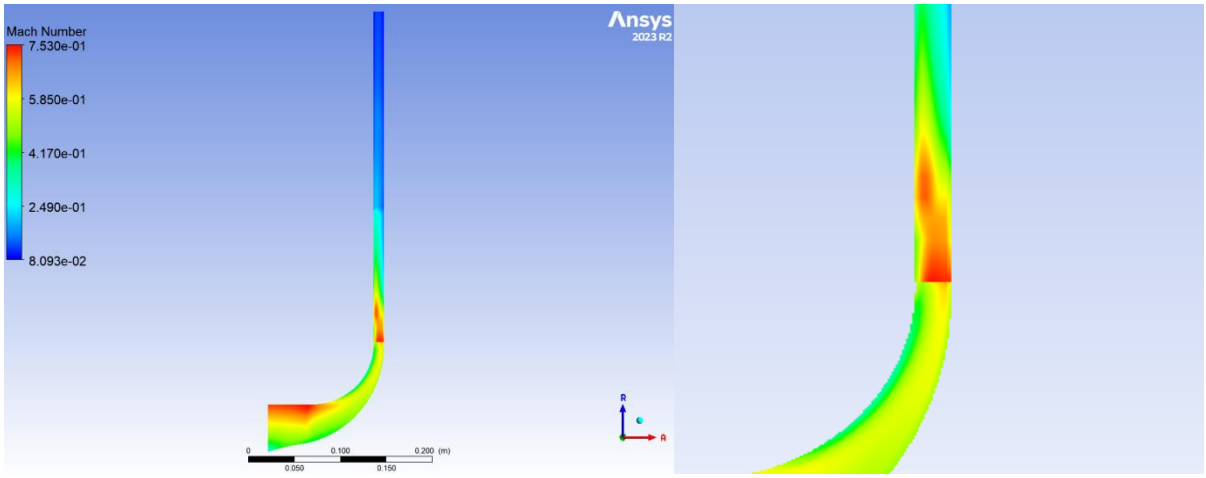

Figure 4.70: Mach number contour
R_4/R_2= 1.18; $\dot{m}_{corr}$= 2,09083

. Blade to blade plane

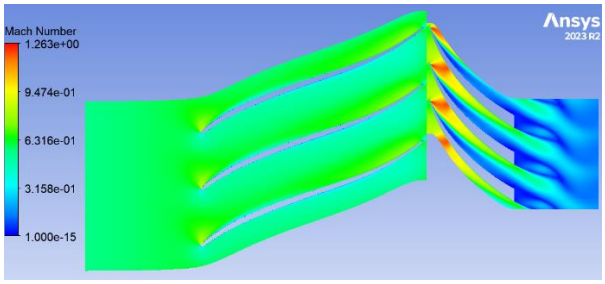

Figure 4.71: Mach number contour
R_4/R_2= 1.06; $\dot{m}_{corr}$= 2,10482

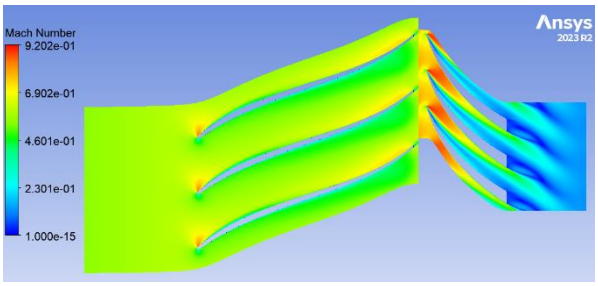

Figure 4.72: Mach number contour
R_4/R_2= 1.10; $\dot{m}_{corr}$= 2,09801

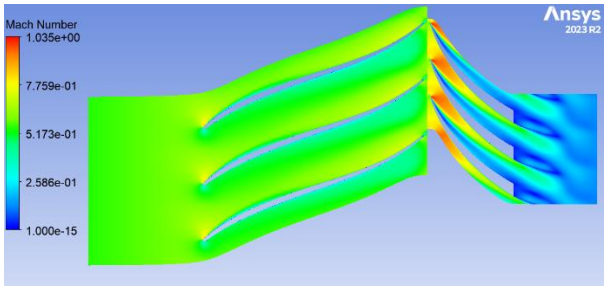

Figure 4.73: Mach number contour
R_4/R_2= 1.14; $\dot{m}_{corr}$= 2,1021

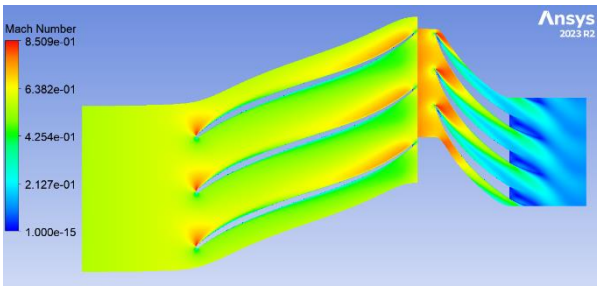

Figure 4.74: Mach number contour
R_4/R_2= 1.18; $\dot{m}_{corr}$= 2,09083

The shock is further more apparent in the Mach contours shown above..

Orthogonal plane

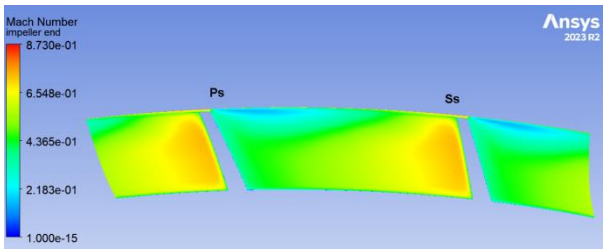

Figure 4.75: Mach number contour
R_4/R_2= 1.06; $\dot{m}_{corr}$= 2,10482

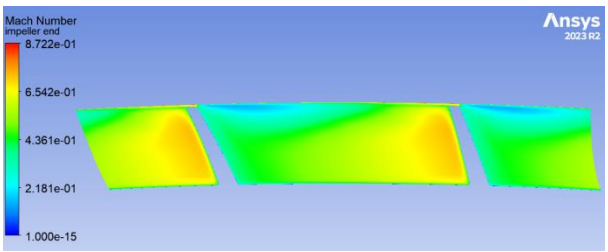

Figure 4.76: Mach number contour
R_4/R_2= 1.10; $\dot{m}_{corr}$= 2,09801

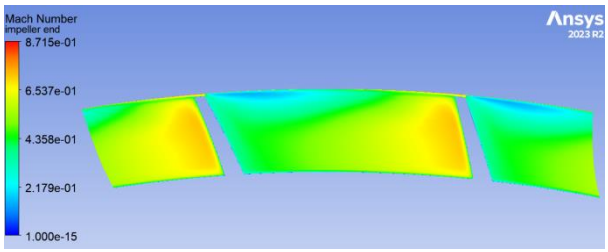

Figure 4.77: Mach number contour
R_4/R_2= 1.14; $\dot{m}_{corr}$= 2,1021

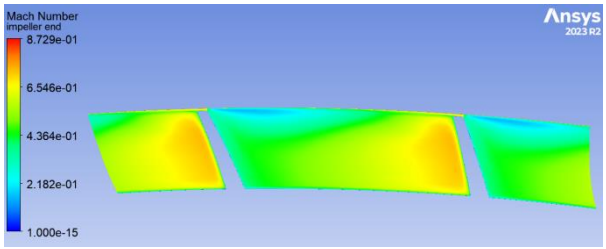

Figure 4.78: Mach number contour
R_4/R_2= 1.18; $\dot{m}_{corr}$= 2,09083

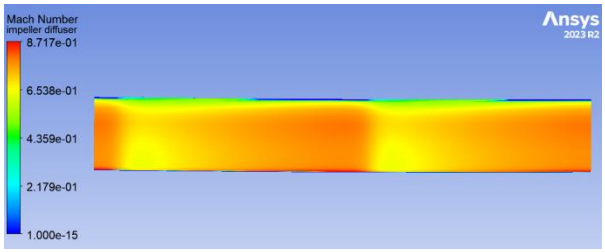

Figure 4.79: Mach number contour
R_4/R_2= 1.06; $\dot{m}_{corr}$= 2,10482

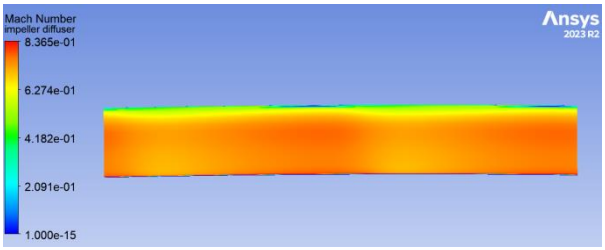

Figure 4.80: Mach number contour
R_4/R_2= 1.10; $\dot{m}_{corr}$= 2,09801

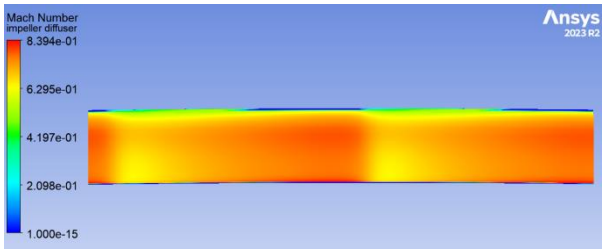

Figure 4.81: Mach number contour
R_4/R_2= 1.14; $\dot{m}_{corr}$= 2,1021

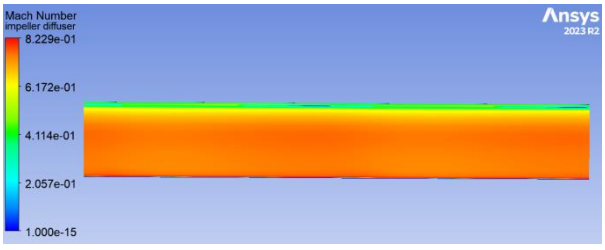

Figure 4.82: Mach number contour
R_4/R_2= 1.18; $\dot{m}_{corr}$= 2,09083

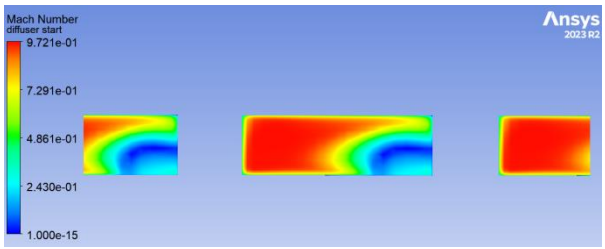

Figure 4.83: Mach number contour
R_4/R_2= 1.06; $\dot{m}_{corr}$= 2,10482

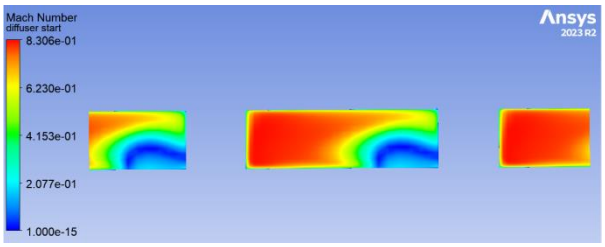

Figure 4.84: Mach number contour
R_4/R_2= 1.10; $\dot{m}_{corr}$= 2,09801

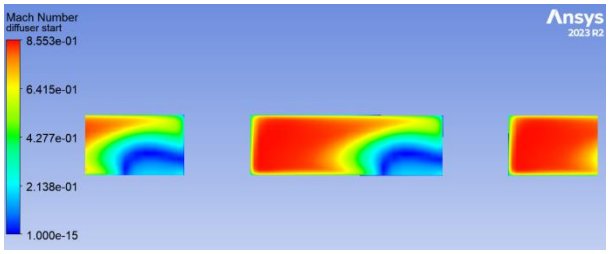

Figure 4.85: Mach number contour
R_4/R_2= 1.14; $\dot{m}_{corr}$= 2,1021

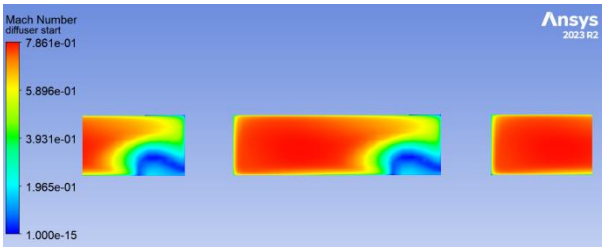

Figure 4.86: Mach number contour
R_4/R_2= 1.18; $\dot{m}_{corr}$= 2,09083

4.4.6 Static entropy: To identify where the most significant energy losses occur and highlight the regions with substantial losses, we will present the static entropy contours.

. Meridional plane

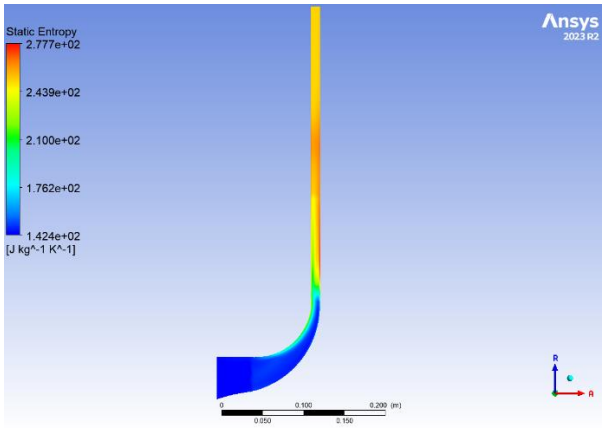

Figure 4.87: Static entropy contour
R_4/R_2= 1.06; $\dot{m}_{corr}$= 2,10482

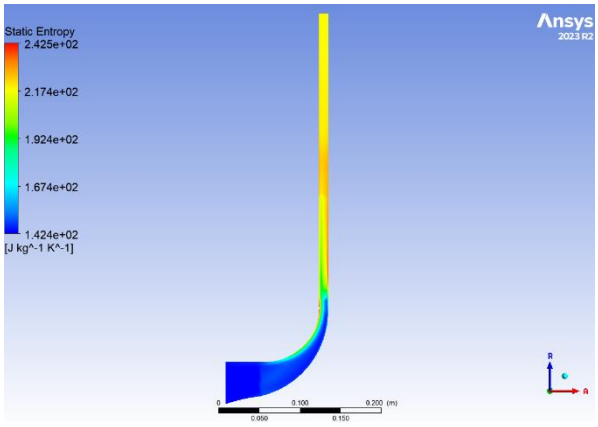

Figure 4.88: Static entropy contour
R_4/R_2= 1.10; $\dot{m}_{corr}$= 2,09801

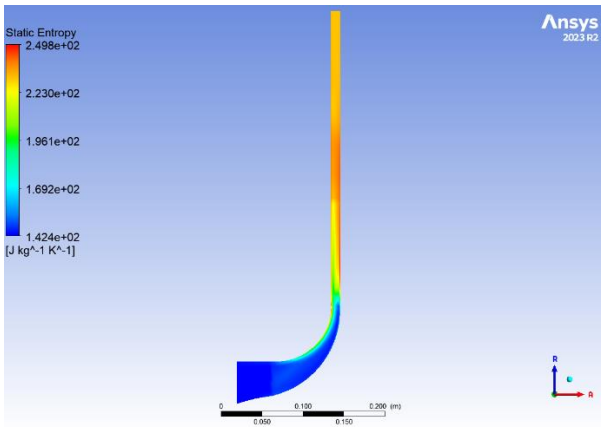

Figure 4.89: static entropy contour
R_4/R_2= 1.14; $\dot{m}_{corr}$= 2,1021

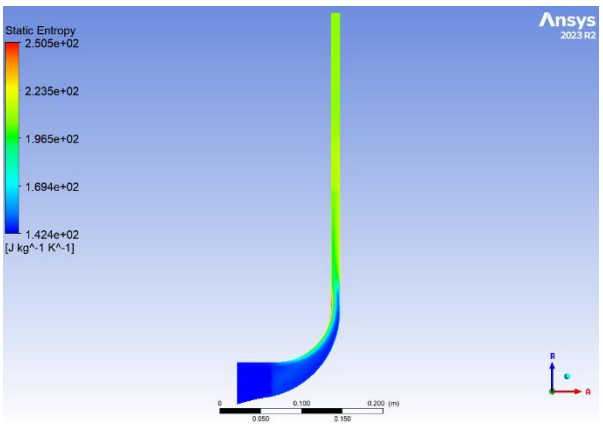

Figure 4.90: static entropy contour
R_4/R_2= 1.18; $\dot{m}_{corr}$= 2,09083

Here, the high entropy region in the radial gap between the impeller and shroud indicates the creation of high-energy small eddies. the significant entropy in the shock wave region aligns with theoretical principles of shock wave phenomena.

. Blade to blade plane

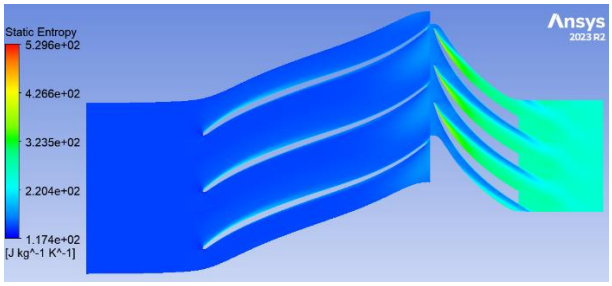

Figure 4.91: Static entropy contour
R_4/R_2= 1.06; $\dot{m}_{corr}$= 2,10482

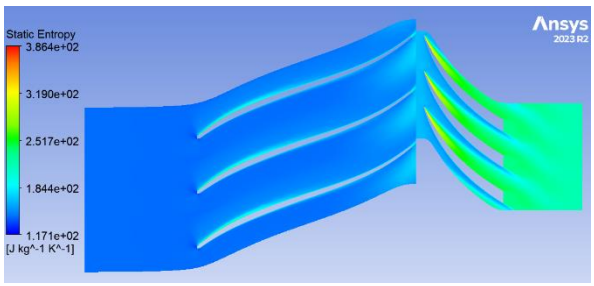

Figure 4.92:Static entropy contour
R_4/R_2= 1.10; $\dot{m}_{corr}$= 2,09801

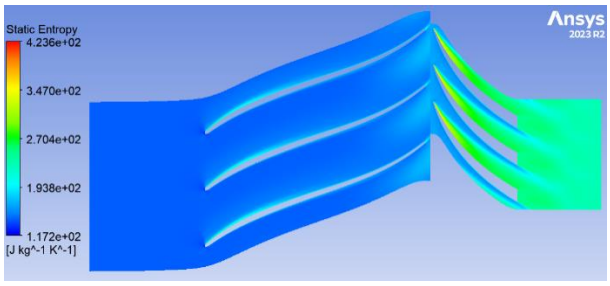

Figure 4.93: Static entropy contour
R_4/R_2= 1.14; $\dot{m}_{corr}$= 2,1021

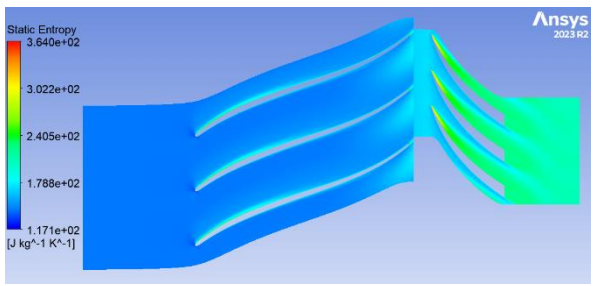

Figure 4.94: Static entropy contour
R_4/R_2= 1.18; $\dot{m}_{corr}$= 2,09083

Here, we can see that the significant entropy in the shock wave region aligns with theoretical principles of shock wave phenomena.

4.4.7 Performance charts

To examine the influence of varying the radial gap between the impeller and diffuser, we present the blade loading curves for both the impeller and diffuser in the configurations $R_4/R_2 = 1.06$, $R_4/R_2 = 1.10$, $R_4/R_2 = 1.14$, and $R_4/R_2 = 1.18$.

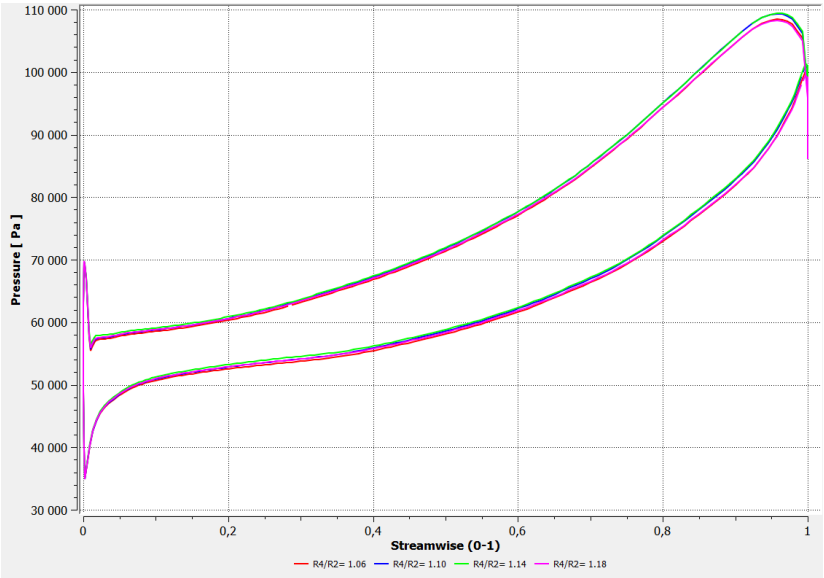

Figure 4.95: Impeller blade loading chart

As we can see all the configurations have practically the same impeller blade loading and show minimal difference.

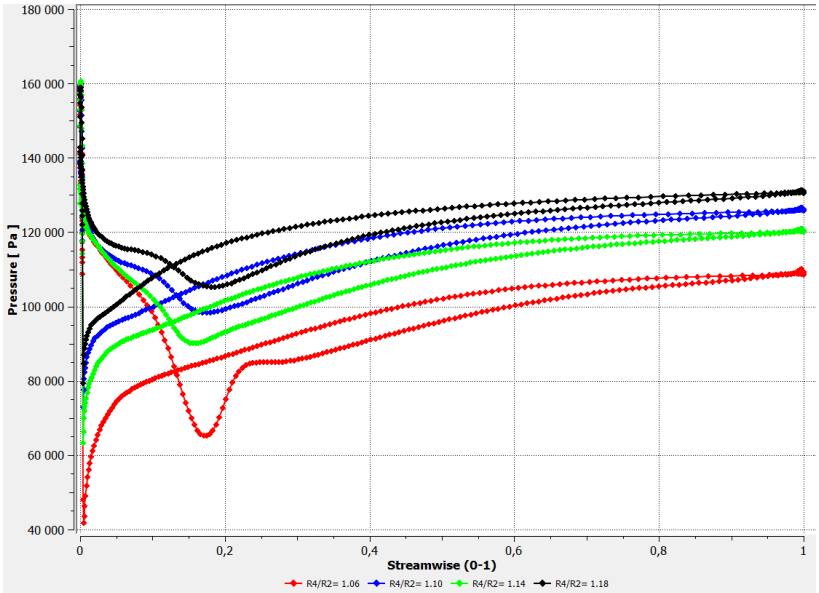

Figure 4.96: Diffuser blade loading chart

Here we can see that a transitional point is observed at approximately 0.18 of the streamwise location. This inconsistency is primarily due to the shock wave formed within the diffuser.

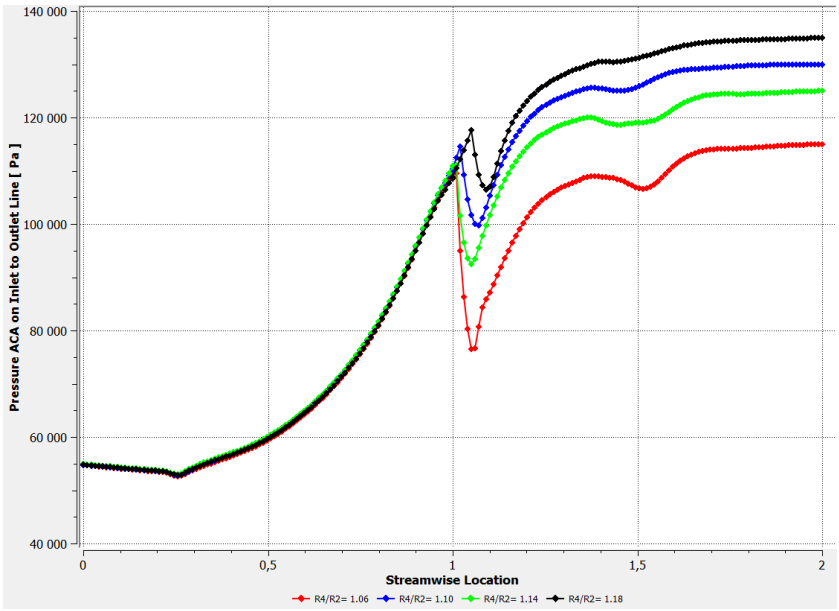

Figure 4.97: Static pressure chart for all configurations

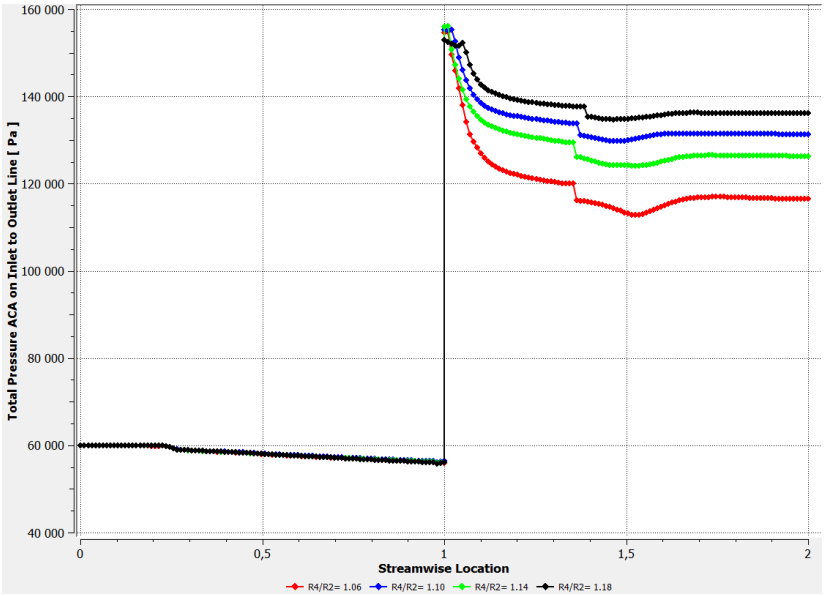

Figure 4.98: Total pressure chart for all configurations

The static and total pressure curves for both the impeller and diffuser in all configurations are almost overlapped and show minimal difference from 0 to 1 streamwise location which means the impeller side, and the difference appears in the diffuser side.

Now we will see the static and total temperature charts.

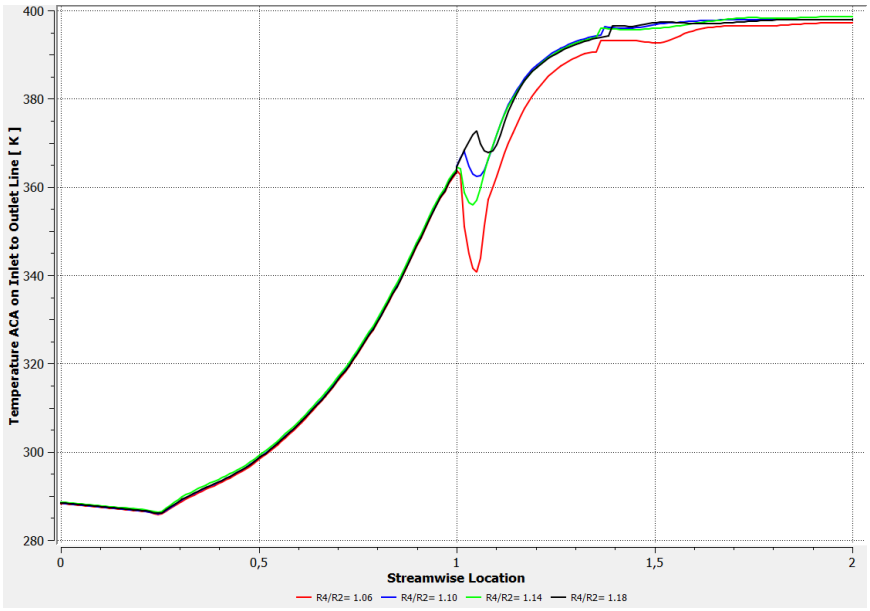

Figure 4.99: Static temperature chart for all configurations

Here we can also see that The static temperature curves for both the impeller and diffuser in all configurations are almost overlapped and show minimal difference from 0 to 1 streamwise location which means the impeller side, and the difference appears in the diffuser side.

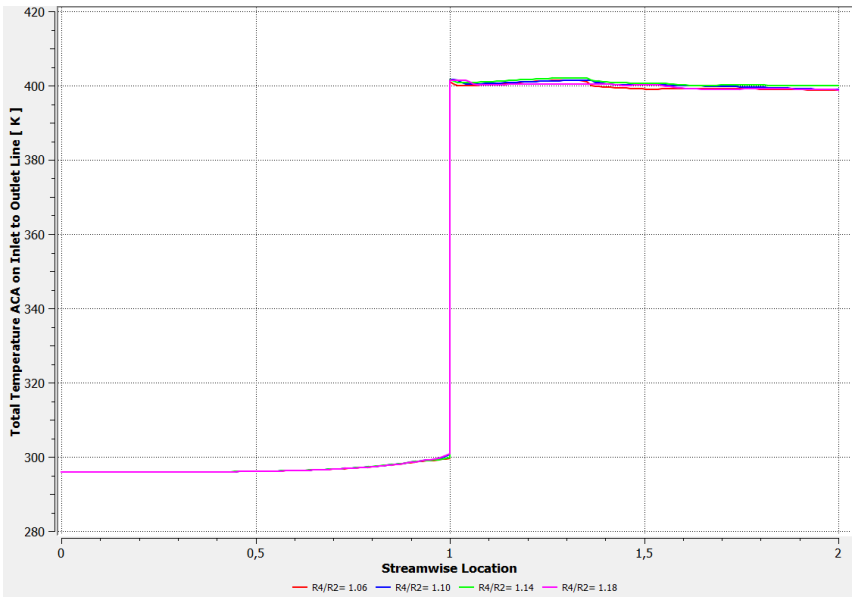

Figure 4.100: Total temperature chart for all configurations

Here, the total temperature curves for both the impeller and diffuser in all configurations are almost overlapped and show minimal difference.

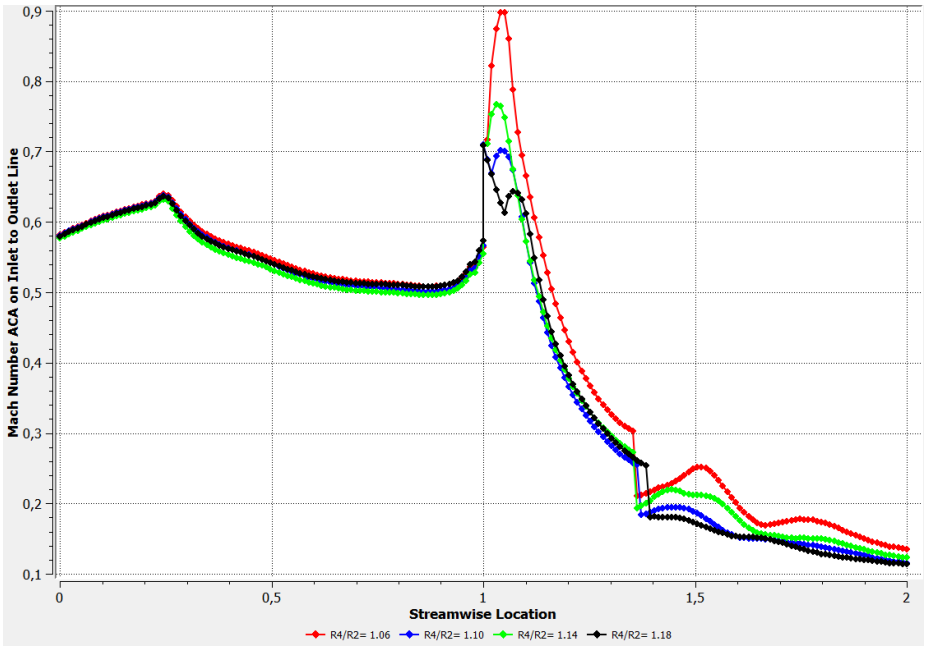

Figure 4.101: Mach number chart for all configurations

Here we can see a minimal difference in the impeller side (from 0 to 1 streamwise location), and we can notice also a sudden downward slope on about 1.35 streamwise location, and this is due to the shockwave formed in the diffuser.

General Conclusion

The study of internal flow in turbomachines, particularly centrifugal compressors, highlights the importance of understanding various factors such as viscosity, compressibility, three-dimensionality, and vortices. Researchers have extensively used numerical and experimental methods, employing tools like ANSYS CFX software and the k-ω SST turbulence model, to analyze aerothermodynamic parameters and the critical interaction between the impeller and diffuser. These studies aim to optimize geometric and operational parameters, enhancing isentropic efficiency and corrected mass flow rate for better energy efficiency.

As the R4/R2 ratio increases, the total isentropic efficiency as well as total pressure ratio also generally increases. A higher total isentropic efficiency, and total pressure ratio signifies better compression performance. Which means that R4/R2= 1.18 configuration gave us the best performances.

Centrifugal compressors play a pivotal role across industries and small gas turbine engines, where achieving a high-pressure ratio stands as a primary objective for enhancing energy efficiency, reducing emissions, and increasing power density. Each stage of a centrifugal compressor comprises two essential components: the rotor (impeller) and the stator (diffuser). The rotor, a dynamic assembly of blades attached to a central hub, accelerates the gas by imparting swirl motion. In contrast, the stator, composed of fixed blades, diffuses the accelerated gas to convert kinetic energy into elevated pressure. Designing the optimal fluid interaction between these components is a sophisticated endeavor, often driven by numerical simulations and Computational Fluid Dynamics (CFD) models. These simulations allow engineers to refine geometric and operational parameters, aiming to maximize compressor performance and energy efficiency. Such advancements not only improve overall system reliability but also contribute significantly to sustainable energy practices by reducing operational costs and environmental impact. Through ongoing research and innovation, engineers continue to push the boundaries of centrifugal compressor design, paving the way for more efficient industrial processes and cleaner energy solutions globally.

Bibliography

[1] Jeske.H, O.Tepel. A theoretical investigation of transonic flows in radial compressor diffusers.1983.

[2] Michael D. Hathaway, Randall M. Chriss, Jerry R. Wood, and Anthony J. Strazisar. Experimental and Computational Investigation of the NASA Low-Speed Centrifugal Compressor Flow Field. NASA Technical Memorandum 4481. September 1993.

[3] Kai U .Ziegler, Heinz E .Gallus, Reinhard Niehuis. A study on impeller-diffuser interaction: part i –influence on the performance. In Turbo Expo: Power for land, Sea, and Air, volume3610, pages545-556, 2002.

[4] Kai U Ziegler. Experimentale untersuchung der laufrad-diffusor-interaktion in einem radialverdichter variable geometrie. Shaker, 2003.

[5] Guillaume Dufour. Contributions à la modélisation et au calcul des écoulements dans les compresseurs centrifuges : application à la conception par lois de similitude. PHD thesis, 2006.

[6] Nicolas Rochuon. Analyse de l'écoulement tridimensionnel et instationnaire dans un compresseur centrifuge à fort taux de pression. Ecole centrale de Lyon 2007.

[7] Ozturk Tatar, Adnan Ozturk, and Ali Pinarbasi. Flow analysis in centrifugal compressor vaneless diffusers 2008.

[8] Moustafa Maammeur. Simulation de l'écoulement de l'air dans la roue d'un compresseur centrifuge. PHD thesis

[9] Michael Casey and Chris Robinson. Radial Flow Turbocompressors, Design, Analysis, and Applications.2021

[10] Dr. Meherwan P. Boyce, P.E. Centrifugal Compressors A Basic Guide.2003.

[11] Kwang-Yong Kim, Abdus Samad, Ernesto Benini. Design optimization of Fluid Machinery, Applying Computational Fluid Dynamics And Numerical Optimization.2019.

[12] Robert D.Cook, David S.Malkus, Michael E. Plesha. Concepts and Applications of Finite Element Analysis. Third Edition. 1989.

[13] ANSYS Inc. Ansys CFX-Solver theory guide, 2023.

[14] Andrew Louis De Wet. Performance investigation of a turbocharger compressor.2011.